Open Access Theses & Dissertations

2024-08-01

Establishment Of A Novel Prairie Vole (microtus Ochrogaster) Sars-Cov-2 Infection And Transmission Model

Stephanie Rebecca Kehl
University of Texas at El Paso

ESTABLISHMENT OF A NOVEL PRAIRIE VOLE (*MICROTUS OCHROGASTER)* SARS-

COV-2 INFECTION AND TRANSMISSION MODEL

STEPHANIE REBECCA KEHL

Doctoral Program in Biosciences

APPROVED:

Hugues Ouellet, Ph.D., Chair

Charles Spencer, Ph.D.

Manuel Llano, Ph.D.

Bruce S. Cushing, Ph.D.

Md Nurunnabi, Ph.D.

Stephen L. Crites, Jr., Ph.D.
Dean of the Graduate School

ESTABLISHMENT OF A NOVEL PRAIRIE VOLE (*MICROTUS OCHROGASTER)* SARS-

COV-2 INFECTION AND TRANSMISSION MODEL

by

STEPHANIE REBECCA KEHL, MS

DISSERTATION

Presented to the Faculty of the Graduate School of

The University of Texas at El Paso

in Partial Fulfillment

of the Requirements

for the Degree of

DOCTOR OF PHILOSOPHY

Department of Biological Sciences

THE UNIVERSITY OF TEXAS AT EL PASO

August 2024

Abstract

Considering that the number of SARS-CoV-2 cases and deaths continues to increase three years after the onset of the pandemic, the need for animal models to study disease pathology and test antiviral effectiveness remains paramount. Prairie voles offer unique advantages as an infection model, such as mirroring human social behavior, including pair bonding and biparental offspring rearing, having inducible estrus and ovulation cycles, and not being overly domesticated. Based on the sequence homology of the vole ACE2 receptor to that of other species that are susceptible to SARS-CoV-2, such as the ferret and hamster, we hypothesized that the vole ACE2 receptor would bind to the receptor binding domain (RBD) within the Spike protein of SARS-CoV-2. Using VSV pseudoparticles expressing the Spike protein, we determined that the vole ACE2 receptor facilitated viral entry. Intranasal and aerosol inoculation of the voles resulted in a peak in viral RNA levels in the lungs of the animals 4 dpi. Additionally, at 7 dpi, we observed viral RNA levels in the lungs, brain, and nasal wash of uninfected voles housed with an infected cage mate. Viral RNA levels detected in the voles following either inoculation method were comparable to those observed in the K18hACE2 transgenic mouse model. Finally, we observed a significant reduction in both viral RNA copies and titer following treatment of SARS-CoV-2 infected voles with remdesivir. Our findings demonstrate that the prairie voles are susceptible to SARS-CoV-2 infection, can transmit the virus to uninfected cage-mates, and can be treated with an established antiviral.

Table of Contents

List of Tables

List of Figures

List of Abbreviations

µg – Micrograms

µL – Micrograms

α – Alpha

ACE2 – Angiotensin converting enzyme 2

Amp – Ampicillin

Ang – Angiotensin

AP-1 – Activator protein-1

APCs – Antigen presenting cells

BAC – Bacterial Artificial Chromosome

BCA – Bicinchoninic acid

BSL – Biosafety level

CARD – Caspase-recruitment domain

cDNA – Complementary DNA

cGAS – Cyclic GMP-AMP synthase

CN – Calcineurin

COVID-19 – Coronavirus disease 19

CPE – Cytopathic effect

CSA – Cyclosporine A

CTL – Cytotoxic T cells

CTSL – Cathepsin L

CV – Column volume

DAMPs – Danger-associated molecular pattern molecules

diH$_2$O – Deionized water

DMEM – Dulbecco's Modified Eagle Medium

dpi – Days post-infection

EQU-BAC – Equilibration buffer

ERGIC – Endoplasmic reticulum-Golgi intermediate compartment

ExoN – Exonuclease

FBS – Fetal bovine serum

G418 – Geneticin

GE – Genome equivalents

hACE2 – Human ACE2

HEK – Human Embryonic Kidney

HHS – US Department of Health and Human Services

His – Histidine

hTMPRSS2 – Human TMPRSS2

IACUP – Institutional Animal Care and Use Program

IFN – Interferon

IL – Interleukin

IP – Intraperitoneal

IPA – Isopropanol

IRFs – Interferon regulatory factors

IVC – Individually ventilated cages

JAK1 – Janus kinase 1

kDa – Kilodaltons

LB – Luria-Bertani

MAPKs – Mitogen-activated protein kinase

MDA5 – Melanoma differentiation-associated gene 5

MERS-CoV – Middle east respiratory syndrome coronavirus

mL – Milliliters

moACE2 – Prairie vole ACE2

MOI – Multiplicity of infection

mRNA – Messenger RNA

MWCO – Molecular weight cut-off

MyD88 – Myeloid differentiation factor 88

N7-MTase - N7-methyltransferase

NEAA – Non-essential amino acids

NFAT - Nuclear factor of activated T cells NFAT

NF-κB – Nuclear factor (NF)-κB

NGS – Next generation sequencing

NHP – Non-human primates

NIH – National Institutes of Health

NLR – Nucleotide-binding and oligomerization domain (NOD)-like receptors

NLRP3 – NOD-like receptor protein 3

Nsps – Nonstructural proteins

NTD – N terminal domain

OLAW – Office of Laboratory Animal Welfare

p1 – Passage 1

p2 – Passage 2

p8 – Passage 8

p12 – Passage 12

p15 – Passage 15

PAMPs – Pathogen-associated molecular pattern molecules

PBS – Phosphate Buffered Saline

PD – Postnatal day

PEG – Polyethylene glycol

PHS – Public Health Service

PL-pro – Papin-like protease

PMSF – Phenylmethylsulfonyl fluoride

PRR – Pattern recognition receptors

PS – Penicillin and streptomycin

qRT-PCR – Quantitative reverse transcription polymerase chain reaction

RAS – Renin-aldosterone system

RBD – Receptor binding domain

RdRp – RNA-dependent RNA polymerase

RLR – Retinoic acid-inducible gene-I (RIG-I-)like receptors

RNA – Ribonucleic acid

ROS – Reactive oxygen species

rpm – Rotations per minute

SARS-CoV – Severe acute respiratory syndrome coronavirus

SARS-CoV-2 – Severe acute respiratory syndrome coronavirus 2

SDS-PAGE – Sodium Dodecyl-Sulfate Polyacrylamide Gel Electrophoresis

sg mRNA – Subgenomic mRNA

SIG – SARS-CoV-2 Interagency Group

STING – Stimulator of interferon genes

Tfh – Follicular helper T cells

Th – T helper cells

TLR – Toll-like receptors

TNF – Tumor necrosis factor

TRIF – Toll/interleukin (IL)-1 receptor domain-containing adaptor inducing IFN-β

TTSP – Type II transmembrane serine protease

USDA – U.S. Department of Agriculture

UTEP – University of Texas at El Paso

VBM – Variants being monitored

VeroE6 – African green monkey kidney cells

VeroE6/TMPRSS2 – African green monkey kidney cells expressing TMPRSS2

VOC – Variants of concern

VOHC – Variants of high consequence

VOI – Variants of interest

VSV – Vesicular Stomatitis Virus

WHO – World Health Organization

WT – Wildtype

Chapter 1: Introduction

1.1   SARS-CoV-2 PANDEMIC

Severe acute respiratory syndrome coronavirus 2 (SARS-CoV-2), commonly known as coronavirus disease 19 (COVID-19), emerged in December 2019, instigating a global health crisis of unprecedented proportions (Gorbalenya et al., 2020). The cumulative toll of cases has surpassed 770 million, with related deaths exceeding 6.9 million (WHO, 2021). The sheer scale of those affected by COVID-19 has posed an exceptional challenge to healthcare systems, exacerbated economic hardships, and mandated unparalleled efforts to control and mitigate the virus's impact (Nicola et al., 2020).

1.2   SARS-CoV-2 GENEALOGY

SARS-CoV-2 is an RNA virus belonging to the genera Betacoronavirus (β-CoV) within the Coronaviridae family of viruses (H. Li et al., 2020). This family, classified under the Nidovirales, is a diverse group of positive-sense single-stranded RNA viruses with genomes greater than 26,000 nucleotides. As a result, they possess the largest genomes of all known RNA viruses (Mousavizadeh & Ghasemi, 2020; Tokarz et al., 2015). This family includes four genera of viruses: Alphacoronaviruses, Betacoronaviruses, Gammacoronaviruess, and Deltacoronaviruses, which have been grouped primarily based on serology and phylogenic clustering (Pal et al., 2020). The Conoraviridea family has a broad host range, predominantly associated with mammals and birds, and has been implicated in human disease (Miller et al., 2021). Notably, two highly pathogenic members of this family caused the 2002 and 2013 severe acute respiratory syndrome coronavirus (SARS-CoV) and Middle East respiratory syndrome coronavirus (MERS-CoV) outbreaks in China and the Middle East, respectively. These outbreaks resulted from zoonotic spillover from intermediate hosts to humans (Gu et al., 2020; H. Li et al.,

2020; Ma & Gong, 2021). Consequently, SARS-CoV-2 marks the third coronavirus causing severe human disease through a zoonotic spillover event (Gorbalenya et al., 2020). Phylogenetic analysis indicates bats are the natural host for all three coronaviruses (Boni et al., 2020; Hu et al., 2021). However, viral adaptation within an intermediate host can facilitate transmission to humans (Gu et al., 2020; Wahl et al., 2021). While intermediate hosts for SARS-CoV (civets) and MERS-CoV (camels) have been identified (Gu et al., 2020), it remains unclear whether an intermediate host was involved in the SARS-CoV-2 pandemic, given the presence of a SARS-CoV-2 progenitor circulating in bats capable of infecting human cells (Boni et al., 2020; Wahl et al., 2021).

1.3   SARS-CoV-2 GENOME

SARS-CoV-2 is known for its relatively extensive RNA genomes that encode numerous proteins and can form elaborate structures (Bassett et al., 2022). By utilizing several viral proteases and open reading frames (ORFs) that work as templates for the production of subgenomic mRNAs, these viruses can encode upwards of 30 proteins (Mousavizadeh & Ghasemi, 2020). For instance, the SARS-CoV-2 genome encodes 29 proteins from eleven ORFs (Mousavizadeh & Ghasemi, 2020). The 5' end of the genomic RNA contains two large ORFs, ORF1a and ORF1b (V'kovski et al., 2021). These ORFs constitute two-thirds of the genome and are responsible for producing two large polypeptides that are cleaved by two viral proteases (PL^{pro} and 3CL^{pro}/M^{pro}) into 16 nonstructural proteins (Nsps) (H. Li et al., 2020; Mousavizadeh & Ghasemi, 2020). These Nsps, which include enzymes with RNA-processing, RNA-modifying, and RNA-proofreading functions, compose the viral replication and transcription complex (RTC) and are vital to maintaining the integrity of the viral genome (V'kovski et al., 2021). ORFs in the remaining one-third of the genome are dedicated to encoding four structural proteins with well-defined functions and five accessory proteins whose functions are not wholly understood but are thought to be

involved in the evasion of the host immune system (Mousavizadeh & Ghasemi, 2020; V'kovski et al., 2021). Transcription of these proteins at the 3' end of the genome results in the formation of subgenomic mRNA (sg mRNA) (V'kovski et al., 2021).

The structural proteins that are required for viral assembly and infection include the following: the spike (S) protein, which mediates viral entry into host cells; the membrane (M) and the envelope (E) proteins, which form the viral envelope; and the nucleocapsid (N) protein, which binds to the viral RNA genome (H. Li et al., 2020). The S protein is a surface glycoprotein protruding from the viral surface, as seen in Figure 1.1, and regulates coronavirus diversity and host tropism (Yuki et al., 2020). As a result, it is the principal inducer of neutralizing antibodies (Mousavizadeh & Ghasemi, 2020). This highly immunogenic viral protein consists of two functional subunits (outlined in Figure 1.2), each modulating different host-pathogen interactions. In particular, the S1 subunit contains the receptor binding domain (RBD) that interacts with the host cell receptor. Conversely, the S2 subunit containing the fusion peptide is involved in membrane fusion events (Yuki et al., 2020).

SARS-CoV and SARS-CoV-2 share a high degree of similarity in their protein sequences, with SARS-CoV-2 sharing almost 80% of its genome with SARS-CoV. For example, the M protein of SARS-CoV-2 has been shown to share 90% homology with the M protein of SARS-CoV (Thomas, 2020). Furthermore, the shared sequence homology of the RBD within the S protein of both SARS-CoV-2 and SARS-CoV indicates a significant level of genetic similarity (C. Wu et al., 2020). However, it is important to note that while most of the proteins in SARS-CoV-2 show extremely high homology (95-100%) with the proteins of SARS-CoV, two proteins, ORF8 and ORF10, in SARS-CoV-2 have no homologous proteins in SARS-CoV (Xu et al., 2020). In addition, SARS-CoV-2 exhibits notable variations within the RBD of the S protein. The SARS-

CoV-2 S protein differs from SARS-CoV by 380 amino acid substitutions, yielding mutations in five of the six vital amino acids involved in receptor binding (A. Wu et al., 2020). Since these six amino acids within the RBD are critical for receptor binding, mutations within this domain can affect virulence and host tropism (Andersen et al., 2020; Yuki et al., 2020).

Further variations within the RBD of SARS-CoV-2 arise from the insertion of four amino acids at the S1/S2 protease cleavage site, forming a polybasic furin recognition site (Andersen et al., 2020; Wrapp et al., 2020). The unique expression of a furin cleavage site enhances the pathogenicity of SARS-CoV-2 compared to SARS-CoV (Yuki et al., 2020). Moreover, the active form of the S protein from SARS-CoV-2 has been found to have a significantly lower free energy than the active form of the S protein from SARS-CoV, suggesting that SARS-CoV-2 is more stable and may survive at higher temperatures than SARS-CoV (Govind Kumar et al., 2022; He et al., 2020). While both viruses utilize the same receptor, angiotensin converting enzyme 2 (ACE2), for host cell entry (Markus Hoffmann et al., 2020; H. Li et al., 2020), ACE2 has a 10-20-fold higher binding affinity towards the S protein of SARS-CoV-2, which may explain why this virus is more transmissible than SARS-CoV (Wrapp et al., 2020). These findings collectively suggest a substantial genetic homology between SARS-CoV and SARS-CoV-2, with some variations in specific proteins. Additional comparisons reveal significant genome homology between SARS-CoV-2 and a coronavirus isolated from bats in Yunnan province, China, with specific genes sharing more than 96% of their identity with SARS-CoV-2 (L. Li et al., 2021). Based on these sequence similarities, bats are speculated to be the host reservoir for the SARS-CoV-2 precursor (Andersen et al., 2020).

1.4   SARS-CoV-2 VIRION

The SARS-CoV-2 virion, as seen in Figure 1.1, comprises the + sense single-stranded RNA genome and four structural proteins. The N protein encapsulates the +sense single-stranded RNA, creating the helical capsid structure of the virion. The viral envelope contains a lipid bilayer that anchors the E, M, and S proteins. The E protein mediates budding and release of viral progeny (Mandala et al., 2020). The M and E proteins ensure the incorporation of the RNA genome in the particles during viral assembly. Both proteins play important roles in immune evasion (Jackson et al., 2022; Samavati & Uhal, 2020). The S protein is a type I glycoprotein that forms peplomers on the virion surface, giving the virion its crown-like appearance (Jackson et al., 2022).
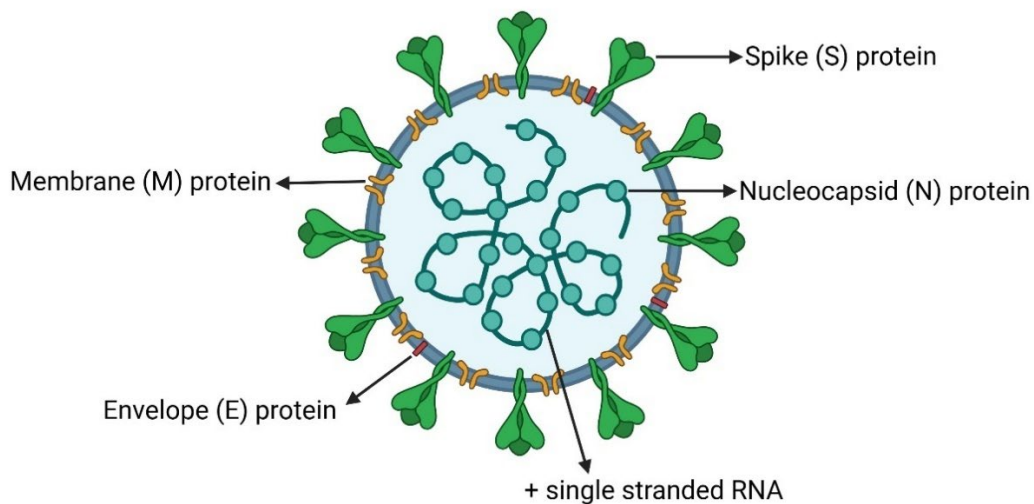
Figure 1.1: The SARS-CoV-2 virion. The virion consists of the RNA genome and four structural proteins. The N protein forms a helical structure around the positive sense single-stranded RNA. The M and E proteins are embedded within the viral membrane, and multiple copies of the S protein protrude from the viral surface. This figure was created using BioRender software.
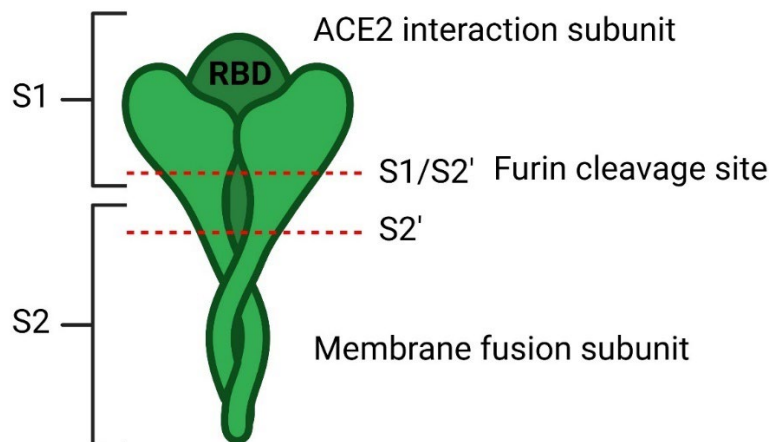
Figure 1.2: SARS-CoV-2 S protein subunits. The S protein comprises of two noncovalently linked subunits separated by two cleavage sites: the S1/S2, or furin cleavage site, and the S2 cleavage site. The S1 subunit contains the RBD and interacts with the host ACE2 cellular receptor. The S2 subunit contains a fusion peptide that mediates viral-host membrane fusion. This figure was created using BioRender software.

1.5 SARS-CoV-2 ENTRY

The primary route of SARS-CoV-2 transmission is person-to-person via respiratory droplets. However, other routes of transmission include aerosol transmission and contact with surfaces, items, and food contaminated by infectious respiratory droplets (Ong et al., 2020; Pitol & Julian, 2021; Setti et al., 2020). The entry of SARS-CoV-2 into host cells is an essential step for viral tropism and pathogenesis (Amraei et al., 2022). SARS-CoV-2 predominantly infects lung epithelium cells but is also detected in other epithelial tissues as it disseminates throughout the host (Koch et al., 2021).

To initiate viral replication, RNA viruses must release their genome into the cytosol of host cells (Salonen et al., 2005), and to gain access to the cytosol, enveloped viruses must fuse with the cell membrane (Koch et al., 2021). During SARS-CoV-2 entry (outlined in Figure 1.3), membrane fusion is achieved by proteolytically activating the S protein, performed by host-encoded proteases (Markus Hoffmann et al., 2020; Peacock et al., 2021). Several proteases, including furin, the

6

transmembrane serine protease 2 (TMPRSS2), and cathepsin L, have been proposed to prime and activate the S protein (Gomes et al., 2020; Koch et al., 2021).

For proper activation, the S protein undergoes sequential cleavage at the S1/S2 and S2 cleavage sites (Markus Hoffmann et al., 2020; Peacock et al., 2021). This process begins in the infected cell during virion biosynthesis. It involves the cleavage of the S protein at the S1/S2 site, also called the furin cleavage site, by furin within the Golgi apparatus (Jackson et al., 2022; Peacock et al., 2021). As a result, the S protein on mature virions consists of the non-covalently linked S1 and S2 subunits (Jackson et al., 2022). Moreover, cleavage of the S1/S2 site allows for further processing of the S protein by revealing the S2 cleavage site responsible for mediating viral-host membrane fusion (Markus Hoffmann et al., 2020; Jackson et al., 2022; Peacock et al., 2021).

SARS-CoV-2 entry is initiated by the interaction between the RBD within the S1 subunit of the S protein and the ACE2 cellular receptor expressed on the surface epithelial cells. This interaction mediates viral attachment to the host cell's surface, enabling proteolytic processing of the S protein that triggers membrane fusion and the subsequent release of the viral genome into the cytosol (Markus Hoffmann et al., 2020; Peacock et al., 2021). SARS-CoV-2 virions can release their genetic material into the cytosol by fusing their envelope with the cell membrane or through receptor-mediated endocytosis (Gomes et al., 2020). Differential expression of ACE2, TMPRSS2, and cathepsin L proteins within epithelial cells influences the entry route employed by the virus.

At the cell surface, RBD-ACE2 binding exposes the S2 cleavage site, which is cleaved by TMPRSS2, releasing the fusion peptide and initiating viral envelope fusion with the plasma membrane (Jackson et al., 2022). S protein priming and activation at the plasma membrane leads to the rapid cytosolic release of the viral genome in an acid-independent manner. In contrast,

during receptor-mediated endocytosis, RBD-ACE2 binding mediates endocytosis of the virion, and S protein proteolysis is completed in the endolysosomal compartment by the lysosomal protease, cathepsin L. Priming and activating the S protein in this manner results in a slow acid-mediated release of the viral RNA into the cytosol (Koch et al., 2021).
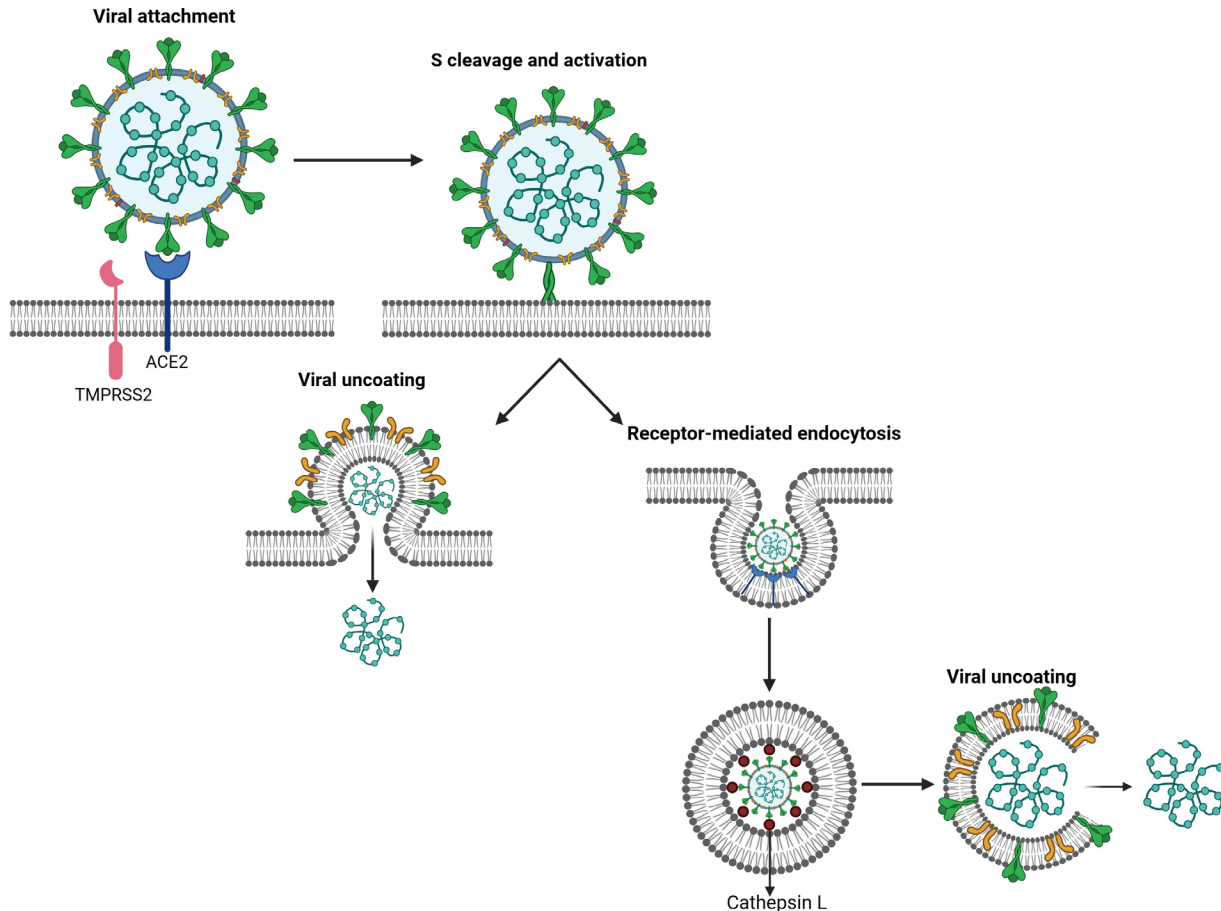
Figure 1.3: SARS-CoV-2 viral entry. Viral attachment is mediated by the proteolytic cleavage of the viral S protein. It is first cleaved at the S1/S2, or furin, cleavage site in the ER of the host cells during virion assembly. This cleavage facilitates the interaction between the RBD within the S1 subunit of the S protein and the host cell receptor ACE2. At this point, the virus can utilize two independent pathways to reach the cytosol of the host cell. One pathway involves the use of TMPRSS2. In this process, sequential cleavage of the of S protein at the S2 site reveals the fusion peptide, enabling host-viral membrane fusion. As a result, the viral genome is released into the cytosol in a rapid, acid-independent manner – the other pathway uptake of the virion via receptor-mediate endocytosis. Within the endosome, the S protein is proteolytically activated by CTSL, and the viral genome is released into the cytosol in a slow, acid-dependent manner. This figure was created using BioRender software.

1.6 ACE2

Aside from its role as the principal receptor for SARS-CoV-2 attachment and entry, ACE2 is a modulator of the renin-aldosterone system (RAS) and an amino acid transporter (Gheblawi et al., 2020). As a regulator of the RAS, ACE2 acts as a carboxypeptidase, converting angiotensin I (Ang) and Ang II into Ang 1-9 and Ang 1-7, respectively, to control blood pressure, hypertension, and fluid balance (Gheblawi et al., 2020; Turner, 2015). Consequently, ACE2 plays a crucial role in heart failure, systemic and pulmonary hypertension, lung disease, myocardial infarction, and diabetes mellitus (Gheblawi et al., 2020). The ACE2 system is a protective pathway against human diseases, including Alzheimer's, as both ACE and ACE2 have been shown to hydrolyze the amyloid-β peptide, inhibiting its aggregation (Hu et al., 2001; Turner, 2015).

ACE2 is widely expressed in various tissues, including the heart, kidney, upper respiratory tract, lungs, gastrointestinal tract, and liver (Gheblawi et al., 2020). In humans, ACE2 is abundantly expressed on the surface of alveolar (Type II) epithelial cells within the lungs and enterocytes of the intestines (Hamming et al., 2004), giving rise to the specific tissue tropism seen in SARS-CoV-2-infected individuals. ACE2 is a type I transmembrane protein with an extracellular N-terminal domain and a C-terminal cytosolic tail. The heavily glycosylated N-terminal domain contains the protease domain that interacts with the RBD of the S protein during viral entry (Gheblawi et al., 2020; Xiao et al., 2020), and the C-terminal domain is referred to as the Collectrin-like domain. The ACE2 protein exists in two forms: a cellular and a soluble form. Cellular ACE2 represents the full-length protein containing the transmembrane structure anchoring it to the membrane, while the soluble form lacks this anchor and circulates in the blood. Circulating ACE2 is cleaved from cellular ACE2 and released into the extracellular matrix by metalloprotease ADAM17 (Xiao et al., 2020).

1.7   TMPRSS2

TMPRSS2 is a transmembrane serine protease that belongs to the type II transmembrane serine protease (TTSP) family and falls under the hepsin/TMPRSS2 subfamily. The characteristic features of the TTSPs are (1) an N-terminal signal anchor domain, (2) a C-terminal trypsin-like serine protease domain, and (3) a stem region containing 1 of 6 different types of protein domains. TMPRSS2 is further classified by the presence of a class A receptor domain and a group A scavenger receptor domain in the hepsin/TMPRSS2 subfamily (Bugge et al., 2009). This protease family is co-expressed with ACE2 (Wruck & Adjaye, 2020), with TMPRSS2 colocalizing with the receptor at the cell membrane (Fraser et al., 2022). Because TMPRSS2 is an important priming enzyme in SARS-CoV-2 infection relevant to viral-host membrane fusion (Rossi Á et al., 2021), its expression dictates the route of entry the virus uses to infect cells (Koch et al., 2021). In the presence of TMPRSS2, the S protein is proteolytically cleaved and activated at the plasma membrane, resulting in a rapid uptake of the virus in a pH-independent manner. Conversely, when TMPRSS2 is absent, the virus is endocytosed in a slow acid-activated pathway that involves cathepsin L proteolytic cleavage of endolysosomes (Koch et al., 2021). Other viruses that rely on TMPRSS2 for proteolytic cleavage and activation of viral envelope glycoproteins include influenza and other human coronaviruses, such as MERS-CoV and SARS-CoV (Meyer et al., 2013; Zmora et al., 2018).

TMPRSS2 is mainly expressed in the lungs, salivary glands, gastrointestinal tract, kidneys, and liver, with the lungs and intestines having the highest levels of expression (Cao et al., 2021), further promoting SARS-CoV-2 tissue tropism of the lungs and intestines. It is also expressed at elevated levels in many male-specific tissues, such as the seminal vesicle, epididymis, and prostate, relative to female-specific tissues, including the breasts, ovaries, and endometrium (42).

Additionally, androgenic hormones play a role in regulating TMPRSS2 expression (Lin et al., 1999), and studies have shown a significant positive correlation between the androgen receptor gene and TMPRSS2 in SARS-CoV-2-infected tissues (Cao et al., 2021). This sex-specific expression and co-expression profile may suggest a role for TMPRSS2 tissue distribution in the higher SARS-CoV-2 infection rate and disease severity in men (Tian & Zhou, 2021).

1.8 CATHEPSIN L

Cathepsins are the most abundant lysosomal proteases found in endolysosomal compartments, where they play a role in diverse physiological functions, including intracellular protein degradation, energy metabolism, and immune responses (Yadati et al., 2020). Cathepsin L (CTSL) is a cysteine protease whose primary function is proteolysis of protein antigens generated by pathogen endocytosis. CTSL is recognized as both a lysosomal and a secreted protease. Lysosomal CTSL cleaves and activates the S protein following endocytosis of SARS-CoV-2, promoting membrane fusion and the subsequent release of the viral genome into the cytosol (Gomes et al., 2020). The significance of this entry mechanism was demonstrated by an *in vitro* study revealing a 76% reduction in SARS-CoV-2 infection after CTSL inhibition (Ou et al., 2020).

Similarly, overexpression of CTSL enhances pseudovirus infection in human cells. Variations in CTSL levels throughout infection indicate a significant association between CTSL and SARS-CoV-2 *in vivo*. Researchers detected elevated CTSL levels in the plasma of SARS-CoV-2-infected patients following the early onset of symptoms, but at 28 days post-infection (dpi), these levels had dramatically decreased. Additionally, since SARS-CoV-2 infection has been shown to promote CTSL expression, which enhances viral infection, CTSL expression has been associated with disease severity (Zhao et al., 2021).

1.9   FURIN

Furin is a calcium-dependent serine endoprotease belonging to the proprotein convertase family that has been extensively studied due to its involvement in various physiological and pathological processes (Koch et al., 2021; Nakayama, 1997). It is widely expressed in many tissues and plays a critical role in processing a wide range of precursor proteins, including growth factors, receptors, extracellular matrix proteins, and pathogenic agents (Koch et al., 2021; Nakayama, 1997). Since furin proteolytically activates a variety of mammalian, bacterial, and viral substrates, it has been implicated in various health conditions ranging from cancer to infectious and viral diseases, including SARS-CoV-2 (Braun & Sauter, 2019; Gomes et al., 2020). The membrane-bound form of furin is localized on the Golgi apparatus, acting as the central processing enzyme of the secretory pathway (Vidricaire et al., 1993) and proteolytically actives the S protein of SARS-CoV-2 (Jackson et al., 2022). Posttranslational modifications to the membrane-bound form of furin produce a soluble form of the enzyme that can be secreted and act on substrates in the extracellular matrix (Vidricaire et al., 1993; Zhang et al., 2022).

Furin proteolytically activates the glycoproteins expressed by various viral envelopes and, as a result, enhances viral fusion to host cell membranes. The presence of a furin cleavage site increases the pathogenicity of certain viruses, including influenza and SARS-CoV-2 (Gomes et al., 2020). The SARS-CoV-2 furin cleavage site refers to a polybasic insertion of five amino acids (proline, arginine, arginine, alanine, and arginine) that can be cleaved by furin. This site, which is absent in SARS-CoV, is located at the boundary between the S1 and S2 subunits of the S protein and improves the efficiency of S protein priming for viral-host membrane fusion. As a result, its presence has been associated with increased virulence, disease severity, and transmissibility of SARS-CoV-2 (Peacock et al., 2021).

1.10   SARS-CoV-2 REPLICATION

Once the viral genomic RNA is released into the cytosol of the infected cell, the virus hijacks the host cell machinery to replicate its genome. Viral replication (outlined in Figure 1.4) begins with the translation of ORF1a and ORF1b by host ribosomes, producing two viral replicase polyproteins, pp1a and pp1b (Yang & Rao, 2021). Co-translational and post-translation processing of these polyproteins by two cysteine proteases located within the Nsp3 (PL^pro) and Nsp5 (3CL^pro/M^pro) induces the production of sixteen individual Nsps. Nsp2-16 are targeted to the endoplasmic reticulum, where they remodel intracellular membranes to form viral replication organelles (Jackson et al., 2022; V'kovski et al., 2021). These organelles provide a secluded environment for viral RNA synthesis carried out by the Nsp12 RNA-dependent RNA polymerase (RdRP) and its two cofactors, Nsp7 and Nsp8. Nsp12 is assisted by Nsp14, which provides RNA proofreading through 3'-5' exonuclease activity (Gao et al., 2020; Jackson et al., 2022). Viral RNA capping is executed by Nsp10, which acts as a cofactor; Nsp13, which provides the RNA 5'-triphosphatase activity; Nsp14, which functions as the N7-methyltransferase; and Nsp16, which supplies the 2'-O-methyltransferase activity (Chen et al., 2009; Chen et al., 2011; V'kovski et al., 2021).

During SARS-CoV-2 replication, newly synthesized full-length negative-sense genomes are either used as templates for generating new positive-sense genomes, translated into more Nsps and RTCs, or packaged into newly forming virions (Jackson et al., 2022). Notably, when the coronavirus RTC encounters a transcription regulatory sequence (TRS) on the negative-sense template, it stops transcription and re-initiates the process at the TRS sequence located at the 5' end of the genome. This discontinuous step in RNA synthesis produces a set of negative-sense sgRNA that serve as templates for positive-sense sg mRNA, which are then translated into

structural and accessory proteins (Jackson et al., 2022; Sawicki & Sawicki, 1995; Sola et al., 2015). Once translation is complete, virion assembly begins in the endoplasmic reticulum-Golgi intermediate compartment (ERGIC) (Yang & Rao, 2021). During virion biosynthesis, structural proteins play various roles in viral assembly, ranging from genome packaging to virion budding (V'kovski et al., 2021). Following virion maturation, they exit the infected cell via exocytosis to initiate another round of infection (Yang & Rao, 2021).
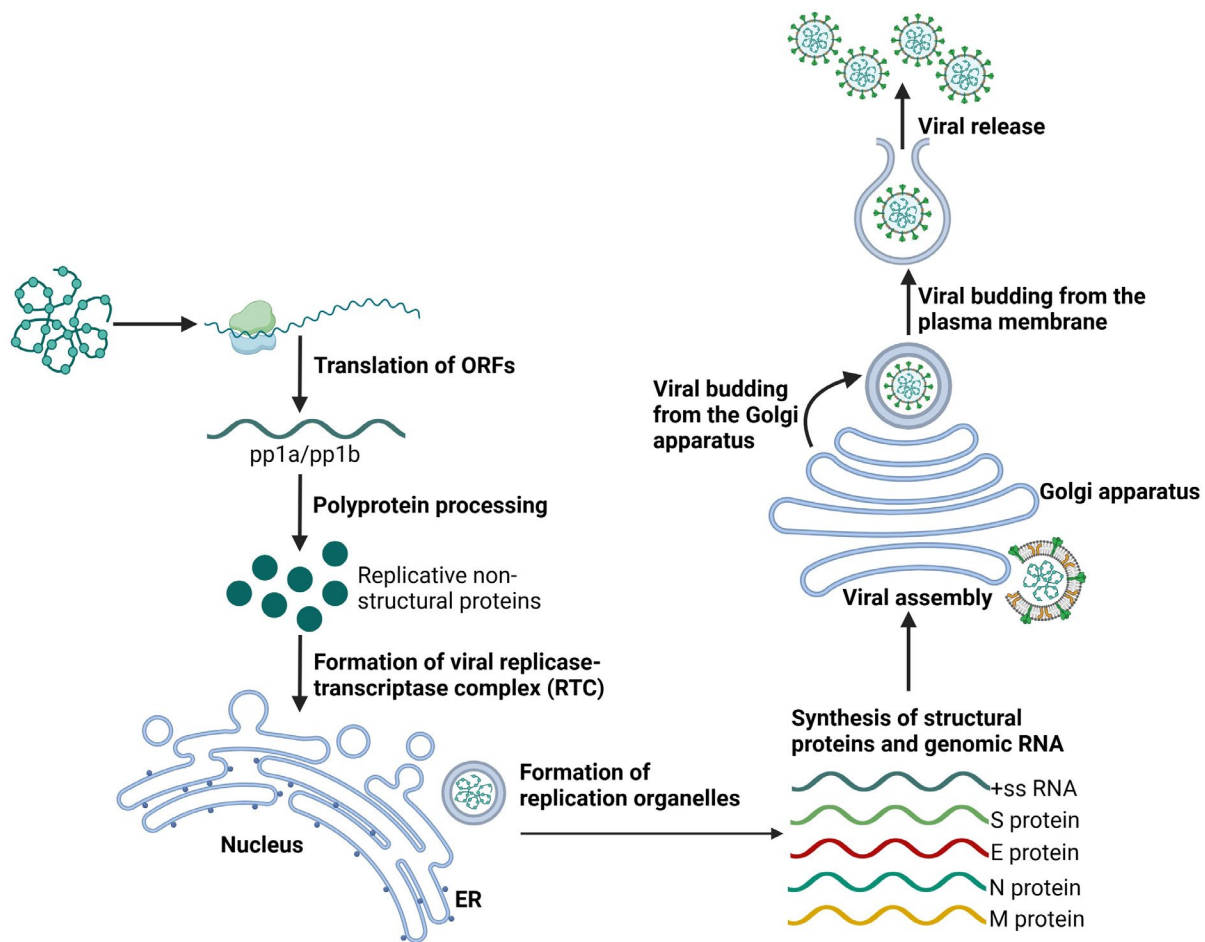
Figure 1.4: SARS-CoV-2 viral replication. Inside the host cytosol, translation of the viral genome results in the production of two polyproteins, pp1a and pp1b. Viral proteases process these polyproteins to produce the Nsps, which are targeted to the ER, where they form replication organelles. Within these organelles, viral structural proteins and genomic RNA are synthesized. They are then translocated to the ER-Golgi intermediate compartment, where virus biosynthesis and maturation occur. Virions are released from the cell via exocytosis. This figure was created using BioRender software.

1.11   HOST IMMUNE RESPONSE TO SARS-CoV-2

1.11.1 Symptoms of SARS-CoV-2 infection

SARS-CoV-2 mainly causes upper and lower respiratory tract infections, frequently accompanied by symptoms such as fever, cough, and shortness of breath (Dixon et al., 2020; Lovato & Filippis, 2020). However, SARS-CoV-2 infection can affect various body systems, including the cardiovascular, gastrointestinal, and nervous systems (Lovato & Filippis, 2020; Schmithausen et al., 2020). While most SARS-CoV-2 infections remain mild, with up to 20-40% of patients being asymptomatic (Boyton & Altmann, 2021), some patients develop acute respiratory distress syndrome (ARDS) or cytokine storm, which are marked by systemic inflammation and tissue damage and can be fatal. Other SARS-CoV-2-associated lung injuries, such as pulmonary edema and hypoxemia, have been reported in hospitalized patients. In other instances, infected patients have experienced cardiac complications, including hypertension, cardiomyopathy, and cardiogenic shock (Esakandari et al., 2020). Within the gastrointestinal tract, SARS-CoV-2 infection induces symptoms such as nausea, vomiting, diarrhea, and hemorrhage (Corso et al., 2022). A broad range of symptoms, including confusion, delirium, dizziness, encephalopathy, anosmia, seizure, and stroke, have been associated with the effects of SARS-CoV-2 infection on the nervous system (Esakandari et al., 2020; Süzgün et al., 2023). Risk factors for increased disease pathogenesis include diabetes, hypertension, obesity, and age (Zhang et al., 2023).

1.11.2 Role of the innate immune system in SARS-CoV-2 infection

The innate immune system, which acts as the first line of defense against foreign body invasion, employs several pattern recognition receptors (PRRs) that sense and respond to SARS-CoV-2 infection, as outlined in Figure 1.5 (Diamond & Kanneganti, 2022). This list includes toll-

like receptors (TLRs), retinoic acid-inducible gene-I (RIG-I)-like receptors (RLRs), and nucleotide-binding and oligomerization domain (NOD)-like receptors (NLRs), and once activated, they stimulate inflammatory pathways that promote viral clearance (Diamond & Kanneganti, 2022; Yamada & Takaoka, 2023). PRRs are expressed at various locations throughout the cell and share a similar function of recognizing pathogen-associated molecular pattern molecules (PAMPs) and damage-associated molecular pattern molecules (DAMPs) (Yamada & Takaoka, 2023). PAMPs, such as lipopeptides, lipopolysaccharides, and bacterial or viral RNA, are highly conserved pathogenic molecular structures expressed in pathogens and their products. At the same time, DAMPs represent intracellular host proteins or nucleic acids released by necrotic cells (Diamond & Kanneganti, 2022).

TLRs are localized on the cell surface or within endosome membranes and are classified as type I integral membrane glycoproteins composed of an extracellular domain and a cytoplasmic signaling domain (Mantovani et al., 2023). When stimulated, TLRs transduce signals through two key adaptor molecules, myeloid differentiation factor 88 (MyD88) or Toll/interleukin (IL)-1 receptor domain-containing adaptor inducing IFN-β (TRIF) (Diamond & Kanneganti, 2022; Yamada & Takaoka, 2023). Most TLRs utilize the MyD88 signaling pathway to induce host immune responses (Figure 1.5, pathway 1). Myd88 activation can lead to the activation of nuclear factor (NF)-κB and mitogen-activated protein kinases (MAPKs) such as p38 and ERK. Activation of the MAPKs leads to activation of activator protein-1 (AP-1). Once activated, NF-κB and AP-1 translocate to the nuclease and stimulate the production of proinflammatory cytokines and other viral mediators. TLR3, which is localized in endosomal compartments, exclusively uses the TRIF adaptor protein to activate NF-κB and interferon (IFN) regulatory factors (IRFs) with various antiviral functions (Kawasaki & Kawai, 2014; Yamada & Takaoka, 2023) (Figure 1.5, pathway

2). In contrast, TLR4, expressed on the cell surface, can activate downstream transcription factors using either adaptor protein (Kawasaki & Kawai, 2014) (Figure 1.5, pathway 2). Several TLRs, including TLR2, 3, and 4, have been associated with SARS-CoV-2 severity (Mantovani et al., 2023). To combat SARS-CoV-2 infection, TLR2 senses the viral E protein and stimulates immune signaling through the MyD88 pathway. Evidence suggests that TLR1, 4, and 6 in the plasma membrane and TLR3 in the endosomal membrane recognize the viral S protein to induce anti-SARS-CoV-2 immune responses (Diamond & Kanneganti, 2022).

RLRs, including RIG-1 and melanoma differentiation-associated gene 5 (MDA5), are intracellular sensors that recognize double and single-stranded viral RNA from various viruses (Mantovani et al., 2023; Yamada & Takaoka, 2023). Specifically, RIG-I senses single-stranded RNA with 5'-triphosphate caps and short double-stranded RNA, while MDA5 primarily recognizes long kilobase-scale double-stranded RNA (Kato et al., 2008; Yamada & Takaoka, 2023). RIG-I and MDA5 provide critical regulation of the IFN pathway and contain two caspase-recruitment domains (CARDs), a DExD/H-box helicase domain (HD), and a C-terminal domain (CTD) (Reikine et al., 2014). RNA ligand binding through the CTD domains releases the CARDs, which then interact with the mitochondrial antiviral signaling (MAVS) adaptor protein to trigger the production of type I and type III IFNs and inflammatory cytokines (Reikine et al., 2014; Yamada & Takaoka, 2023). During SARS-CoV-2 infection, RIG-I and MDA5 can sense single-stranded viral RNA derived from genomic, subgenomic, or replicative intermediates to stimulate viral countermeasures (Diamond & Kanneganti, 2022) (Figure 1.5, pathway 3).
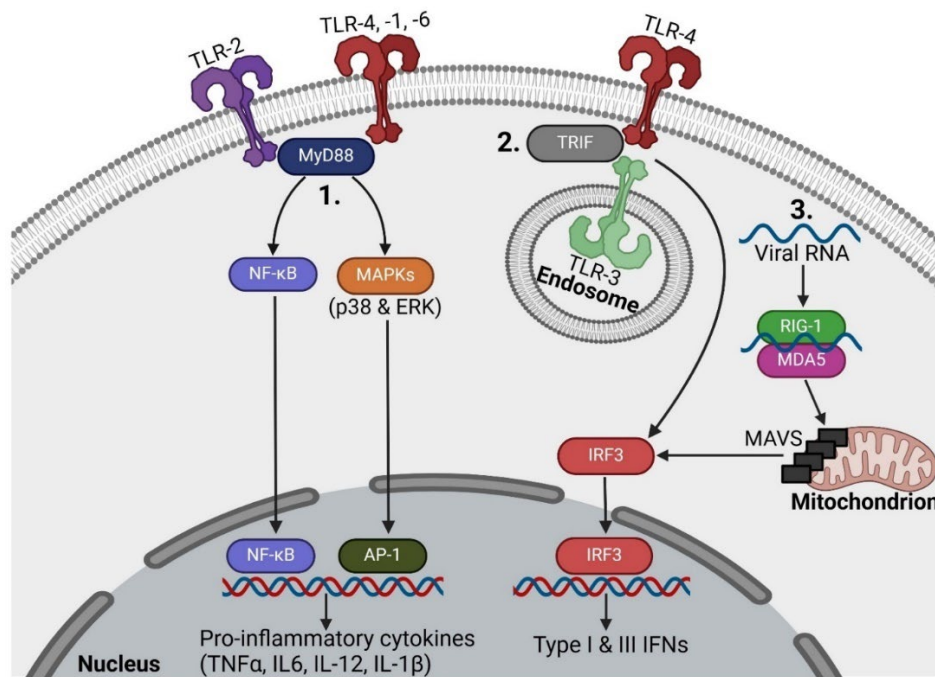
Figure 1.5: PRR signaling pathways triggered during SARS-CoV-2 infection. **1.** Activation of surface TLRs stimulates MyD88 signaling pathways, leading to the nuclear translocation of NF-κB and AP-1, where they induce the transcription of genes encoding proinflammatory cytokines and other antiviral products. **2.** Activation of TLR-3 and 4 stimulates the TRIF signaling pathway, activating IRF3 and inducing the expression of type I and III IFNs. **3.** Sensing of viral RNA by the cytosolic RLRs (RIG-I and MDA5) stimulates the formation of a MAVS signalosome and ultimately results in the transcription of type I and III IFNs and the production of ISGs with various antiviral functions. This figure was created using BioRender software.

NLRs form an extensive family of intracellular PRRs featuring a central NOD and a C-terminal domain containing leucine-rich repeats. They play a critical role in monitoring the intracellular environment for signs of infection (Yamada & Takaoka, 2023). NLRs generally recognize Gram-negative bacterial cell wall components; however, they have also been reported to respond to SARS-CoV-2, inducing the production of type I IFNs and inflammatory cytokines (Diamond & Kanneganti, 2022; Mantovani et al., 2023). One of the best-studied members of the NLR family is the NOD-like receptor protein 3 (NLRP3), which forms a multiprotein complex, or inflammasome, upon its activation (Yamada & Takaoka, 2023). NLRP3 inflammasome activation

(outlined in Figure 1.6), triggered in response to PAMPs and DAMPs and aimed at inducing inflammatory responses against infections or cellular damage, respectively, initiates a series of events that ultimately result in cell death via pyroptosis. The first event in this series is the recruitment and activation of Caspase-1, which then mediates the production of bioactive interleukin (IL)-1β and IL-18 and cleavage of Gasdermin D (GSDMD). Once activated, GSDMD forms pores in the plasma membrane, which drives membrane rupture, releases IL-1β and IL-18, and sparks pyroptotic cell death (Diamond & Kanneganti, 2022). In SARS-CoV-2 infection, NLRP3 inflammasome assembly has been associated with different PAMPs ranging from GU-rich single-stranded RNA to structural and accessory proteins (Castaño-Rodriguez et al., 2018; Diamond & Kanneganti, 2022). The structural E protein can act as a viroporin in addition to its genome-packaging role during virion formation. Viroporins are small hydrophobic multifunctional viral proteins that form hydrophilic pores in the membrane of host cells and play a critical role in virion release from host cells (Nieva et al., 2012). SARS-CoV-2 encodes two additional viroporins, the accessory proteins ORF3a and ORF8a. These proteins have ion channel activity and enhance viral replication and virulence (Castaño-Rodriguez et al., 2018; Yamada & Takaoka, 2023). Other structural proteins, including S and N, have been shown to play a role in NLRP3 inflammasome development (Diamond & Kanneganti, 2022).

Aside from PRRs, other cytosolic sensors have been known to respond to SARS-CoV-2 infection (Diamond & Kanneganti, 2022; Yamada & Takaoka, 2023). For example, cyclic GMP-AMP synthase (cGAS) is an essential cytosolic DNA sensor that interacts with the adaptor molecule, stimulator of interferon genes (STING), to induce the production of type II and III IFNs and inflammatory cytokines during viral infection (Yamada & Takaoka, 2023). In addition to exogenous DNA, the cGAS-STING pathway is also stimulated by endogenous DNA released from

damaged mitochondria. SARS-CoV-2 infection has been associated with mitochondrial damage, including membrane depolarization, dysregulated membrane permeability, and reactive oxygen species (ROS) release. Mitochondrial damage during SARS-CoV-2 infection has been linked to the localization of viral replicative intermediates in the form of double-stranded RNA to the mitochondria (Shang et al., 2021). Thus, cGAS activation can occur through the direct sensing of viral DNA or the indirect sensing of the destructive effects of viral infection (Shang et al., 2021). For this reason, cGAS can elicit antiviral activity against both DNA and RNA viruses and plays a critical role in limiting their replication (Diamond & Kanneganti, 2022; Shang et al., 2021).
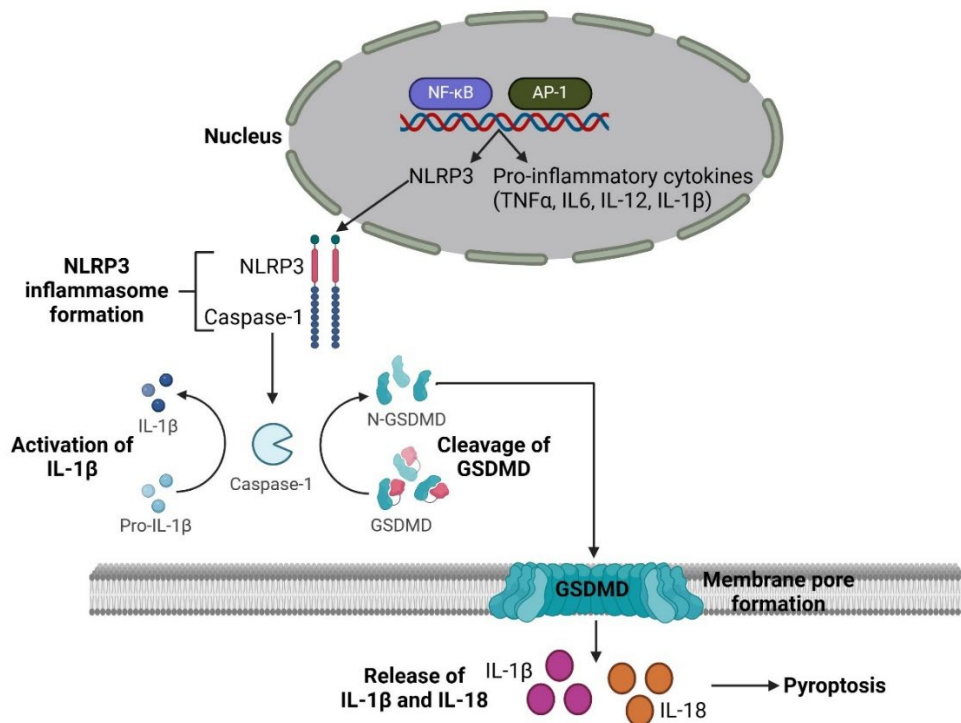
Figure 1.6: NLRP3 inflammasome formation during SARS-CoV-2 infection. Within the nucleus, NF-κB and AP-1 induce the transcription of NLRP3, which interacts with various cellular molecules, including Caspase-1, to form a multiprotein complex or inflammasome. Caspase-1 proteolytically activates IL-1β and GSDMD. Once activated, GSDMD forms pores in the plasma membrane, leading to the release of IL-1β and IL-18 and cell death via pyroptosis. This figure was created using BioRender software.

1.11.3 Role of the adaptive immune system in SARS-CoV-2 infection

Successful activation of the innate immune system propels the development of adaptive immunity (Primorac et al., 2022). As a result, the adaptive immune system plays a crucial role in controlling and clearing viral infections (Sette & Crotty, 2021). Adaptive immune responses are initiated by innate immunity and are slow to develop upon initial exposure to a new pathogen; however, once activated, they impart immunological memory, allowing the immune system to remember previously encountered pathogens and respond to them in a rapid and effective manner (B et al., 2002). For this reason, adaptive immunity is pathogen-specific and provides the basis for the development of vaccines (Sette & Crotty, 2021). The fundamental elements of the adaptive immune system are B cells and CD4+ and CD8+ T cells (Sette & Crotty, 2021).

B cells generate antibodies and an antibody-mediated memory response to invading pathogens. Following infection, secreted or membrane-bound antibodies bind to the epitopes, or small sites, within pathogenic molecules, termed antigens. This binding results in neutralization of the pathogen or phagocytosis of the pathogen by phagocytic immune cells, such as macrophages and dendritic cells. Pathogenic proteins are degraded within these antigen presenting cells (APCs), and their fragments are presented on the cell surface to T cells. This process stimulates T cell activation and propels further immune responses, making antigen presentation a critical step in pathogen-specific immune responses. B cells can also activate antigen-specific CD4 and CD8+ T cells, which elicit effector and cytotoxic effects (Rastogi et al., 2022).

CD4+ T cells can differentiate into a range of T helper (Th) cells that possess a variety of helper and effector functions that enable or enhance the activity of other immune cells (Sette & Crotty, 2021). Differentiation into the different Th subsets is induced by TCR stimulation and is regulated by environmental factors (Takeuchi & Saito, 2017). These Th subsets are characterized

by their specific cytokine products that promote various types of immune responses, including antibody production, CD8+ cytotoxic T cell (CTL) proliferation, phagocytic activity, immune cell recruitment, and inflammatory responses (Sette & Crotty, 2021; Takeuchi & Saito, 2017). Some cytokine products can also suppress inflammatory responses, facilitating tissue repair and regulating the immune microenvironment (Takeuchi & Saito, 2017). Follicular helper T (Tfh) cells provide specialized help to B cell maturation and are essential to antibody and memory B cell production (Crotty, 2014). Th1 cells stimulate inflammatory responses and immune cell recruitment by secreting IFNγ (Sette & Crotty, 2021). CD4+ CTLs are a unique Th subset with cytotoxic activity that kill target cells in an antigen-specific manner (Takeuchi & Saito, 2017). CD8+ T cells are stimulated to release cytokines and chemokines or directly lyse infected cells in response to TCR engagement by various antigens presented on the surface of APCs (Berg & Forman, 2006).

SARS-CoV-2-specific antibodies, CD4+, and CD8+ T cells are produced in response to infection (Sette & Crotty, 2021). B cell-mediated immunity is induced at the onset of SARS-CoV-2 infection. It involves the activation and maturation of naïve B cells, leading to the production of neutralizing antibodies that mainly target the N and S proteins within 7-10 dpi (Shen et al., 2023; Sosa-Hernández et al., 2020). SARS-CoV-2 neutralizing antibody titers increase with disease severity (Lau et al., 2021). However, low antibody titers in some patients suggest that the virus may trigger other adaptive immune responses (Shen et al., 2023). Anti-S neutralizing antibodies explicitly targeting the RBD are detectable up to 75 days after symptom onset (Iyer et al., 2020).

Additionally, SARS-CoV-2-specific immunoglobulin (IgG) antibody titers remain relatively robust for at least five months post-infection, significantly reducing the risk of reinfection (Shen et al., 2023). Cross-reactive immunity, resulting from exposure to similar human

coronaviruses, such as MERS-CoV and SARS-CoV, may affect SARS-CoV-2 outcomes (Shen et al., 2023). For instance, anti-S antibodies with cross-reactivity to the S protein of MERS-CoV and SARS-CoV were detected in SARS-CoV-2 naïve individuals (Hicks et al., 2021). Other SARS-CoV-2 S-reactive antibodies targeting the S2 subunit rather than the RBD and the S1 subunit have been isolated from SARS-CoV-2-unifected individuals (Ng et al., 2020). In addition, memory B cells obtained from SARS-CoV-infected individuals showed potent neutralizing activity towards SARS-CoV-2 (Shen et al., 2023). Not surprisingly, memory B cells are positively associated with increased clinical outcomes in hospitalized SARS-CoV-2 patients and are detectable for at least three months after recovery (Rodda et al., 2021; Zhu et al., 2022).

CD4+ T cell responses to SARS-CoV-2 are more prominent than CD8+ T cell responses and can be detected as early as 2 to 4 days post symptom onset. Compared to CD8+ T cells and antibodies, SARS-CoV-2-specific CD4+ T cells have the strongest association with disease outcome (Sette & Crotty, 2021). Rapid induction of CD4+ T cells during SARS-CoV-2 infection is linked to mild disease and accelerated viral clearance, while delayed production of SARS-CoV-2-specific CD4+ T cells is correlated with severe or fatal disease (Tan et al., 2021). SARS-CoV-2-specific CD4+ T cells are prominently produced in response to the S, M, and N proteins but also to ORF3a and Nsp3. The magnitude of CD4+ T cell responses to these specific proteins corresponds to their level of expression (Grifoni et al., 2020). SARS-CoV-2-specific CD4+ T cells generally differentiate into Th1 and Tfh cells. IFNγ production by Th1 cells during SARS-CoV-2 infection is associated with decreased disease severity.

Similarly, SARS-CoV-2-specific Tfh cells, which are required for the development of anti-S antibodies, correspond to reduced disease severity (Rydyznski Moderbacher et al., 2020). Although SARS-CoV-2-specific CD8+ T cells have been associated with immune protection,

circulating levels of these cells in infected individuals are less common than CD4+ T cells (Grifoni et al., 2020; Rydyznski Moderbacher et al., 2020). CD8+ T cells specific for S, N, M, and ORF3a have been reported as early as one day post symptom onset (Sette & Crotty, 2021). During infection, SARS-CoV-2-specific CD8+ T cells express high levels of cytotoxic molecules, including IFNγ, granzyme B, and perforin. IFNγ stimulates inflammatory responses and the recruitment of immune cells, while granzyme B and perforin kill target cells (Rydyznski Moderbacher et al., 2020).

1.11.4 Immune dysfunction during SARS-CoV-2 infection

Although host inflammatory immune responses are intended to promote viral clearance, they can have detrimental effects on the host. For example, dysfunctional immune responses can lead to excessive inflammation, acute lung injury, and organ failure (Zhu et al., 2022). Expression profiles of SARS-CoV-2-infected patients reveal elevated levels of inflammatory cytokines, including IFNγ, IL-1β, tumor necrosis factor (TNF), and IL-6 (Rabaan et al., 2021). Properly regulated expression of these pro-inflammatory cytokines facilitates viral clearing; however, dysregulated secretion of these cytokines is positively associated with disease severity as they contribute to cytokine storm production, a life-threatening condition that mediates inflammatory cell death, or PANoptosis (Karki & Kanneganti, 2022). This inflammatory programmed cell death pathway is regulated by the PANoptosome complex composed of caspases, inflammasome components, and RHIM domain-containing proteins (Samir et al., 2020). In SARS-CoV-2 infection, IFNγ and TNF signal cooperatively to transduce downstream signaling through STAT1 (signal transducer and activator of transcription-1) and IRF1, leading to the activation of caspases within the PANoptosome and subsequent cell death (Karki et al., 2021). Because PANoptosis is accompanied by the release of inflammatory cytokines such as IL-1β and IL-18, there is a positive-

feedback loop in which cytokine secretion causes PANoptosis that results in more cytokine release, culminating in a cytokine storm that causes life-threatening tissue and organ damage (Karki & Kanneganti, 2022; Karki et al., 2021).

1.12   SARS-CoV-2 IMMUNE EVASION

Several SARS-CoV-2-encoded proteins disrupt host immune responses during infection (Rashid et al., 2022). These proteins employ various strategies, such as inhibiting host recognition and IFN production and signaling pathways, to evade antiviral responses (Kim & Shin, 2021). Numerous viral proteins play a role in blocking PAMP recognition by host sensors, which interrupts downstream signaling pathways activated by these sensors (Minkoff & tenOever, 2023). For example, the intracellular viral RNA sensors, RIG-I and MDA5, are targets for several structural and accessory proteins. The papin-like protease (PLpro) domain in Nsp3, which is essential for the production of viral Nsps, inhibits MDA5 activation, thereby blocking the IFN signaling pathway and the subsequent production of type I and III IFNs (G. Liu et al., 2021). Similarly, Nsp5 utilizes two mechanisms to inhibit the RIG-I signaling pathway. Through its protease activity, Nsp5 cleaves the N-terminal domain of RIG-1, preventing MAVS activation. Additionally, Nsp5 promotes ubiquitination and degradation of MAVS, solidifying the disruption of this signaling pathway and deterring the production of antiviral IFNs (Y. Liu et al., 2021). Other viral proteins that interfere with the RIG-I and MDA5 signaling pathway include ORF7b, ORF9b, the N protein, and the M protein. In this context, these viral proteins mediate the suppression of IFNβ production (K. Chen et al., 2020; Shemesh et al., 2021). To mediate IFNβ repression, the N protein binds to the DexD/H box helicase of RIG-I and blocks its interaction with TRIM25. In contrast, the M protein antagonizes MAVS activation by impairing its ability to recruit signaling adaptors (Fu et al., 2021; Gori Savellini et al., 2021).

Many SARS-CoV-2 proteins target distinct steps in type I IFN production and signaling to evade type I-mediated immune responses (Minkoff & tenOever, 2023; Xia et al., 2020). Nsp6 and Nsp13 are involved in suppressing type I IFN production by blocking the phosphorylation of IRF3 and TBK1, respectively (Xia et al., 2020). Type I IFN signaling suppression is mediated by the inhibition of STAT1 and STAT2 phosphorylation and their nuclear translocation (Minkoff & tenOever, 2023). STAT1 phosphorylation is inhibited by Nsp1, ORF3a, and the M protein, while STAT2 phosphorylation is uniquely inhibited by ORF7a. Nsp6, Nsp13, and ORF7b prevent the phosphorylation of both STAT1 and STAT2, and ORF6 inhibits STAT1 nuclear translocation (Xia et al., 2020). Additionally, the viral S protein antagonizes type I IFN signaling by inducing proteasomal degradation of IRF3 and preventing STAT1-Janus kinase (JAK)1 interactions (Freitas et al., 2021; Zhang et al., 2021). Given that reduced IFN levels are a significant determinant of disease severity, targeting this pathway is an effective strategy for SARS-CoV-2 propagation (Kim & Shin, 2021).

Other SARS-CoV-2 proteins ensure that viral translation occurs and is not detected by the host cell. For example, Nsp1 ensures viral protein production by promoting the degradation of cellular mRNA lacking a 5' viral sequence (Finkel et al., 2021). Additionally, Nsp10, 12, 13, 14, and 16 add a 5' cap to nascent viral RNA before translation. The resulting viral transcripts mimic host transcripts, preventing their detection. The capping process begins with the removal of the phosphate and transfer of a guanosine monophosphate to the 5' end of the viral RNA by Nsp13 and Nsp12, respectively, and is finalized by Nsp14 and Nsp16 with the help of Nsp10 (Minkoff & tenOever, 2023). Likewise, Nsp15 and the N protein mask cytosolic viral RNAs by cleaving 5'-polyuridienes from negative-sense viral RNAs and destabilizing dsRNA, respectively (Caruso Í et al., 2021; Frazier et al., 2021).

SARS-CoV-2 also employs tactics and proteins to mask viral replication within host cells. For instance, during viral replication, immunogenic negative-sense and double-stranded RNA intermediates are sequestered inside replication organelles to minimize host detection (Caruso Í et al., 2021; Frazier et al., 2021).

1.13   SARS-CoV-2 VARIANTS

Mutations within the SARS-CoV-2 genome give rise to different SARS-CoV-2 variants. These mutations are commonly found within but are not limited to the highly variable S protein. Within the S protein, a large portion of mutations are observed in the RBD (Perez-Gomez, 2021). Given that this region interacts with the ACE2 receptor on host cells, mutations within this region are involved in tissue and species tropism, thereby playing an essential role in zoonotic spillover (Dhama et al., 2020). The list of current SARS-CoV-2 variants ranges from Alpha to Omega and beyond and continues to increase. The SARS-CoV-2 Interagency Group (SIG), established by the US Department of Health and Human Services (HHS), characterizes emerging variants into four classes based on their disease severity, transmissibility, and impact on medical countermeasures. These classes are as follows: variants being monitored (VBM), variants of interest (VOI), variants of concern (VOC), and variants of high consequence (VOHC). VBM are variants that do not pose a significant or imminent risk to public health. VOIs possess genetic markers that enhance transmission and immune escape while negatively impacting diagnostic and therapeutic interventions. Variants associated with increased morbidity and mortality coupled with reduced treatment, vaccine, and diagnostic testing effectiveness are classified as VOC, and variants that cause even worse disease outcomes based on their reduced susceptibility to medical intervention are classified as VOHC ((CDC), 2023; Thakur et al., 2022). Currently, Omicron (B.1.1.529) is the only variant classified as a VOC; variants containing the F456L S protein mutation, which have

not yet been labeled by the World Health Organization (WHO), are classified as VOI, and the remaining variants are classified as VBM ((CDC), 2023).

1.13.1 S protein mutations within the variants

Mutations within the S protein not only contribute to tropism but also to viral transmission and virulence. Considering the immunogenic nature of the S1 subunit, frequent mutations in this region, especially the RBD and N terminal domain (NTD), can reduce antibody neutralization and vaccine efficacy, leading to viral adaptation that directs immune escape. Several substitution mutations have been identified within the RBD that enhance viral infectivity and transmissibility (Thakur et al., 2022). For instance, D614G is a highly prevalent substitution within the RBD that increases S protein expression on the virion surface, thus enhancing viral infectivity (Zhang et al., 2020). Similarly, the N501Y substitution within the RBD enhances the affinity of the S protein for the ACE2 receptor, thereby enhancing both viral infectivity and transmissibility (Liu et al., 2022). Other prevalent RBD substitutions, such as D364Y and E484K, have been identified in variants with higher transmission rates (Barton et al., 2021; Thakur et al., 2022). The D364Y substitution enhances the structural stability of the S protein, resulting in increased receptor affinity and SARS-CoV-2 infectivity (J. Chen et al., 2020). In contrast, the E484K substitution impairs neutralization antibody activity and has been associated with reinfections and reduced vaccine effectiveness.

Apart from the RBD, various mutations have been identified within the N terminal domain (NTD) of the S protein. Most of these mutations result in the deletion of regions within the NTD, which culminates in the elimination of epitopes and facilitates immune evasion (Harvey et al., 2021).

1.14   SARS-CoV-2 TREATMENTS

The current list of SARS-CoV-2 treatments includes Paxlovid, remdesivir, immune modulators, and monoclonal antibodies. Administration of these treatments depends on the severity of the infection. Paxlovid, a combination of nirmatrelvir and ritonavir, is prescribed to patients 12 years and older with mild or moderate SARS-CoV-2 (Drożdżal et al., 2021). Remdesivir is a broad-spectrum antiviral that targets the viral RNA-dependent RNA polymerase (RdRp) and inhibits RNA synthesis and viral replication (Lin et al., 2021). It has been shown to improve clinical outcomes of hospitalized patients (Drożdżal et al., 2021). Baricitinib and tocilizumab are immune modulators that inhibit JAK1 and IL-6, respectively and have been used in tandem with systemic administration of steroids to control hyperinflammatory responses in hospitalized SARS-CoV-2 patients (Masiá et al., 2021). Monoclonal antibody cocktails that neutralize the viral S protein, such as casirivimab/imdevimab and bamlanivimab/etesevimab, have been used to treat hospitalized pediatric and adult patients (Falcone et al., 2021). Additionally, canakinumab is an anti-IL-1β antibody that has been shown to enhance clinical outcomes in hospitalized patients by reducing SARS-CoV-2 pneumonia-related symptoms, including the need for ventilator assistance (Generali et al., 2021).

1.15   SARS-CoV-2 POTENTIAL DRUG TARGETS

Given the importance of its protease activity during SARS-CoV-2 entry, TMPRSS2 has been identified as a potential drug target. Protease inhibitors and androgen blockers have been used to investigate the impact of direct and indirect TMPRSS2 inhibition on SARS-CoV-2 infection. The androgen receptor antagonist, enzalutamide, was ineffective in limiting SARS-CoV-2 infection in human airway cells (Guo et al., 2022). In contrast, inhibition of TMPRSS2 by the serine protease inhibitor, camostat mesylate, blocks SARS-CoV-2 entry and is detrimental to

viral replication (Guo et al., 2022; M. Hoffmann et al., 2020). Camostat mesylate is an orally available drug approved for the treatment of pancreatitis in Japan (M. Hoffmann et al., 2020). While *in vivo* studies show the potential of camostat mesylate to be repurposed as a SARS-CoV-2 drug, the results from clinical trials show otherwise. Camostat mesylate treatment failed to reduce the viral loads within the upper airways of patients with mild to moderate SARS-CoV-2 and, therefore, ineffective as a SARS-CoV-2 antiviral (Kinoshita et al., 2022; Tobback et al., 2022).

Although camostat mesylate inhibits TMPRSS2-mediated viral entry, it does not block viral entry via the endosome (Peacock et al., 2021). For this reason, inhibitors of the CTSL have also been investigated for their SARS-CoV-2 antiviral potential. Amantadine is a prophylactic agent approved for the treatment of influenza and Parkinson's disease and has been reported to suppress CTSL transcription. Consequently, researchers have recently tested its ability to prevent SARS-CoV-2 infection. Amantadine was shown to inhibit SARS-CoV-2 pseudovirus infection in both human cells and humanized mice (Zhao et al., 2021). However, a clinical trial with 121 participants concluded that amantadine did not affect the progression of SARS-CoV-2 disease (Weis et al., 2023). Another study has demonstrated the potential of using CRISPR technology to treat SARS-CoV-2 infection. In this study, the researchers developed a CasRX-based nanosystem targeting lung CTSL mRNA and observed reduced viral burden, cytokine levels, and lesions in the lungs of SARS-CoV-2-infected transgenic mice (Cui et al., 2022).

Since SARS-CoV-2 can utilize two independent pathways to access host cells, blocking one pathway may not prevent viral entry, as seen by camostat mesylate and amantadine clinical trials. As a result, researchers have hypothesized that simultaneously blocking both pathways will improve clinical outcomes. One group of researchers performed an *in silico* investigation of

approved drugs that can target both pathways and identified cyclosporine A (CSA) as a potential SARS-CoV-2 drug candidate (Prasad et al., 2021). CSA is a calcineurin (CN) inhibitor peptide. CN is a protein phosphatase that regulates the nuclear factor of activated T cells (NFAT) and thereby plays a key in controlling immune responses (Wang et al., 2022). Accordingly, CSA has immunosuppressive activity, has been used to treat various autoimmune conditions, and is administered to transplant recipients to reduce tissue and organ rejection (D'Angelo et al., 2023). *In vitro* studies reveal that CSA treatment impairs viral protein expression, hampers virion release, and dampens inflammatory cytokine production in SARS-CoV-2-infected human lung cells (Fenizia et al., 2022). Pre-clinical and phase I trials have shown that CSA improved patient outcomes in hospitalized SARS-CoV-2 patients who require oxygen (Blumberg et al., 2022; Devaux et al., 2021).

RNA methyltransferases and their associated molecules are another group of potential drug targets. Methyltransferases transfer a methyl group from a donor molecule, such as S-adenosyl methionine (SAM), to a target molecule, such as RNA (Fischer et al., 2022). RNA methyltransferases play a vital role in viral replication by regulating the stability and translation efficiency of viral RNA (Sulimov et al., 2022). SARS-CoV-2 encodes two methyltransferases, Nsp14 and 16. Together, these enzymes catalyze the final steps of viral RNA cap formation, essential for RNA stability and immune system evasion. Nsp14 exhibits enzymatic functions: an N7-methyltransferase (N7-MTase) and a 3'-5' exonuclease (ExoN) activity. The ExoN activity is responsible for proofreading, while the N7-MTase activity is responsible for the methylation of the N7 position of the guanosine residue at the 5' end of viral RNA. This modification enhances viral RNA stabilization.

Further methylation of the viral RNA cap structure is executed by the 2'-O-MTase activity of Nsp16, which forms an active complex with Nsp10 (Nencka et al., 2022). In this process, Nsp16 utilizes SAM to add a methyl group to the 2' OH group of the first nucleotide within the cap structure (Nencka et al., 2022; Sulimov et al., 2022). This final cap modification helps viral RNA evade host immune detection (Nencka et al., 2022). As a result, the binding of a small molecule within the SAM binding site of Nsp16 can disrupt viral translation and replication (Sulimov et al., 2022). *In silico* studies calculating binding energies and predicted docking have revealed numerous compounds with the potential to inhibit Nsp16 (Sulimov et al., 2022). Another study showed that several synthesized compounds capable of binding to the SAM of Nsp16 and the RNA-binding site of Nsp14 had potent activity against both enzymes but lacked antiviral activity *in vitro (Štefek et al., 2023)*. Hence, more testing is required to determine whether methyltransferase inhibitors are effective SARS-CoV-2 drug targets.

1.16 ESTABLISHED SARS-COV-2 ANIMAL MODELS

Animal models have played a pivotal role in investigating the origin of SARS-CoV-2, understanding viral affinity, and evaluating vaccine efficacy (Gu et al., 2020; Ma & Gong, 2021). During SARS-CoV-2 infection, receptor recognition is crucial in determining cross-species transmission and host permissiveness and susceptibility (Li, 2013). For instance, the acquisition of the polybasic cleavage site, consisting of four amino acid residues within the RBD of the S protein, significantly enhances SARS-CoV-2's ability to interact with human ACE2 (Wan et al., 2020). Beyond human ACE2, SARS-CoV-2 also recognizes ACE2 from a wide range of hosts (Hu et al., 2021). While this broad species tropism suggests the potential for diverse animal models, susceptibility varies among hosts, partly attributed to different S protein-ACE2 interactions (Hu et al., 2021; Li et al., 2006). Host susceptibility to SARS-CoV-2 is additionally contingent on the

32

expression of the cellular transmembrane serine protease, TMPRSS2, which facilitates viral attachment by cleaving the S protein (Markus Hoffmann et al., 2020; Peacock et al., 2021).

Studies have demonstrated the susceptibility of various animal species, such as cats, dogs, pigs, and bats, to SARS-CoV-2 and have provided insights into potential reservoirs and transmission dynamics (AboElkhair et al., 2023; Ma & Gong, 2021; Shi et al., 2020). As a result, various animal species have been investigated for their susceptibility to SARS-CoV-2 infection, leading to an upsurge in SARS-CoV-2 animal models. These models, exhibiting varying degrees of susceptibility, offer distinct advantages and present unique disadvantages. Notable examples include non-human primates (NHP), ferrets, Golden Syrian hamsters, and mice (Singh et al., 2020).

1.16.1 NHP SARS-CoV-2 infection models

Animal models that recapitulate clinical conditions are integral to evaluating disease pathology and drug development. For this reason, NHPs are considered the gold standard for infectious disease models as they closely resemble human disease pathology (Singh et al., 2020). Compared to other NHP models, rhesus macaques and African green monkey models demonstrate heightened susceptibility to SARS-CoV-2 infection. Both models exhibited pulmonary infiltration and elevated levels of viral RNA, with the latter producing viral pneumonia and inflammatory mediators mirroring human immune signatures (Lu et al., 2020; Singh et al., 2020; Woolsey et al., 2021). Consequently, NHPs have become valuable pre-clinical models for SARS-CoV-2 studies, contributing to a deeper understanding of viral pathogenesis and the development of potential therapeutic interventions (Meekins et al., 2021). More importantly, NHP studies have played a critical role in evaluating the safety and efficacy of various SARS-CoV-2 vaccine candidates. A

series of DNA vaccine candidates expressing different forms of the S protein and the mRNA-1273 vaccine candidate were evaluated in rhesus monkeys (Corbett et al., 2020; Yu et al., 2020).

Additionally, NHPs have been used to assess the potential for viral spillover in natural settings (Sacchetto et al., 2021). Despite their value in infectious disease research, NHPs present significant challenges, including availability, handling, and cost (Singh et al., 2020). Aside from these issues, working with NHPs is considered ethically controversial due to their complexity and human resemblances (Au et al., 2022).

VeroE6 cells isolated from African green monkey kidneys have been extensively utilized in the study of SARS-CoV-2 (Zaliani et al., 2022). These cells have been instrumental in the isolation and propagation of SARS-CoV-2; however, studies have shown that propagation of the virus in VeroE6 cells lacking TMPRSS2 can lead to loss of the polybasic furin cleavage site, resulting in attenuation of the virus (Aiewsakun et al., 2023; Johnson et al., 2021). Therefore, scientists have utilized VeroE6 cells expressing TMPRSS2 (VeroE6/TMPRSS2) to enhance viral isolation and propagation and study viral pathogenesis (Matsuyama et al., 2020). Furthermore, VeroE6/TMPRSS2 cells have been employed to assess the antiviral activity of various compounds and to study the signaling pathways and cellular responses associated with SARS-CoV-2 infection (Pires De Souza et al., 2022).

1.16.2 Ferrets as a SARS-CoV-2 infection model

Ferrets are a well-established model for studying the pathogenesis and transmission of human respiratory viruses such as influenza, human respiratory syncytial virus, and SARS-CoV (Wong et al., 2019; Zhao et al., 2023). Ferrets are highly susceptible to influenza infection and mimic many clinical symptoms observed in humans, making them valuable in testing influenza therapeutics. Their ability to cough and sneeze makes them optimal for studying the transmission

of respiratory viruses (Zhao et al., 2023). Regarding SARS-CoV-2, ferrets are susceptible to infection, exhibiting high viral titers in the upper respiratory tract, and they can directly or indirectly transmit the virus to naïve ferrets (Au et al., 2022; Kim et al., 2020). Accordingly, ferrets recapitulate certain aspects of SARS-CoV-2 human infection and are used as a model to study infection, transmission, and pathology (Kim et al., 2020).

Furthermore, like humans, ferrets show age-related disease severity, with animals three years or older exhibiting higher viral loads and inflammatory cytokines in the lungs and prolonged nasal viral shedding compared to younger animals (Zhao et al., 2023). SARS-CoV-2-infected ferrets show a lack of clinical symptoms, with no change in body weight observed during infection. However, they develop an immune response as evidenced by the production of neutralizing antibodies (Kim et al., 2020; Zhao et al., 2023). For this reason, ferrets are considered a suitable animal model for asymptomatic or mild SARS-CoV-2 infection (Everett et al., 2021; Zhao et al., 2023). While ferrets offer some advantages as a SARS-CoV-2 infection model, such as being more accessible and cheaper to work with than NHPs, they exhibit disease pathology that is less comparable to humans, making them less suited to explore the efficacy of potential therapeutics than other models (Kim et al., 2020; Singh et al., 2020).

1.16.3 Golden Syrian hamsters as a SARS-CoV-2 infection model

Golden Syrian hamsters have proven to be invaluable to SARS-CoV-2 research. As an infection model, golden Syrian hamsters exhibit several characteristics associated with mild SARS-CoV-2 in humans (Imai et al., 2020; Sia et al., 2020). For example, the virus replicates efficiently in the lungs of these animals and causes severe pathological lung lesions similar to those observed in SARS-CoV-2 patients with pneumonia. As a result, Syrian hamsters are considered a useful small animal model for the evaluation of SARS-CoV-2 vaccines, immunotherapies, and

antiviral drugs (Imai et al., 2020). In addition, the virus can be transmitted among infected and uninfected hamsters via direct contact or aerosol droplets. As measured by body weight loss and neutralizing antibodies, clinical symptoms were reported in both inoculated and naturally infected hamsters, making them a valuable animal model to study SARS-CoV-2 pathogenesis and transmissibility (Sia et al., 2020). The production of neutralizing antibodies facilitated recovery and protected hamsters from SARS-CoV-2 reinfection. Similarly, inoculation of naïve hamsters with serum from infected animals prevented viral infection (Imai et al., 2020).

Although Syrian hamsters are highly regarded for their ability to recapitulate human aspects of SARS-CoV-2 infection, they exhibit notable sex-related differences in their condition. These differences can contribute to variations in disease pathology and therapeutic response, especially for diseases where sex disparities have been observed in humans, like SARS-CoV-2, which shows increased infectivity and worse overall outcomes for males than females (Chaturvedi et al., 2022; Sia et al., 2020).

1.16.4 Mouse SARS-CoV-2 infection models

Mice are a stable animal model because they are inexpensive, relatively simple to handle, and easy to obtain; however, they present several problems when studying SARS-CoV-2 (Singh et al., 2020). Most notably, standard laboratory mice are not susceptible to infection with wild-type (or Wuhan) SARS-CoV-2 (Gu et al., 2020). Therefore, viral or host adaptation was required to study SARS-CoV-2 pathogenesis and potential countermeasures in mice at the beginning of the pandemic. Adaptation of SARS-CoV-2 to mice resulted in the production of a mouse-adapted variant capable of infecting BALB/c mice and causing interstitial pneumonia and inflammatory responses after intranasal inoculation. This variant allows researchers to test vaccine and antiviral candidates using standard laboratory mice (Gu et al., 2020).

Conversely, host adaptation led to the production of transgenic mice expressing the human ACE2 receptor, or K18-hACE mice (Singh et al., 2020). These transgenic mice are highly susceptible to SARS-CoV-2 infection. Intranasal inoculation of these mice results in high viral titers and the production of inflammatory cytokines within the lungs, leading to pulmonary dysfunction and viral dissemination to other organs. Therefore, the K18-hACE2 mouse model shares many features of severe SARS-CoV-2 infection in humans and can be used to study severe disease pathology and investigate therapeutic interventions (Winkler et al., 2020). Despite the advantages offered by the mouse-adapted variant, the relevance of this strain to human disease pathology is limited.

Similarly, while transgenic mice have contributed significantly to SARS-CoV-2 infection studies, variations in gene expression within tissues and among individual mice render this model less comparable to human pathology (Singh et al., 2020). However, a recent study shows BALB/c mice are susceptible to SARS-CoV-2 infection without needing viral or host adaptation. In particular, this study shows that the SARS-CoV-2 Beta variant (B.1.351) replicates efficiently and induces significant pathological changes coupled with inflammatory cytokine production in the lungs of BALB/c mice (Pan et al., 2021). This variant allows researchers to study SARS-CoV-2 pathogenesis and evaluate therapeutics in mice in a manner that is more relatable to humans.

1.17 PRAIRIE VOLES

Prairie voles (*Microtus ochrogaster*) are small rodents, typically weighing 30 to 60 grams, that inhabit the grasslands of central North America (McGraw & Young, 2010). Individual male and female prairie vole territories broadly overlap in the field, allowing them to interact and potentially form pair bonds (Hofmann et al., 1984; Kenkel et al., 2021). Pair bonding in prairie voles forms the cornerstone of their social organization and monogamy (Blocker & Ophir, 2016).

Regarding social organization, prairie vole family units consist of a pair-bonded male and female and one or two reproductively quiescent offspring generations (Getz et al., 1981). Family units remain together until the fall and winter when juveniles leave the nest and form communal groups with unrelated individuals. These individuals pair up in the spring and form their own familial nests (Getz & Carter, 1996).

Regarding their relationships, prairie voles form long-term pair bonds – a mating strategy observed in a select group of mammals, including humans. This strategy involves coupling unrelated individuals with the shared purpose of mating and rearing offspring for life (Johnson & Young, 2015; Young et al., 2011). Prairie voles are defined as being monogamous but not necessarily sexually exclusive (Blocker & Ophir, 2016). In this mating scenario, referred to as social monogamy, a mating partner may have a preferred mate who receives most of their attention and casual mating partners (Blocker & Ophir, 2016; Getz et al., 1993; McGuire & Getz, 2010). Social monogamy in prairie voles has been hypothesized as a strategy to nurture and safeguard vulnerable offspring (Emlen & Oring, 1977). Typically, the survival of offspring from pair-bonded animals relies on the collaborative efforts of both parents and prairie voles exhibit the practice of bi-parental care for their offspring. Male prairie voles significantly contribute to various parental behaviors, including pup huddling and retrieval, nest building, and nest guarding (Getz & Carter, 1996; Gruder-Adams & Getz, 1985). Prairie voles also exhibit alloparental care in which a parental-offspring bond is formed between unrelated individuals. These behavioral phenomena, not commonly seen in traditional rodent models, overlap with human social behavior (McGraw & Young, 2010), making them an interesting novel candidate for modeling human disease transmission.

Studies have shown that prairie voles exhibit distinct social behaviors, such as selective aggression, affiliation, and social organization, which make them an ideal model for studying social attachment and bonding (Insel & Shapiro, 1992; Lee et al., 2019; Yee et al., 2016). The distribution of oxytocin and vasopressin receptors in the brain of prairie voles has been associated with their social organization, providing insights into the neural mechanisms underlying their monogamous behavior (Insel et al., 1994; Kitano et al., 2022; Ross et al., 2009). Prairie voles have also been used to investigate the role of neuropeptides, such as oxytocin and vasopressin, in regulating social attachment and pair bonding, highlighting their significance in understanding the neurobiology of social behavior (31, 37). Moreover, the use of prairie voles has extended to investigating the impact of prenatal stress, aging, and microbiota on social behavior, providing valuable insights into the environmental and physiological factors influencing social interactions (38, 39).

1.17.1 Advantages of using Prairie voles as a SARS-CoV-2 infection model

In addition to their distinct social behaviors, prairie voles offer other unique advantages as an infection model. Unlike mice and rats (who experience spontaneous estrus and ovulation), estrus and ovulation are inducible in prairie voles by either brief physical contact with a male or male urine (Becker et al., 2005; Dluzen et al., 1981; McLean et al., 2012). As a result, both sexes can be used in a study without complications due to hormonal differences. Additionally, the effect of female hormones on disease pathology can be examined before and after estrus induction, allowing researchers to draw a more precise association between hormone profile and disease pathology. This aspect is essential in disease studies because physiological sex differences also account for prominent differences in mental health. For instance, estrus has been shown to induce

anxiety behavior in female rats, which leads to an increased proinflammatory state and reduced immune responses (Hawkley & Capitanio, 2015; Mora et al., 1996).

Compared to mice, prairie voles offer other discernable advantages as a SARS-CoV-2 infection model. For example, prairie voles have not undergone substantial domestication, which can trigger behavioral changes in aspects such as temperament and stress reactivity (Chalfin et al., 2014). It can also alter microbiome diversity, resulting in an acritical microbiome that can decrease translational relevance (Kitano et al., 2022; Rosshart et al., 2019). Additionally, as hamster-sized rodents, they provide similar simplicity, cost-effectiveness, and practicality as transgenic mice. They also facilitate infection without necessitating host or virus adaptation, potentially rendering them more suitable for researching human disease interventions. More importantly, as an established behavioral model to explore anxiety and depression (i.e., social defeat), a prairie vole infection model would offer a unique perspective on the correlation between SARS-CoV-2 infection and mood and anxiety disorders observed in patients months after their initial infection (Klaser et al., 2021).

1.18 Hypothesis and Justification of Experiments

At the beginning of the pandemic, there was a surge in animal models being evaluated for their ability to recapitulate SARS-CoV-2 symptoms and disease pathology observed in humans. This surge was due to the race to understand SARS-CoV-2 pathogenesis and host-viral interactions, to validate vaccine candidates, and to examine potential therapeutic countermeasures. Since wild-type (WT) mice are not susceptible to SARS-CoV-2 and ACE2 gene expression in transgenic mice is not comparable to human levels, we assessed the potential of other rodents as a SARS-CoV-2 infection model. We decided to use prairie voles due to their human-like social behavior compared to other common laboratory rodents such as rats and hamsters. Based on ACE2

sequence homology, we tested the hypothesis that *prairie voles are susceptible to SARS-CoV-2 following in vivo inoculation.*

The following specific aims were carried out to test the hypothesis:

1) To determine the susceptibility of the prairie vole to SARS-CoV-2 infection using *in vitro* screening assays using SARS-CoV-2 pseudoviral particles and various SARS-CoV-2 variants.

2) To assess the susceptibility of the prairie vole to SARS-CoV-2 infection *in vivo* using quantitative reverse transcription PCR (qRT-PCR) and $TCID_{50}$ and plaque assay to determine the number of viral RNA copies and titer, respectively, within the tissues and nasal wash of the animals following intranasal and aerosol inoculation.

3) To enhance the virulence of SARS-CoV-2 in the prairie voles and increase their utility as a pre-clinical model by generating a prairie vole-adapted SARS-CoV-2 variant through *in vivo* serial passage in the lungs of the animals.

The studies described in the subsequent chapters mark the first attempt to employ prairie voles as an infection model. The overall goal of this project was to establish the prairie vole as a pre-clinical model to study SARS-CoV-2 infection and transmission. The novelty of this research lies in its utilization of an animal model typically employed in behavior studies to investigate a viral infection that has been associated with cognitive disorders like depression and anxiety.

Chapter 2: Materials and Methods

2.1 **ANIMALS**

The animal work for this research was performed in the biosafety level-3 (BSL-3) facility at the University of Texas at El Paso (UTEP) in El Paso, Texas, USA. All work with live animals was approved by the Institutional Animal Care and Use Program (IACUP) in accordance with guidelines from the National Institutes of Health (NIH) Office of Laboratory Animal Welfare (OLAW) in compliance with the Public Health Service (PHS) Policy on Human Care and Use of Laboratory Animals and in accordance with US Department of Agriculture (USDA) Animal and Plant Health Inspection Service in compliance with the Animal Welfare Act.

All animals were acclimated to the BSL-3 facility for at least seven days prior to entering an infection study, given food and water ad libitum, monitored daily, and provided with environmental enrichment throughout each study. In the BSL-3 facility, all animals were maintained on a 12:12 hour light: dark cycle (lights on at 07:00) and housed within individually ventilated (IVC) Tecniplast Sealsafe Plus GM500 cages with a floor area of 501cm^2. Cages were stored on a Tecniplast Sealsafe Plus DGM80 rack with an 8w X 10h, single-sided configuration.

2.1.1 K18hACE2 transgenic mice

The K18hACE2 transgenic BALB/cJ (BALBcJ.K18-hACE2) mice express the human ACE2 receptor. The human keratin 18 promoter directs expression of the human ACE2 receptor to epithelia, including airway epithelia. The K18hACE2 transgenic mice [C.Cg-Tg(K18-ACE2)2Prlmn/ J (Strain#: 035247) (RRID: IMSR_JAX:035247)] were obtained from Jackson Laboratories at six weeks of age. Mice were housed in the BSL-3 IVC system with 4-5 mice per cage.

2.1.2 Prairie voles

All prairie voles were generously provided by Dr. Bruce Cushing at UTEP. These laboratory-reared prairie voles were derived from wild-caught founders initially captured near Champaign, IL. Within the BSL-2 vivarium, the voles were housed in polysulfonate cages measuring 25 X 45 X 60cm. They were supplied with high-fiber rabbit food and water ad libitum, along with cotton nestlets for environmental enrichment. The voles adhered to a 14:10 hour light: dark cycle, with lights turning on at 06:00. Following the establishment of breeder pairs, pups were weaned into same-sex sibling pairs at postnatal day (PD) 21. Litter sizes were regulated to 6 pups to mitigate competition for nourishment and associated complications. Experimental subjects were same-sex siblings aged PD 60 or older. Voles were housed in the BSL-3 IVC system with two voles (forming one pair bond) per cage.

2.2 MAMMALIAN CELLS AND MAINTENANCE MEDIA

All adherent cells were incubated at 37°C, 5% CO_2, and 90% humidity in 1X Dulbecco's Modified Eagle Medium (DMEM) (Ref#10-017-CV, Corning). All culture media was supplemented with 10% Fetal Bovine Serum (FBS) (Ref#35-011-CV, Corning) and 1mM sodium pyruvate (Ref#25-000-CI, Corning). VeroE6 cells stably expressing human TMPRSS2 were obtained from Dr. Stefan Pohlmann at the University Gottingen, Gottingen, Germany, and were maintained in DMEM supplemented with 1 µg/mL blasticidin (Cat#3513-03-9, Millipore Sigma). VeroE6 cells stably expressing human TMPRSS2 cells were also obtained from Sekisui Xeno Tech, LLC (JCRB#1819) and maintained in DMEM supplemented with 1mg/mL geneticin (G418) (Ref#10131-027, Gibco). Human Embryonic Kidney (HEK) 293T cells stably expressing human and vole ACE2 and human TMPRSS2 cells were generated by lentiviral transduction and puromycin and hygromycin B-based selection and were maintained in DMEM supplemented with

3ug/mL puromycin (Cat#P-600-100, Gold Biotechnology) and 0.3mg/mL hygromycin B (Cat#H-270-25, Gold Biotechnology). For subculturing and seeding of adherent cells, cells were washed with 1X Dulbecco's phosphate-buffered saline (PBS) without Ca^{+2} and Mg^{+2} (Ref#21-040-CV, Corning) and subsequently incubated in 0.05% trypsin-EDTA (Cat#T3924, Sigma) until they detached.

Expi293F suspension cells were purchased from ThermoFisher Scientific (Cat#A14527, Gibco), maintained in Expi293 expression medium (Ref#A14351-01, Gibco) and 125mL Erlenmeyer Shaker Flasks (Cat#4115-0125, ThermoFisher Scientific). Expi293T cells were incubated at 37°C, 8% CO_2, and 90% humidity while shaking at 100 rotations per minute (rpm).

2.3   SARS-CoV-2 isolates

The following SARS-CoV-2 isolates were obtained from BEI Resources: hCoV-19/USA-WA1/2020 (lineage A; Pango v.4.1.3 PANGO-v1.17) (Cat#NR-52281), hCoV-19/England/204820464/2020, or UK/VUI/3/2020 and VUI-2020 12/01 (linage B.1.1.7; Alpha variant) (Cat#NR-54000), hCoV-19/USA/MD-HP01542/2021, or GH/501Y.v2 (lineage B.1.351; Beta variant) (Cat#NR-55282), hCoV-19/USA/MD-HP05647/2021 (lineage B.1.617.2; Delta variant) (Cat#NR-55672), USA/CA/VRLC009/2021, or USA/CA-Standford-02_S43/2021 (lineage B.1.427; Epsilon variant) (Cat#NR-55308), USA/CA/VRLC012/2021, or USA/CA-Standford-04_S01/2021 (lineage P.2; Zeta variant) (Cat#NR-55439), hCoV-19/USA/CA-Standford-15_S02/2021, or hCoV-19/USA/CA-SU-15_S02/2021 (lineage B.1.617.1; Kappa variant) (Cat#NR-55486), hCoV-19/Peru/un-CDC-2-4069945/2021 (lineage C.37; Lambda variant) (Cat#NR-55654), and an infectious clone of isolate MA10 (ic2019-nCoV MA10) (mouse-adapted, MA variant in isolate USA-WA1/2020 backbone) (Cat#NR-55329). The recombinant reporter

virus, SARS-CoV-2-Nluc-2A, was kindly provided by Dr. Luis Martinez-Sobrido at the Texas Biomedical Research Institute, San Antonio, Texas, USA.

Isolate USA-WA1/2020 was isolated from an oropharyngeal swab from a patient who had traveled to China and developed COVID-19 on January 19, 2020, in Washington, USA. Isolate hCoV-19/England/204820464/2020 (Alpha (α), or UK variant) was isolated from a 58-year-old man on November 24, 2020, in England, United Kingdom. Isolate hCoV-19/USA/MD-HP01542/2021 (Beta variant) was isolated from a human nasal swab in January 2021 in Maryland, USA. Isolate hCoV-19/USA/MD-HP05647/2021 (Delta variant) was isolated from a patient in Maryland, USA, on April 27, 2021. Isolate USA/CA/VRLC009/2021 (Epsilon variant) was isolated from a nasopharyngeal swab in California, USA, on January 13, 2021. Isolate USA/CA/VRLC012/2021 (Zeta variant) was isolated from a mid-turbinate nasal swab in California, USA, on January 23, 2021. Isolate hCoV-19/USA/CA-Standford-15_S02/2021 (Kappa variant) was isolated from a mid-turbinate nasal swab from a 29-year-old male on March 5, 2021, in California, USA. Isolate hCoV-19/Peru/un-CDC-2-4069945/2021 (Lambda variant) was isolated from a human nasopharyngeal swab in Peru on February 20, 2021. Isolate MA10 (mouse-adapted variant) was developed by 10 *in vivo* serial passages of SARS-CoV-2, isolate MA, in BALB/c mice, followed by plaque purification in VeroE6 cells.

2.4   PRODUCTION OF SARS-CoV-2/VENUS-2A STRAIN

2.4.1   pBAC-SARS-CoV-2/Venus-2A plasmid

This plasmid utilizes a bacterial artificial chromosome (BAC) promoter. It was constructed by inserting the full-length SARS-CoV-2 genome sequences into the pBeloBAC vector and replacing the viral ORF7a gene with a fluorescent (Venus) reporter gene, producing reporter-expressing recombinant viruses.

2.4.2 Bacterial Cells and Media

Bacterial cells containing pBAC-SARS-CoV-2/Venus-2A plasmids were obtained from Texas Biomedical Research Institute and grown in Luria-Bertani (LB) broth or on LB agar (Cat#BP1423-2, Fisher Scientific) containing 34μg/mL of chloramphenicol (Cam) (Cat#BP904-100, Fisher BioReagents).

2.4.3 pBAC-SARS-CoV-2/Venus-2A Plasmid isolation

Bacterial cells were streaked onto LB agar plates containing 34μg/mL of CAM and incubated at 37°C overnight. A liquid culture was prepared in a 14mL round-bottom polypropylene test tube (Cat#14-959-11B, Falcon) by inoculating 5mL of LB broth containing 34μg/mL of CAM with cells selected from a single, isolated colony. This culture was incubated at 37°C and 250rpm for 8 hours. Next, 250μL of the 8-hour culture was used to inoculate 250mL of LB broth containing 34μg/mL. This culture was then incubated overnight at 37°C and 250rpm. The overnight culture was transferred to a 500mL RC-6 centrifuge tube and centrifuged at 8,000rpm for 15 minutes at 4°C.

After pelleting the culture, the plasmid was isolated using the NucleoBond Xtra BAC kit for large construct plasmid DNA from Macherey-Nagel (Cat#740436.10). The supernatant was discarded, and the pellet was resuspended in 60mL of resuspension buffer containing 100μg/mL of RNase A. Next, 60mL of lysis buffer was added to the suspension. The suspension was mixed thoroughly by inverting the tubes 4-5 times and incubated at room temperature for 5 minutes. Then, 60mL of neutralizing buffer was added to the tube. The tube was inverted to mix and incubated on ice for 5 minutes. The lysate was loaded onto the column after equilibrating the column filter with 30mL of equilibration (EQU-BAC) buffer. The column was filtered via gravity flow and washed with 15mL of EQU-BAC buffer and then with 45mL of wash buffer. Next, 15mL

of heated elution buffer was added to the column to elute the DNA into a 35mL RC-6 centrifuge tube. The elution was mixed with 6mL of room temperature isopropanol (IPA) and incubated at room temperature for 2 minutes. This mixture was centrifuged at 17,000rpm for 30 minutes at 4°C. After discarding the supernatant, the pellet was washed with 5mL of room temperature 70% ethanol and centrifuged at 17,000rpm for 5 minutes at 4°C. The supernatant was discarded from the tube, and the pellet was air-dried for 15 minutes at room temperature. Then, the pellet was resuspended in 400μL of TE buffer.

The concentration and purity of the eluted DNA were measured with a NanoDrop One Microvolume UV-Vis Spectrophotometer (Cat#13-400-519, ThermoScientific). DNA purity of isolated plasmids was confirmed by agarose gel electrophoresis. The 0.8% agarose gel containing 0.025mg of ethidium bromide was visualized using an iBright FL1000 imaging system (Cat#A32752, Invitrogen).

2.4.4 Transfection of pBAC-SARS-CoV-2/Venus-2A into VeroE6/TMPRSS2 cells

Since this procedure involved generating a recombinant virus, it was conducted in the BSL-3 facility. VeroE6/TMPRSS2 cells were seeded at $2.0*10^5$ cells/well in a 6-well plate and incubated at 37°C and 5% CO_2 overnight until ~90% confluent. The following day, 750μL of OptiMEM and 15μL of lipofectamine 2000 transfection reagent (Cat#11668027, Invitrogen) were combined in a microcentrifuge tube and mixed via inversion 4-5 times. The mixture was incubated for 10 minutes at room temperature. In a separate microcentrifuge tube, 150μL of OptiMEM and 7.5μg of the plasmid were combined and mixed via inversion 4-5 times. This mixture was added to the OptiMEM-lipofectamine mixture, and the tube was inverted 4-5 times to mix. This mixture was incubated at room temperature for 20 minutes. After replacing the maintenance media (1X DMEM + 10% FBS + 2% G418) in the 6-well plate with 1mL of transfection media (1X DMEM

+ 10% FBS), 300µL of the OptiMEM-lipofectamine-DNA mixture was added to each well. The plate was then incubated at 37°C and 5% CO_2 overnight. On day 2, the transfection media was removed and replaced with 2mL of post-transfection media (1X DMEM + 2% FBS + 1X penicillin and streptomycin (PS)). The plate was incubated for an additional 48 hours. After removing the post-transfection media (1X DMEM + 2% FBS + 1X PS) from the wells of the plate, the cells were washed with 1X PBS and treated with 0.5mL of 0.05% trypsin-EDTA for 3 minutes at 37°C and 5% CO_2. After adding 2.5mL of post-transfection media (1X DMEM + 2% FBS + 1X PS) to each well, the media was collected and transferred to a 15mL conical tube. The tubes were centrifuged at 1,000rpm for 5 minutes at room temperature. Next, the supernatant was discarded, and the pellets were resuspended in 12mL of post-transfection media (1X DMEM + 2% FBS + 1X PS). This viral suspension was transferred to a T-75 flask containing VeroE6/TMPRSS2 cells at ~95% confluency. The flask was incubated at 37°C and 5% CO_2 for 48 hours and monitored for cytopathic effect (CPE) daily. At six days post-transfection, the media from the inoculated T-75 flask was transferred to a 15mL conical tube and centrifuged at 1,000rpm for 5 minutes at room temperature. The supernatant was transferred to 2mL microcentrifuge tubes with screw caps (Cat#4305936, ThermoFisher Scientific) in 1mL aliquots for storage at -80°C.

2.5 VIRAL STOCK PREPARATION AND STORAGE

All *in vitro* viral work was conducted in the BSL-3 facility. Working stocks of each variant were created by passaging each virus a single time (P1) in VeroE6/TMPRSS2 cells maintained in DMEM (Ref#10-017-CV, Corning) supplemented with 2% FBS (Ref#35-011-CV, Corning), 1mM sodium pyruvate (Ref#25-000-CI, Corning), and 1mg/mL geneticin (Ref#10131-027, Gibco). The inoculated T-25, T-75, or T-300 flasks were incubated at 37°C and 5% CO_2. Viral suspensions were harvested once ~90% CPE was observed and clarified by centrifugation at

1,000rpm for 5 minutes before being concentrated with Polyethylene Glycol (PEG) 8000 (Cat#V3011, Promega) overnight at 4°C. The concentrated isolates were clarified by centrifugation at 3500rpm for 30 minutes, pooled, and stored at -80°C. Viral titers of all stocks were determined via plaque assay or $TCID_{50}$ assay.

2.6 VSV PSEUDOPARTICLE PRODUCTION

VSV pseudoparticles carrying the SARS-CoV-2 S protein were produced in the BSL-2 facility by transfecting HEK293T cells with 6μg of pCG1-SARS-2-S using X-tremeGENE 9 DNA transfection reagent (Cat#6365779001, Millipore Sigma). After a 16-hour incubation at 37°C and 5% CO_2, the cells were inoculated with a replication-competent vesicular stomatitis virus (VSV) containing an expression cassette for luciferase in place of the VSV-G open reading frame (VSV-ΔG-luciferase), which was kindly provided by Dr. Stefan Polhmann at the University Gottingen, Gottingen, Germany. The cells were incubated for an additional 2 hours at 37°C and 5% CO_2 before removing the inoculum and washing the cells twice with FBS-free DMEM. Twenty hours later, the pseudoparticles were collected, passed through a 0.45μ filter, and stored at -80°C.

2.7 VSV PSEUDOPARTICLE INFECTION

HEK293T cells expressing human ACE2 (hACE2) or prairie vole ACE2 (moACE2) alone or in combination with the human TMPRSS2 protease (hTMPRSS2) were seeded in 6-well plates at $1.5*10^5$ cells/mL and incubated at 37°C and 5% CO_2 until ~80% confluent. The cells were infected with pseudoparticles in the BSL-3 facility, and 18 hours post-infection, 100μL of the cell supernatant was transferred to a white 96-well plate with a clear bottom and mixed with 50μL of Bright NanoLuc reporter (Cat#N1110, Promega). Luciferase activity was then measured using a plate reader.

2.8   IN VITRO SARS-CoV-2 INFECTIVITY ASSAY

HEK293T expressing prairie vole ACE2 (moACE2) and human ACE2 (hACE2) and HEK293T cells expressing hACE2 and hTMPRSS2 were seeded at $1.0*10^5$ cells/mL in 24-well plates. Plates were incubated at 37°C and 5% CO_2 overnight. The following day, the cells were inoculated with SARS-CoV-2 isolates at a multiplicity of infection (MOI) of 0.01 in the BSL-3 facility. Inoculation of the cells with infectious virus particles began by removing the media from each well. During this process, 40μL was left in the wells to keep the cells from drying out. After washing the wells with 500μL of 1X PBS, 100μL of virus stock diluted in infection media (1X DMEM + 2% FBS + 1X PS) was added to the corresponding wells. The plates were incubated at 37°C and 5% CO_2 for 1 hour, rocking every 15 minutes to disseminate the viral particles. Then, 400μL of maintenance media containing 10% FBS and 1X PS was added to each well, and the plates were incubated for three days at 37°C and 5% CO_2 with daily CPE checks. To collect samples for RNA extraction, 250μL of media from each well was transferred to a 2mL microcentrifuge tube with a screw cap containing 750μL of TRIzol LS (Cat#10296010, ThermoFisher Scientific) and 200μL of chloroform (Cat#AC423550010, Fisher Scientific). The tubes were inverted 4-5 times to mix, and the samples were stored at -80°C in the BSL-2 facility. The remaining 250μL of media within the wells was transferred to a separate 2mL microcentrifuge tube with a screw cap and stored at -80°C in the BSL-3 facility to be analyzed via TCID$_{50}$ assay.

2.9   VIRAL RNA EXTRACTION

Viral RNA was extracted from *in vitro* and *in vivo* samples using the PureLink RNA Mini Kit from Invitrogen (Cat#12183018A) according to the manufacturer's instructions. RNA samples were thawed on ice, vortexed briefly to mix, and centrifuged at 13,000rpm for 10 minutes at 4°C. After centrifugation, 250μL of the top layer of each sample was transferred to a microcentrifuge

tube containing 250µL of 70% ethanol. The tubes were briefly vortexed to mix, and the mixture was transferred to the spin column and centrifuged at 10,000rpm for 30 seconds. After discarding the flow through from the collection tube, 700µL of wash buffer I was added to each spin column. The columns were centrifuged at 10,000rpm for 30 seconds, and the collection tubes were discarded. The spin columns were placed in new collection tubes and washed twice with 500µL of wash buffer II. Following centrifugation of the spin columns at 10,000rpm for 1.5 minutes, the RNA was eluted by adding 100µL of RNase-free water to each spin column and centrifuging at 10,000rpm for 2 minutes. RNA yield and purity were determined via NanoDrop.

2.10   QUANTIFICATION OF VIRAL RNA COPIES VIA qRT-PCR

The presence of SARS-CoV-2 RNA in the extracted nasal wash and tissue samples was assessed by qRT-PCR targeting the SARS-CoV-2 nucleocapsid (N) gene using the TaqMan Fast Virus 1-Step Master Mix for qPCR (Cat#4444434, Applied Biosystems) with the following primers and TaqMan probe: SARS-CoV-2-N-forward (5'-GACCCCAAAATCAGCGAAAT-3'), SARS-CoV-2-N-reverse (5'-TCTGGTTACTGCCAGTTGAATCTG-3'), and SARS-CoV-2-N-Probe (5'-ACCCCGCATTACGTTTGGTG GACC-3'). Tissue samples were diluted to 150ng/µL for a total of 600ng per reaction. qRT-PCR reactions were created by mixing 4µL of diluted or undiluted (nasal wash) RNA samples with 3µL of TaqMan Master Mix, 0.6µL corresponding primers (900nM) and probe (250nM), and 4.4µL. PCR was performed at 50°C for 5 minutes, 95°C for 20 seconds, 95°C for 3 seconds, and 60°C for 30 seconds for 45 cycles using the StepOnePlus Real-Time PCR System from Applied Biosystems. Each experimental or control sample was run in duplicate. Positive results were defined by a cycle threshold (Ct) value of ≤ 33. The Ct values were calculated from a standard curve generated from a synthetic standard diluted from 10^4 to 10^8. To quantify the viral RNA copies per tissue, the Ct value was multiplied by the RNA yield of the

total sample divided by 600 and then multiplied by the tissue factor (the number of times the tissue was sectioned during the harvesting process). For the viral RNA copies per nasal wash, the Ct value was multiplied by ¼ of the total volume of the extracted RNA (100µL).

2.11 QUANTIFICATION OF VIRAL LOAD VIA TCID$_{50}$ ASSAY

The viral titer of *in vitro* and *in vivo* samples was determined or confirmed by TCID$_{50}$ assay in a 96-well plate format. VeroE6/TMPRSS2 cells were seeded at $1.0*10^5$ cells/mL in 96-well plates and incubated at 37°C and 5% CO$_2$ overnight. Tenfold serial dilutions of *in vitro* or *in vivo* samples were created in infection media (1X DMEM + 2% FBS + 1X PS). Next, 50µL of the sample dilutions were added to the first row of wells of the plate. After mixing, 50µL of the solution in the first row of wells was transferred to the second row of wells. This process was repeated for the subsequent rows, resulting in a 1/3 dilution of the samples down the plate. The plates were incubated at 37°C and 5% CO$_2$ and monitored daily for CPE. Three days post-infection, viral titers were calculated based on the lowest dilution at which 50% of the wells exhibited CPE.

2.12 VIRULENCE ASSAY OF SARS-COV-2 ISOLATES

2.12.1 Sample Preparation

VeroE6/TMPRSS2 cells were seeded in a T-150 flask at $1.4*10^5$ cells/mL. Flasks were incubated at 37°C and 5% CO$_2$ for three days until the cells reached ~95% confluency. Cells were inoculated with SARS-CoV-2 isolates at an MOI of 0.01 in the BSL-3 facility. The maintenance media (1X DMEM + 10% FBS + 2% G418) was removed from the flasks and replaced with 10mL of virus diluted in infection media (1X DMEM + 2% FBS + 1X PS). Flasks were incubated at 37°C and 5% CO$_2$ for 1 hour and rocked every 15 minutes to ensure the dispersal of the viral particles. After the 1-hour incubation, 20mL of maintenance media (1X DMEM + 10% FBS) was added to each flask, and the flasks were incubated for three days at 37°C and 5% CO$_2$. Flasks were

monitored daily for CPE. At 3dpi, the media from each flask was transferred to a 50mL conical tube, and the samples were centrifuged at 3,500rpm for 15 minutes at room temperature. The supernatants were transferred to 15mL conical tubes in 10mL aliquots and mixed with 2.5mL of PEG 8000. The tubes were inverted 4-5 times to mix and incubated at 4°C overnight. The overnight precipitations were centrifuged at 3,500rpm for 30 minutes at room temperature, and the pellets were resuspended in a total of 3mL of 1X PBS and mixed with 800μL of PEG 8000. Samples were incubated at 4°C overnight before being centrifuged at 3,500rpm for 30 minutes at room temperature. After decanting the supernatants, the pellets were resuspended in 300μL of 1X PBS.

2.12.2 SDS-PAGE

To create sodium dodecyl-sulfate polyacrylamide gel electrophoresis (SDS-PAGE) samples at 2μg/μL, the bicinchoninic acid (BCA) assay was performed in the BSL-3 facility. SDS-PAGE samples were deactivated in the BSL-3 facility by boiling at 100°C for 15 minutes. Samples were then stored at -20°C in the BSL-2 facility.

SDS-PAGE samples were thawed at room temperature and denatured at 65°C for 10 minutes. Next, 10μL of each sample and 3μL of Precision Plus Protein Dual Color Standards ladder (Cat#1610374, BioRad) were loaded into the 4-20% Mini-PROTEAN TGX Precast Protein Gel (Cat#4561096, BioRad).

2.12.3 Western blot

After the gel was run at 200 voles for 30 minutes, proteins were transferred to a nitrocellulose membrane for 2 hours at 4°C and 200 volts. Next, the membrane was cut in half and blocked in 5% milk in 1X PBS for 30 minutes at room temperature. Membranes were washed twice in 1X PBS at room temperature for 5 minutes and then incubated in the primary antibodies diluted in 3% BSA in 1X PBS containing 0.1% Tween-20 (Cat#P1379-500mL, Sigma-Aldrich)

overnight at 4°C. Refer to table 2.1 for primary antibody information. Membranes were washed twice in 1X PBS containing 0.1% Tween-20 at room temperature for 5 minutes and then incubated in the secondary antibodies diluted in 3% BSA in 1X PBS containing 0.1% Tween-20 for 1 hour at room temperature. Refer to table 2.1 for secondary antibody information. Membranes were washed twice in 1X PBS containing 0.1% Tween-20 at room temperature for 5 minutes. Protein bands were visualized using the SuperSignal West Pico PLUS Chemiluminescent Substrate (Cat#34580, ThermoFisher Scientific) and an IBright FL1000.

Table 2.1: Primary and secondary antibodies for Western blot of SARS-CoV-2 isolates

Antibody	Catalog #	Vender	Dilution
Anti-SARS-CoV-1/2-S protein clone 2BBE5 mouse monoclonal	Cat#ZMS1076-25μL	Sigma-Aldrich	1/2000
Anti-SARS-CoV-1/2-N protein clone 2BBE5 mouse monoclonal	Cat#ZMS1075-25μL	Sigma-Aldrich	1/5000
Goat Anti-Mouse IgG, HRP conjugate polyclonal	Cat#12-349	Millipore	1/2000

2.13 IN VIVO SARS-COV-2 INOCULATION

For intranasal inoculum administration, the animals were placed in an anesthesia chamber and anesthetized with isoflurane (Cat#RXISO-250, Medical and Veterinary Supplies) for 3 minutes. Once anesthetized, 35μL/nostril of the SARS-CoV-2 isolate diluted to $1*10^6$ PFU/mL in 1X PBS containing 0.3% BSA (Cat#A3294-100G, Sigma-Aldrich) was delivered via a 100μL micropipette tip. For aerosol inoculation, the animals were placed into an Inhalation Exposure System (Cat#099C-A4212/099C-A4224, Glas-Col LLC) and exposed to 5mL of the SARS-CoV-2 variant at $1*10^6$ PFU/mL. Body weight, physical activity, and lethargy were monitored daily following inoculation.

2.14   TISSUE SAMPLE COLLECTION

At the terminal endpoint, the animals were subjected to an isoflurane overdose followed by cervical dislocation. After confirmation of death, the nasal wash, lungs, and brains of the animals were collected. Nasal washes were collected by rinsing each nostril with 20µL of DMEM + 2% FBS + 1X PS. To prepare the nasal washes for RNA extraction, the 250µL of the samples were mixed with 750µL TRIzol LS and 200µL of chloroform. Extracted lungs were rinsed in 1X PBS before being placed in a gentleMACS M tube (Cat#130-093-236, Miltenyi Biotec) containing 1.2mL of 1X PBS or TRIzol (Cat#15596026, ThermoFisher Scientific) to collect the lung homogenates for viral titer testing or samples for RNA extraction, respectively. The lungs were homogenized in TRIzol or 1X PBS using the gentleMACS Tissue Dissociator (Cat#130-093-235, Miltenyi Biotec). These samples were then clarified via centrifugation at 500rpm for 5 minutes. The supernatant from the lung homogenate was transferred to 2mL microcentrifuge tubes with screw caps and further clarified via centrifugation at 1,000rpm for 3 minutes. The resulting supernatant was transferred to 2mL microcentrifuge tubes with screw caps for storage at -80°C. The lung supernatant bound for RNA extraction was transferred to 2mL microcentrifuge tubes with screw caps containing 200µL chloroform and stored at -80°C. The brains of the animals were harvested, placed in 2mL microcentrifuge tubes with screw caps containing 0.5mL 1.0mm Zirconia Beads (Cat#11079110Z, BioSpec Products), and homogenized in a Sonibeast cell disrupter (Cat#BS:715-12, BioSpec Products) for 2 minutes. The brain samples were then centrifuged at 1,000rpm for 3 minutes, and the supernatant was transferred to 2mL microcentrifuge tubes with screw caps for storage at -80°C. Before storage, 200µL of chloroform was added to the RNA extraction samples.

2.15   QUANTIFICATION OF VIRAL LOAD VIA PLAQUE ASSAY

Viral titers of viral stocks and tissue samples were determined via plaque assay. VeroE6/TMPRSS2 (JCRB1819) cells were seeded at a density of $1.5*10^5$ cells/mL in 6-well plates and incubated at 37°C and 5% CO_2. Once the cells reached ~95% confluency, the maintenance media (1X DMEM + 10% FBS + 2% G418) was removed, and the wells were washed with 2mL of 1X PBS. Tenfold viral or tissue sample dilutions were created in infection media (1X DMEM + 2% FBS + 1X PS). After removing the 1X PBS from the wells, 200μL of the viral or sample dilutions were added to the cells, and the plates were incubated at 37°C and 5% CO_2 for 1 hour. During the 1-hour incubation, the plates were rocked every 15 minutes to ensure the dispersal of the stock or sample, and the primary overlay components were prepared. The overlay media, containing 2XMEM (Cat#11935046, Gibco) supplemented with 8% FBS, 2% 100X non-essential amino acids (NEAA) (Cat# 11140050, ThermoFisher Scientific), and 2% 1X PS, was prewarmed in a water bath at 45°C. The 2% SeaPlauqe Agarose (Cat#50105, Lonza) was prepared by dissolving 0.22g of agarose in 11mL of HyClone HyPure Cell Culture Grade Water (Cat#SH30529.02, Cytiva). The overlay media (2X MEM + 8% FBS + 2% 100X NEAA + 2% 1X PS) and the agarose were mixed (1:1) to create the primary overlay and incubated in a water bath at 45°C. Following the 1-hour incubation, 3mL of the primary overlay was added to each well in a swirling motion. The overlay was allowed to solidify at room temperature before the plates were incubated at 37°C and 5% CO_2 for 48 hours. After 48 hours, 2mL of 0.1% neutral red (Cat#N4638-5G, Sigma-Aldrich) in 1X PBS was added to each well. Plates were incubated at 37°C and 5% CO_2 for 5 hours before removing the neutral red stain and visualizing the plaques via a transilluminator.

2.16 REMDESIVIR TREATMENT OF SARS-COV-2-INFECTED ANIMALS

Remdesivir or vehicle administration to the prairie voles or K18hACE2 transgenic mice was conducted following aerosol inoculation with the UK (α) variant and SARS-CoV-2-Venus-2A, respectively. Remdesivir (GS-5734) (Cat#S8932, Selleckchem.com) was prepared by dissolving 10mg in 0.5mL of DMSO (Ref# 25-950-CQC, Corning) and mixed with 6mL of 10% Tween-80 (Cat#BP338-500, Fisher BioReagents). For vehicle solution preparation, 6mL of 10% Tween-80 was mixed with 0.5mL of DMSO. At 1 and 2dpi, 0.5mL of remdesivir or vehicle solution was administered via intraperitoneal (IP) injection.

2.17 QUANTIFICATION OF CYTOKINE MRNA VIA QRT-PCR

Table 2.2 lists the primers and TaqMan probes for the prairie vole cytokine and housekeeping genes selected for amplification. After preparing the 12µL volume reactions containing the TaqMan Master Mix, specific primers and probes, and 4µL of extracted RNA, qRT-PCR was performed with the StepOnePlus Real-Time PCR System with the same parameters listed above using the comparative Ct (ΔΔCt) method. For this quantification method, Ct values were expressed relative to a reference sample, a corresponding sample obtained from a uninfected prairie vole. Each experimental or control sample was run in duplicate. Quantification of the cytokine mRNA within the samples involved the following steps. First, the CT values for the target amplicon and the endogenous control (18S) were determined for each sample. Then, the difference between these values, the ΔCt value, was calculated to normalize for variations in the total amount of nucleic acid added to each reaction and the efficiency of the RT step. Next, the ΔCt for each experimental sample was subtracted from the ΔCt of the reference sample, giving the ΔΔCt value. Finally, the amount of target, normalized to 18S and relative to the reference sample, was calculated by $2^{-\Delta\Delta Ct}$.

Table 2.2: Primers and probes for PCR amplification of specific prairie vole cytokines

Cytokine	Fwd primer (5'-3')	Rev primer (5'-3')	Probe (5'-3')
IL-1β	GGCTGATGTTCC CATTCGTC	ATTCTGCCCATT GAGGTGGA	AGCTGCACTGCAGGCT CCGA
IL-6	CCCTCCTACTGG AGAAGCTG	TTGTCGAGTAGC CCTCATGG	TGGTCCTTGACCACTC CTTCTGCG
IL-10	TGGGAATAACTG CACCCACT	TGTCCAGCTGGT CCTTCTTT	TGCTCCGAGAGCTGCG AACAGCC
IFNγ	TTCAACAACAGC GAGGCAAA	TTTCCAACAGCG AAACAGCA	TGACCCGCAGGTCCAA CGCA
TNFα	AACCTGTAGCCC ACGTTGTA	GTACAGTCCATC TGCGGGTA	TGCCCTCCTGGCCAAC GGCA

2.18 RBD-8-HIS PROTEIN PURIFICATION

2.18.1 pcDNA3.1-SARS-CoV-2-RBD-8-His plasmid

This plasmid is a mammalian expression plasmid for the production of an RBD protein with a histidine (His) tag. It utilizes the human cytomegalovirus (CMV) promoter and was constructed by inserting the secreted RBD sequence from the spike protein within SARS-CoV-2 into the pcDNA3.1(+) vector containing a C-terminal 8-His tag.

2.18.2 Bacterial Cells and Media

Bacterial cells containing the pcDNA3.1-SARS-CoV-2-RBD-8-His (Plasmid#145145) plasmids were obtained from Addgene and grown in Luria-Bertani (LB) broth or on LB agar (Cat#BP1423-2, Fisher Scientific) containing 100µg/mL of ampicillin (Amp) (Cat#BP1760-5, Fisher BioReagents).

2.18.3 pcDNA3.1-SARS-CoV-2-RBD-8-His plasmid isolation

Bacterial cells were streaked onto LB agar plates containing 100μg/mL of Amp and incubated at 37°C overnight. A liquid culture was prepared in a 14mL round-bottom polypropylene test tube by inoculating 5mL of LB broth containing 100μg/mL of Amp with cells selected from a single, isolated colony. This culture was incubated at 37°C and 250rpm for 8 hours. Next, 250μL of the 8-hour culture was used to inoculate 250mL of LB broth containing 100μg/mL. Then, this culture was incubated overnight at 37°C and 250rpm. The overnight culture was transferred to a 500mL RC-6 centrifuge tube and centrifuged at 8,000rpm for 10 minutes at 4°C.

After pelleting the culture, the plasmid was isolated using the Purelink HiPure Plasmid Filter Maxi Prep Kit from Invitrogen (Cat#K21007). The supernatant was discarded, and the pellet was resuspended in 10mL of resuspension buffer (containing RNase A) until homogenous. Next, 10mL of lysis buffer was added to the suspension. The suspension was mixed thoroughly by inverting the tubes 4-5 times and incubated at room temperature for 5 minutes. Then, 10mL of neutralizing buffer was added to the tube, which was inverted 4-5 times to mix. After equilibrating the column with 30mL of equilibration buffer, the lysate was transferred to the filtration column and filtered through the column via gravity flow. The column was washed twice, with 10mL and then 50mL of wash buffer, and allowed to drain via gravity flow. Next, 15mL of elution buffer was added to the column to elute the DNA into a 35mL RC-6 centrifuge tube. The elution was mixed with 10.5mL of room temperature IPA and centrifuged at 12,000rpm for 30 minutes at 4°C. The pellet was washed with 5mL of room temperature 70% ethanol and centrifuged at 12,000rpm for 5 minutes at 4°C. The supernatant was discarded from the tube, and the pellet was air-dried for 10 minutes at room temperature. Then, the pellet was resuspended in 500μL of TE buffer.

The concentration and purity of the eluted DNA were measured with a NanoDrop One Microvolume UV-Vis Spectrophotometer. DNA purity of isolated plasmids was confirmed by agarose gel electrophoresis. The 0.8% agarose gel containing 0.025mg of ethidium bromide was visualized using an iBright FL1000 imaging system.

2.18.4 Transfection of pcDNA3.1-SARS-CoV-2-RBD-8-His

Expi293F cells were seeded at $3.0*10^6$ cells/mL in a 1000mL Erlenmeyer Shaker Flask (Cat#4115-1000, ThermoFisher Scientific). The transfection was performed using the Expifectamine 293 Transfection Kit from Gibco (Ref#A14524). To begin this process, 640µL of expifectamine was mixed with 12mL of OptiMEM in a 50mL conical tube. Next, 290µL of the isolated plasmid was mixed with 11.2mL of OptiMEM in a separate 50mL conical tube. Both tubes were incubated at room temperature for 5 minutes before mixing the solutions. The mixture was incubated at room temperature for 20 minutes before adding the mixture to the cells in the 1000mL shaker flask. The transfected cells were incubated overnight at 37°C, 8% CO_2, and 100rpm. The following day, 1.2mL of enhancer one and 12mL of enhancer two were added to the transfected cells. The cells were incubated at 37°C, 8% CO_2, and 100rpm for five days. The cells were collected and purified six days post-transfection using a His Trap HP 5mL purification column (Cat#17524801, Cytiva).

2.18.5 Purification of RBD-8-His protein via affinity chromatography

Transfected cells and media were transferred to 5-50mL conical tubes and centrifuged at 1,000rpm for 5 minutes at room temperature. The supernatant was transferred to a 500mL RC-6 centrifuge tube. Next, 1mM phenylmethylsulfonyl fluoride (PMSF) protease inhibitor (Cat#36978, ThermoFisher Scientific) in 100% ethanol was added to the supernatant, and it was centrifuged at 8,000rpm for 15 minutes at room temperature. After mixing the resulting supernatant with an

additional 1mM PMSF protease inhibitor, it was filtered through a 0.45μM Millex-HV syringe filter unit (Cat#SLHVM33RS, Millipore).

The His Trap HP 5mL purification column was attached to a peristaltic pump and calibrated to a flow rate of 3mL/minute. Next, the column was washed with 5 column volumes (CVs), or 25mL, of 10% ethanol and then 5 CVs of deionized water (diH$_2$O). After the column was equilibrated with 5 CVs of loading buffer, the prepared protein sample was loaded onto the column. Refer to Table 2.3 for buffer composition. The column was washed twice with 5 CVs of loading buffer. The protein was eluted with 5 CVs of elution buffer, and the elution fractions were collected in 2.5mL aliquots.

Table 2.3: RBD-8-His protein purification buffer composition

Buffer	Tris pH 8.0	NaCl	Imidazole pH 8.0	Glycerol
Loading	50mM	500mM	2.5mM	5%
Wash	50mM	500mM	25mM	5%
Elution	50mM	500mM	250mM	5%
Dialysis	50mM	500mM	-	5%

2.18.6 SDS PAGE of column fractions

SDS PAGE samples were prepared by mixing 15μL of the column fractions with 4X SDS PAGE loading dye. The samples were denatured at 65ºC for 10 minutes, and 18μL of samples and 3μL of the Precision Plus Protein Dual Color Standards ladder were loaded onto the 4-20% Mini-PROTEAN TGX Precast Protein Gels. The gel was run at 200 volts for 30 minutes and stained with the GelCode Blue Safe Protein Stain (Cat#24596, ThermoFisher Scientific). In this staining process, the gels were microwaved in 100mL of diH$_2$O for 1.5 minutes in 30-second intervals and then incubated on a shaker for 5 minutes at room temperature. Next, the gels were microwaved in

61

20mL of Blue Safe Protein Stain for 1.5 minutes in 30-second intervals and then incubated on a shaker for 5 minutes at room temperature. The gels were destained overnight in 100mL of diH$_2$O on a shaker at room temperature.

The elution fractions (as determined by SDS PAGE) containing the protein were pooled and concentrated down to 1.5mL in a 10,000 molecular weight cut-off (MWCO) Amicon Ultra-15 Centrifugal Filter Unit (Cat#UFC910008, MilliporeSigma) via centrifugation at 4,000g. The concentrated protein sample was transferred to a 0.5-3mL 10,000 MWCO Slide-A-Lyzer Dialysis Cassette (Cat#66380, Thermo Scientific). The cassette was dialyzed in 1L of dialysis buffer at 4°C overnight. The dialyzed sample was transferred from the cassette to a 2mL microcentrifuge tube with a screw cap and stored at -20°C. The concentration of the purified protein was determined via NanoDrop.

2.19 GENERATION OF A SARS-COV-2 PRAIRIE VOLE-ADAPTED VARIANT

A SARS-CoV-2 prairie vole-adapted variant was generated by 15 *in vivo* serial passages followed by plaque purification in VeroE6/TMPRSS2 cells. For the first passage, prairie voles were intranasally inoculated with the UK (α) variant of SARS-CoV-2 at $1.0*10^5$ PFU/mL. At 3dpi, the lungs of the infected voles were harvested and homogenized in 1X PBS using the gentleMACS Tissue Dissociator. The homogenate was centrifuged at 500rpm for 5 minutes at room temperature, and the supernatant was used for the second passage. Specifically, 70μL (35μL/nostril) of the supernatant was intranasally administered to anesthetized voles. Intranasal inoculation of voles with the lung homogenate of the previous passage was repeated up to passage 15.

2.20   SEQUENCING OF THE SARS-COV-2 VOLE-ADAPTED VARIANT

2.20.1 Plaque purification of passage viruses

VeroE6/TMPRSS2 cells were seeded in 6-well plates at $1.5*10^5$ cells/mL and incubated at

37°C and 5% CO_2 overnight. After removing the maintenance media (1X DMEM + 10% FBS +

2% G418) and washing the wells with 1mL of 1X PBS, the cells were inoculated with 200μL of

the passage viruses diluted in infection media (1X DMEM + 2% FBS + 1X PS). The plates were

incubated at 37°C and 5% CO_2 for 1 hour and rocked every 15 minutes to ensure the dispersal of

the virus particles. The primary overlay was prepared by mixing 2% SeaPlaque agar in Cell Culture

Grade Water and overlay media (2X MEM + 8% FBS + 2% NEAA + 1X PS) in a 1:1 ratio and

incubated at 45°C. Next, 3mL of the primary overlay was added to each well and allowed to

solidify at room temperature. The plates were incubated at 37°C and 5% CO_2 for 48 hours, and the

virus plaques were visualized after staining with 2mL of 0.1% neutral red in 1X PBS for 5 hours.

Individual virus plaques were collected using a micropipette and transferred to a microcentrifuge

tube containing 500μL of maintenance media (1X DMEM + 10% FBS). The tubes were incubated

at 4°C overnight to dissolve the agar. The following day, 250μL of the viral suspension was mixed

with 750μL of TRIzol LS and 200μL of chloroform. RNA of each clonal isolate was extracted in

the BSL-2 facility and used for sequencing analysis.

2.20.2 Next generation sequencing (NGS) and analysis

SARS-CoV-2 whole viral genome targeted NSG was conducted using the following

procedures. First, complementary DNA (cDNA) was generated from viral RNA using the

SuperScript IV First-Strand Synthesis System (Cat#18091050, Invitrogen). Next, cDNA libraries

were constructed using the xGen SARS-CoV-2 Amplicon Panels (Cat#10009832, IDT). Libraries

were generated following the low viral load input plate protocol and quantified with Qubit 1X

dsDNA High Sensitivity (HS) and Broad Range (BR) Assay Kit (Cat#Q33230, Invitrogen). After verifying the quality of the libraries using a 4200 TapeStation with D1000 ScreenTape (TapeStation Instruments), they were normalized using the xGen Normalse Module (Cat#10009793, IDT) and sequenced using a MiSeq System (Illumina) in combination with the MiSeq Reagent Kit v3 (600-cycle) (Cat#MA-102-3003, Illumina). The sequences were demultiplexed and saved as FASTQ files.

Reads were trimmed for quality using Trimmomatic and aligned to the Wuhan COVID-19 reference sequence (NCBI reference sequence: NC045512.2) using Burrows-Wheeler aligner (bwa). Next, PCR duplicates were removed, and the sequences were sorted and indexed using Samtools. A complied VCF file containing the sample sequences was created using Bcftools *mpileup*. Bcftools *consensus* was then used to reconstruct sample sequences. Lastly, the sample and reference sequences were imported into Geneious and aligned using MAFFT.

2.21 DATA ANALYSIS

Figures and schematics were generated using BioRender (BioRender Software, Toronto, Ontario, Canada). Graphs were generated and evaluated for significance using GraphPad Prism 10.1.2.324 for Windows (GraphPad Software, San Diego, California, USA). Differences between means were analyzed using paired or unpaired t-tests and one-way ANOVAs and were deemed significant at $p < 0.05$.

Chapter 3: Results and Discussion

3.1   IN VITRO SUSCEPTIBILITY OF PRAIRIE VOLES TO SARS-COV-2

3.1.1   **In vitro pseudovirus infectivity assay**

Since the beginning of the pandemic, researchers have performed multiple sequence alignments on ACE2 proteins from various species and discovered substantial homology and conservation of specific amino acid residues involved in RBD binding shared among humans and other mammals (Hayashi et al., 2020). These findings indicate a significant level of conservation in the ACE2 protein sequence across different species. To determine the level of conservation between humans and prairie voles, we conducted a Needleman-Wunsch Global (pairwise) alignment (NIH, NCBI Web BLAST, blast.ncbi.nlm.nih.gov) using the hACE2 protein sequence (Gen Bank: BAB40370.1) as the query sequence and the moACE2 protein sequence as the subject sequence. We also conducted pairwise alignments showcasing the homology of the hACE2 protein sequence to that of other species that are established SARS-CoV-2 infection models (Table 3.1). The moACE2 protein sequence shares 84% homology with that of the hACE2 protein sequence (Table 3), which was higher than the 82% homology shared between humans and ferrets and was comparable to the homology shared between humans and the Golden Syrian hamster.

Building on these findings, we hypothesized that the moACE2 receptor would facilitate viral entry. To test this hypothesis, we employed HEK293T cells expressing the hACE2 or moACE2 receptors alone or in combination with the hTMPRSS2. These cells were then infected with VSV-ΔG-luciferase pseudoparticles carrying the SARS-CoV-2 S protein. After an incubation period of eighteen hours, we measured luciferase activity. The results indicated that akin to the hACE2 receptor, the moACE2 receptor mediates viral entry, and this process is further enhanced by the expression of the hTMPRSS2 (Figure 3.1).

Table 3.1: Percent identities of the hACE2 protein sequence compared to subject sequences

Species	NCBI Ref Sequence	%Identities
Chlorocebus sabaeus (African green monkey)	XP_037842285.1	95
Mustela putorius furo (Ferret)	NP_001297119.1	82
Mesocricetus auratus (Golden Syrian hamster)	XP_005074266.1	84
Mus Musculus (Mouse)	NP_001123985.1	82
Microtus ochrogaster (Prairie vole)	XP_005358818.1	84
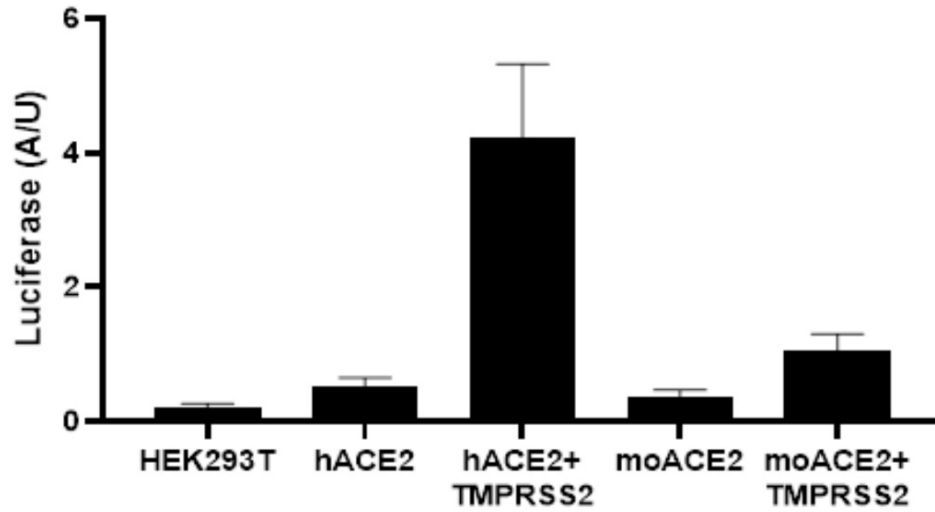
Figure 3.1: In vitro pseudovirus infectivity assay. HEK293T, HEK293T hACE2/hTMPRSS2, and HEK293T moACE2/hTMPRSS2 cells were infected with VSV-ΔG-luciferase-S pseudoparticles. Luciferase activity was measured 18 hours post-infection.

3.1.2 In vitro SARS-CoV-2 infectivity assay

Based on the results of the infectivity assay with the pseudoparticles, we tested the moACE2 receptor's ability to mediate the entry of various SARS-CoV-2 variants *in vitro*. In this experiment, HEK293T hACE2/hTMPRSS2 and moACE2/hTMPRSS2 cells were infected with the WA1/2020 isolate, and the UK (α), Delta, Epsilon, Kappa, Lambda, Mouse-adapted, and Zeta variants. The viral titer ($TCID_{50}$/mL) of each variant was determined at 24-hour intervals post-infection over 72 hours, and the viral RNA levels produced by each variant 3dpi were determined via qRT-PCR. Figure 3.2A illustrates the variants that yielded the highest viral titers as determined via $TCID_{50}$ assay. At 24 hours post-infection, the lambda variant had the highest viral titer at $2.0*10^3$ $TCID_{50}$/mL, but this titer decreased after 72 hours. At 48 hours post-infection, the WA1/2020 isolate plateaued at $2.0*10^3$ $TCID_{50}$/mL. The viral titer of the Delta variant remained steady at $2.0*10^2$ $TCID_{50}$/mL over the 72-hour infection. Figure 3.2B shows the number of viral RNA copies detected via qRT-PCR 72 hours post-infection, with the highest levels of viral RNA copies detected 72 hours post-infection in the Delta variant. These *in vitro* results underscore the moACE2 receptor's ability to mediate viral entry of SARS-CoV-2 variants, and they suggest that the prairie voles are more susceptible to the WA1/2020 isolate and the Delta and Lambda variants.
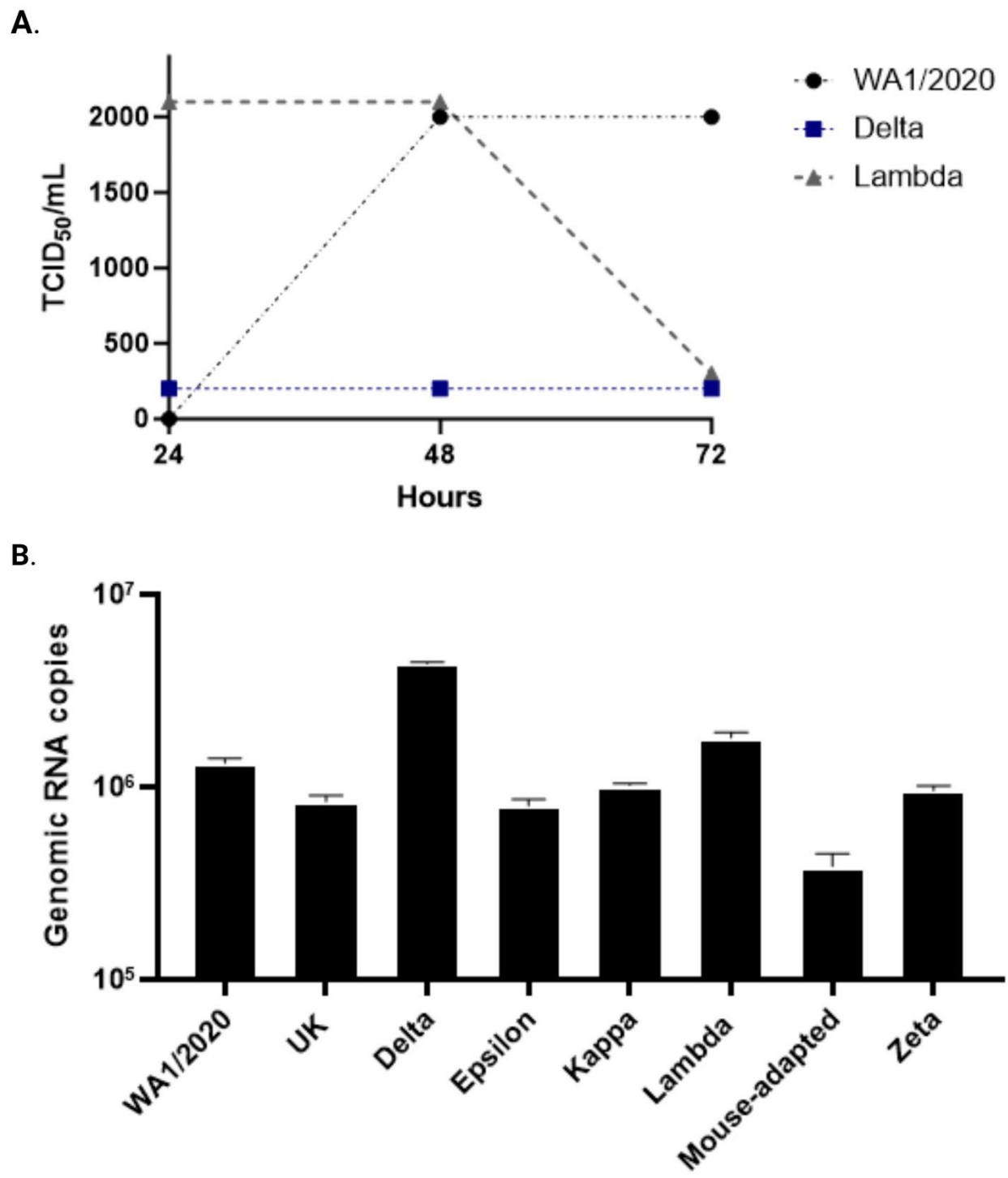
Figure 3.2: In vitro SARS-CoV-2 infectivity assay. HEK293T cells were infected with various SARS-CoV-2 variants. **A**. TCID50/mL of the WA1/2020, Delta, and Lambda variants throughout the 72-hour infection. **B**. Genomic RNA copies detected via qRT-PCR after 72-hour infection with the corresponding SARS-CoV-2 variants. n = 2 for technical replicates.

3.2 VIRULENCE ASSAY OF SARS-COV-2 VARIANTS

Because the S protein regulates viral attachment to the host receptor, it plays a crucial role in defining the virulence of SARS-CoV-2 (Kumavath et al., 2021). Changes in S protein cleavability can significantly impact viral infectivity. For example, increased S1/S2 cleavability enhances membrane fusion and thus enhances viral virulence (Takeda, 2022). Since the UK (α) variant has been associated with increased virulence, we assessed the S protein of the UK (α) variant via Western blot. Compared to the WA1/2020 isolate, we observed a band shift from 180 kilodaltons (kDa) to ~100kDa, as well as two distinct bands at ~100kDa in the UK (α) variant (Figure 3.3). These data suggest that the increase in virulence associated with the UK (α) variant is due to enhanced S protein cleavability.
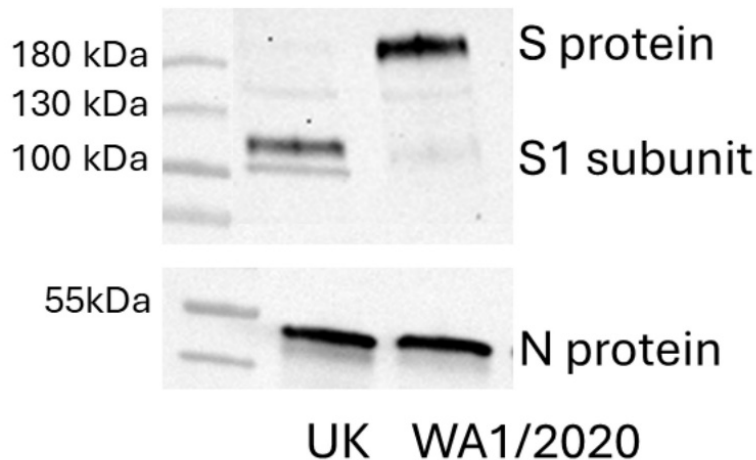
Figure 3.3: Virulence assay of SARS-CoV-2 isolates. The S protein of the UK (α) variant and the WA1/2020 isolate were assessed via Western blot for cleavage. SDS-PAGE was run at 200 volts for 30 minutes with 20μg of each variant. The proteins were transferred to a nitrocellulose membrane at 200 volts for 2 hours at 4°c. The membrane was probed with mouse anti-SARS-CoV-2 S and N protein antibodies and then goat anti-mouse secondary antibody conjugated with HRP. The membrane was visualized using a chemiluminescent substrate and an iBright FL1000. The N protein was used as a loading control.

3.3 **INTRANASAL INOCULATION OF PRAIRIE VOLES WITH THE WA1/2020 ISOLATE**

Given the *in vitro* results, we assessed whether the prairie voles were susceptible to SARS-CoV-2 infection *in vivo*. In this experiment, the prairie voles were subjected to intranasal administration of hCoV-19/USA-WA1/2020 at $7*10^4$ PFU (70µL at $1*10^6$ PFU/mL) (Figure 3.4A). After virus inoculation, the prairie voles were monitored for clinical signs of disease via body weight. Since SARS-CoV-2 predominantly causes acute respiratory disease by infecting the respiratory system (M.-Y. Li et al., 2020), we collected the lungs and nasal wash of the infected animals to quantify the number of RNA copies within each; however, given the large percentage of SARS-CoV-2 patients that have displayed neurological symptoms such as anosmia, confusion, epileptic seizures, and stroke (Helms et al., 2020; Paterson et al., 2020), we also collected the brains of the infection animals for analysis via qRT-PCR. While no fluctuation in body weight was detected after *in vivo* inoculation of the prairie voles with the WA1/2020 isolate (Figure 3.5D), we did detect ~10^4 viral RNA copies in the lungs and brains and ~10^6 viral RNA copies in the nasal wash of the animals 2dpi (Figure 3.4B-D). At 4dpi, we observed an increase of viral RNA copies in the tissues and nasal wash of the prairie voles compared to 2dpi (Figure 3.4B-D). From these data, we concluded that prairie voles are susceptible to intranasal inoculation with the WA1/2020 isolate.
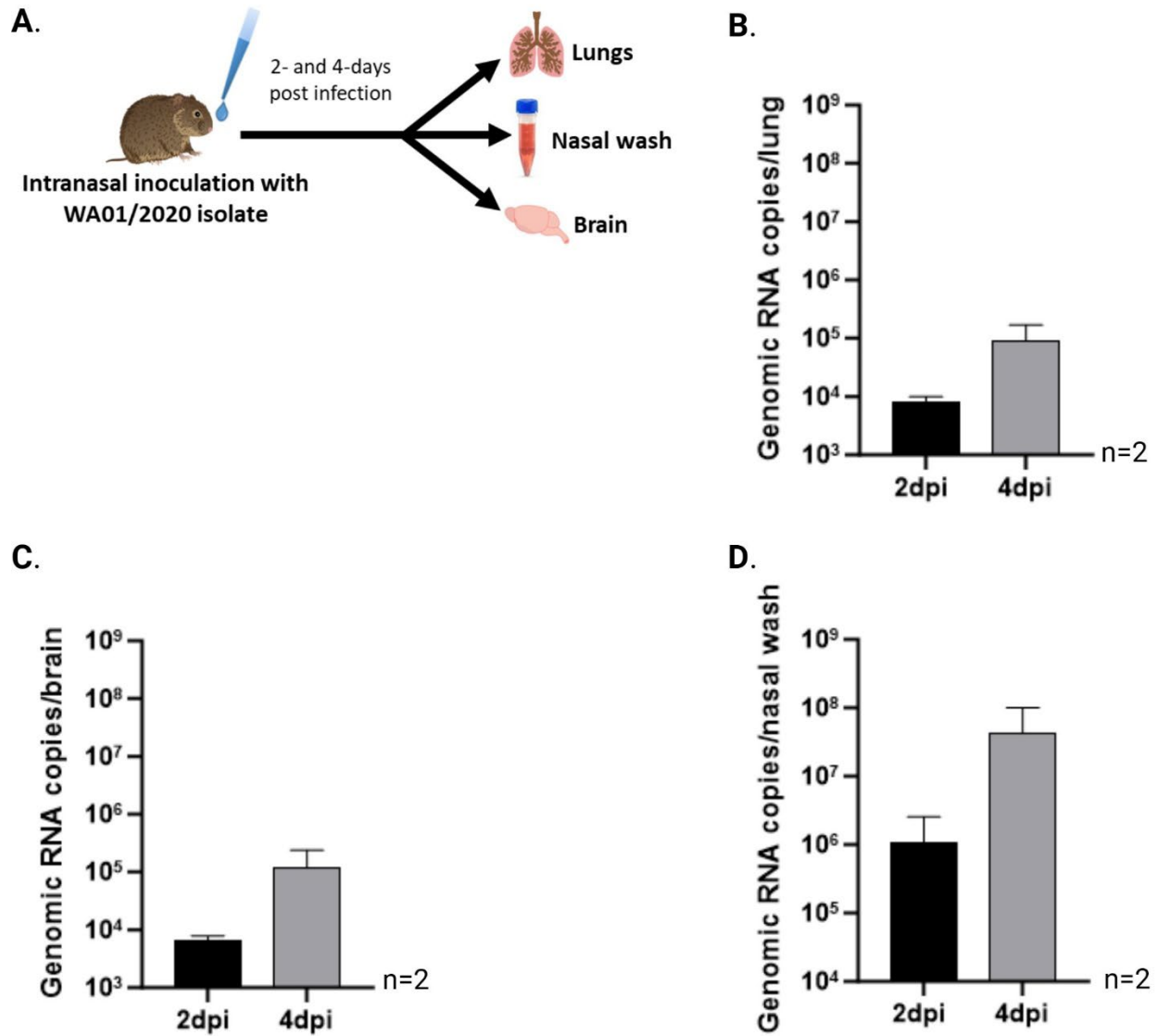
Figure 3.4: Intranasal inoculation of prairie voles with WA01/2020 isolate. **A**. Schematic for animal infection. **B**. The number of viral RNA copies in the lungs of infected prairie voles 2 and 4dpi as determined by qRT-PCR. **C**. The number of viral RNA copies in the brains of infected prairie voles 2 and 4dpi as determined by qRT-PCR. **D**. The number of viral RNA copies in the nasal wash of infected voles 2 and 4dpi as determined via qRT-PCR. n=2 for biological replicates. n=2 for technical replicates.

3.4   INTRANASAL INOCULATION OF PRAIRIE VOLES WITH THE UK (A) VARIANT

Because the UK (α) variant has been associated with a greater risk of mortality (Challen et al., 2021), we compared prairie vole susceptibility between this variant and the WA1/2020 isolate. The prairie voles were intranasally inoculated with $7*10^4$ PFU (70µL at $1*10^6$ PFU/mL) of the UK (α) variant and monitored for clinical symptoms over 10 days. Again, there were no differences in body weight following infection (Figure 3.5D). At 4dpi, we detected significantly higher levels of viral RNA copies in the lungs of the UK (α)-infected prairie voles than those infected with the WA1/2020 isolate (Figure 3.5A). Conversely, we detected no significant difference in the viral RNA copies in the brains and nasal wash of the WA1/2020 or UK (α)-infected animals (Figure 3.5B&C). These data suggest that the UK (α) variant has improved tropism for the lungs of infected prairie voles following intranasal administration.
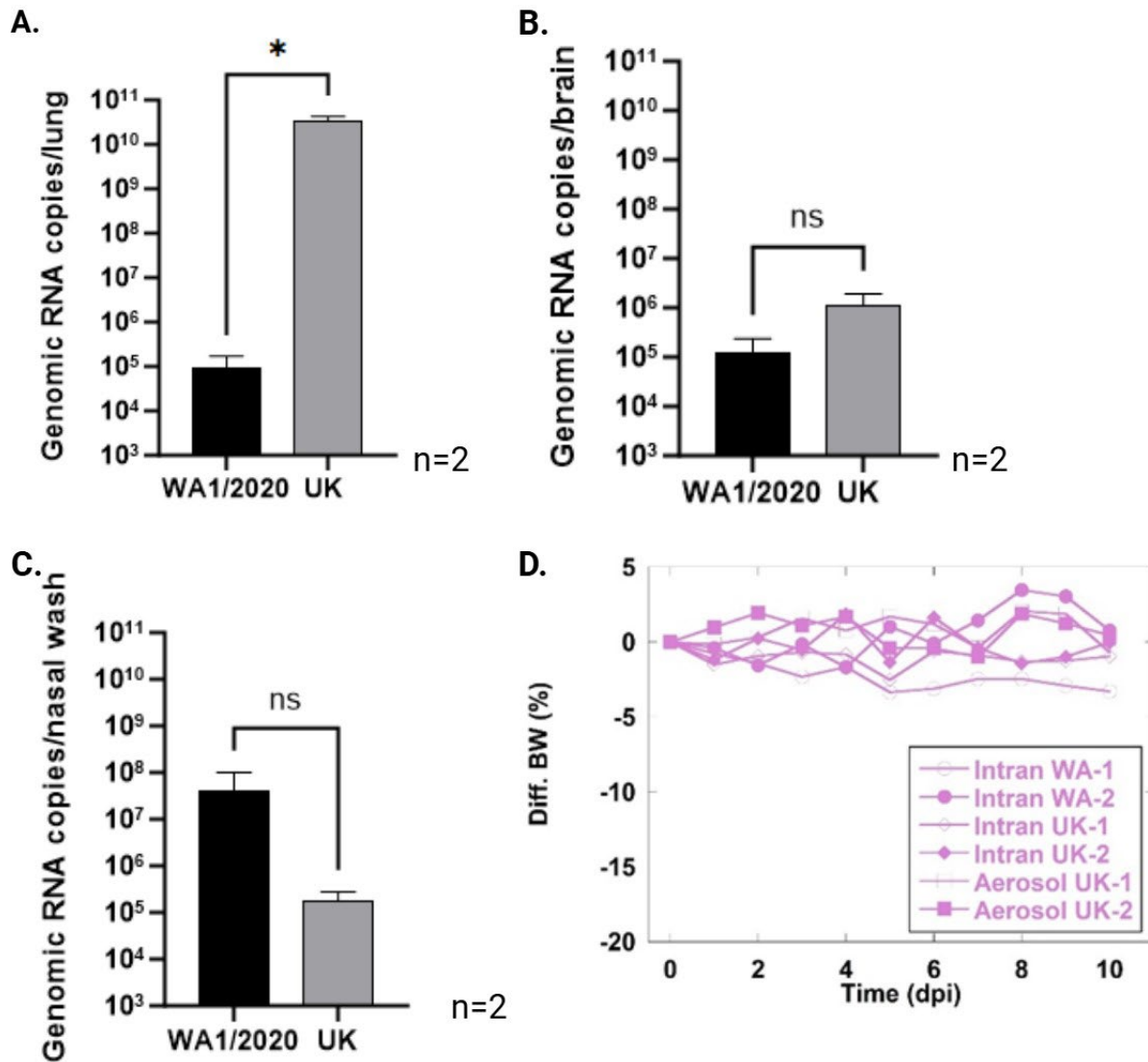
Figure 3.5: Intranasal WA1/2020 vs intranasal UK (α) inoculation of prairie voles 4dpi. **A**. Number of viral RNA copies in the lungs of WA1/2020 and UK (α)-infected prairie voles 4dpi. **B**. The number of viral RNA copies in the brains of WA1/2020 and UK (α)-infected prairie voles 4dpi. **C**. The number of viral RNA copies in the nasal wash of WA1/2020 and UK (α)- infected prairie voles 4dpi. The number of viral RNA copies was determined via qRT-PCR. n=2 for biological replicates and n=2 for technical replicates. **D**. Body weight of WA1/2020 and UK (α)-infected prairie voles.

3.5 AEROSOL INOCULATION OF PRAIRIE VOLES WITH THE UK (Α) VARIANT

Since SARS-CoV-2 is an airborne infectious disease, we tested prairie vole susceptibility to aerosolized SARS-CoV-2 and compared this delivery method to the intranasal method. The animals were placed into an inhalation exposure system for this study and exposed to 5mL of the UK (α) variant at $1*10^6$ PFU/mL (Figure 3.6A). Body weight was measured daily over 4 days with no marked differences noted (Figure 3.5D). Tissues and nasal wash were collected at 2 and 4dpi and analyzed for the presence of viral RNA copies and viral particles. While there was no statistical difference in the number of viral RNA copies in the lungs or brains of the infected prairie voles at 2dpi (Figure 3.6B&C), there was a statistical difference in the number of viral RNA copies in their nasal wash, as seen by the significantly reduced number of viral RNA copies in the infected animals at 4dpi compared to those at 2dpi (Figure 3.6D).

Similarly, the $TCID_{50}$ and plaque assay showed statistically higher viral titers in the nasal wash of the prairie voles at 2dpi than at 4dpi (Figure 3.6E&F). These findings suggest that the viral shedding of the UK (α) variant peaks at 2dpi.

In comparison to the intranasal inoculation, we observed no statistical difference in viral RNA copies in the lungs, brains, and nasal wash (Figure 3.7A-C) or viral titers in the nasal wash (Figure 3.7D&E) of the infected prairie voles 4 days following aerosolized exposure to the UK (α) variant. Since there was no difference in prairie vole susceptibility based on the delivery method of the UK (α) variant, we concluded that aerosol administration was as successful as intranasal administration.
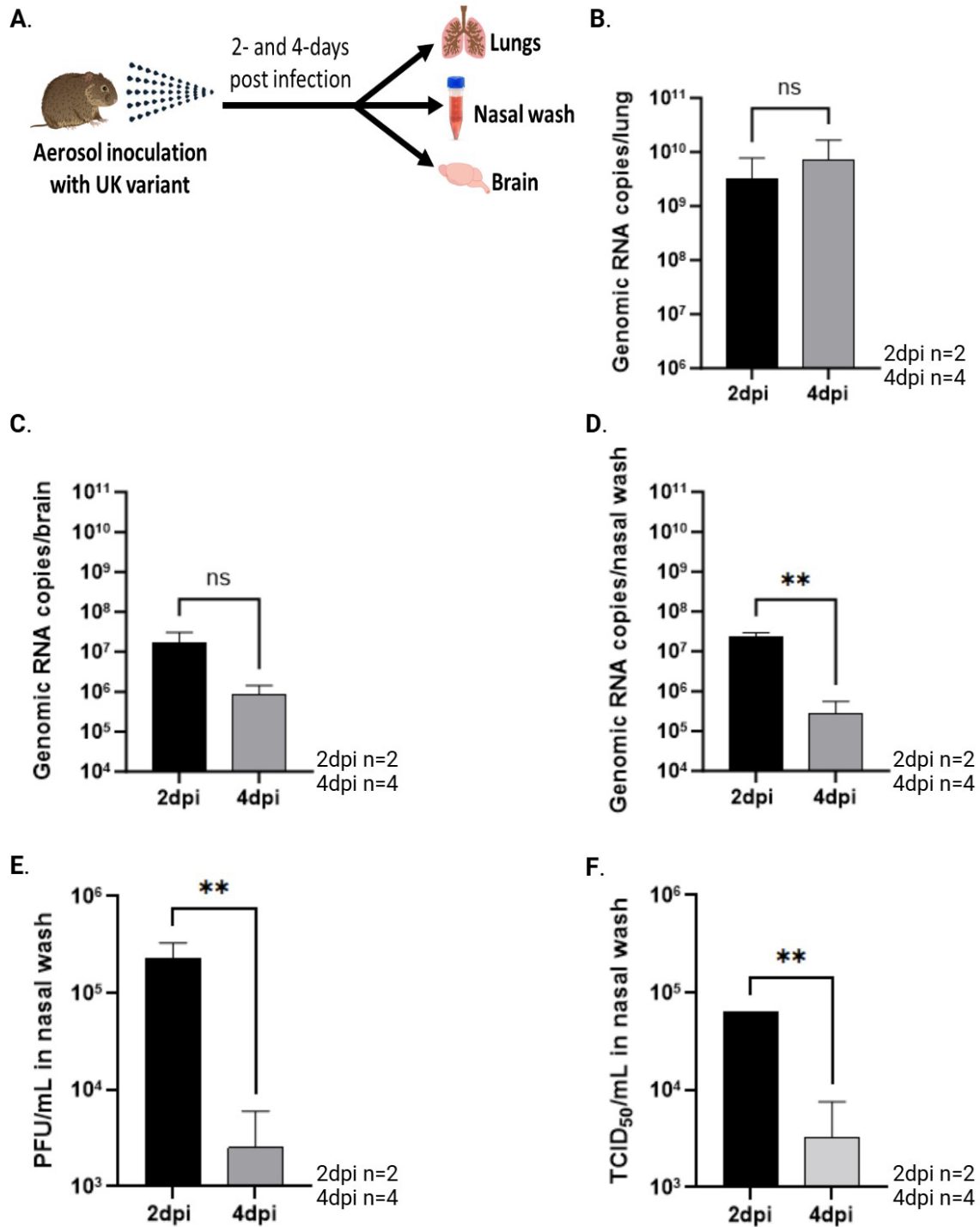
Figure 3.6: Aerosol inoculation of prairie voles with the UK (α) variant. **A**. Schematic for animal infection. **B-D**. The number of viral RNA copies in the lungs, brains, and nasal wash of infected animals 2 and 4dpi determined via qRT-PCR. n=2 for day 2 biological replicates. n=4 for day 4 biological replicates. n=2 for qRT-PCR technical replicates. **E**. PFU/mL in the nasal wash from UK (α)-infected prairie voles 2 and 4dpi. **F**. TCID$_{50}$/mL in the nasal wash from UK (α)-infected prairie voles 2 and 4dpi. n=2 for day 2 biological replicates. n=4 for day 4 biological replicates.
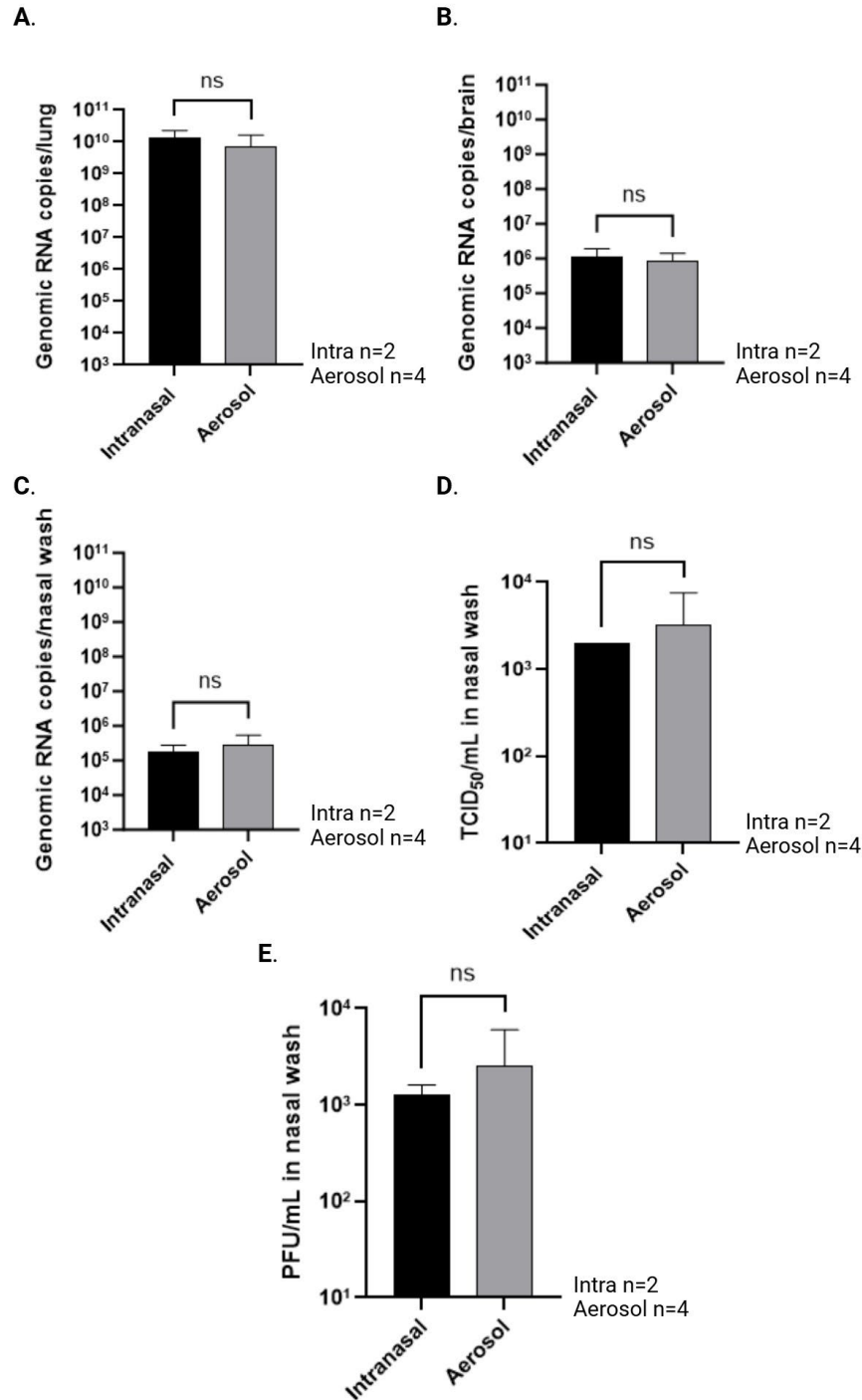
Figure 3.7: UK (α) intranasal vs aerosol inoculation of prairie voles. **A-C**. The number of viral RNA copies in the lungs, brains, and nasal wash of infected animals 4dpi as determined via qRT-PCR. n=2 for intranasal biological replicates. n=4 for aerosol biological replicates. n=2 for qRT-PCR technical replicates. **D**. $TCID_{50}$/mL in the nasal wash from UK (α)-infected prairie voles 4 days after intranasal or aerosol inoculation. **E**. PFU/mL in the nasal wash from UK (α)-infected prairie voles 4 days following intranasal or aerosol inoculation. n=2 for intranasal biological replicates. n=4 for aerosol biological replicates.

3.6   **AEROSOL INOCULATION OF PRAIRIE VOLES WITH THE DELTA VARIANT**

Based on increased disease severity and transmissibility associated with the Delta variant in humans (X. N. Li et al., 2021; Zayet et al., 2022), we evaluated whether this variant would increase disease severity in the prairie voles following aerosol administration. In this study, the prairie voles were subjected to 5mL of the aerosolized Delta variant at $1*10^6$ PFU/mL. Body weight and physical activity were monitored to an experimental endpoint of 14 days, with tissue collections occurring at 3, 7, and 14dpi (Figure 3.8A). Minimal changes in body weight and no changes in physical activity were noted throughout this experiment. Viral RNA copies within the lungs of the Delta-infected prairie voles peaked at 3dpi and were markedly decreased but still detectable at 14dpi (Figure 3.8B).

To assess the host response to this variant, we utilized qRT-PCR to analyze cytokine levels within the lungs of infected prairie voles 3 and 7dpi. Relative to the uninfected animals, the infected animals showed evaluated cytokine expression at 3dpi (Figure 3.8C). At 7dpi, the cytokine levels within the lungs of the infected animals had decreased compared to those at 3dpi but were still evaluated relative to the uninfected animals (Figure 3.8D). As a result, we concluded that infection with the Delta variant induces inflammatory cytokine production in the lungs of prairie voles.
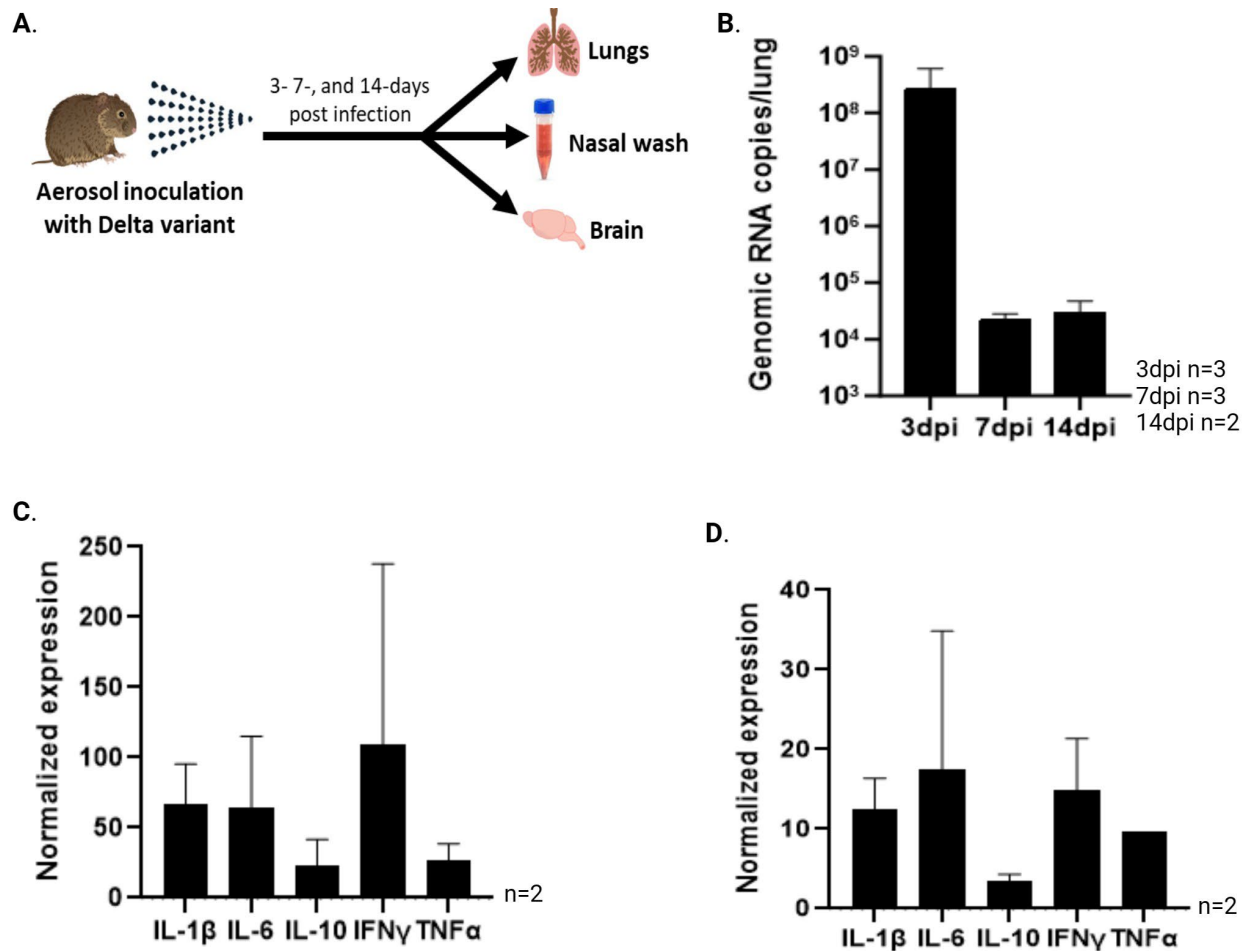
Figure 3.8: Aerosol inoculation of prairie voles with the Delta variant. **A**. Schematic for animal infection. **B**. The number of viral RNA copies in the lungs of Delta-infected animals 3, 7, and 14dpi as determined via qRT-PCR. n=3 for day 3 and 7 biological replicates. n=2 for day 14 biological replicates. n=2 for qRT-PCR technical replicates. **C&D**. Inflammatory cytokine levels in Delta-infected animals 3 and 7dpi determined via qRT-PCR. Expression levels were normalized to inflammatory cytokine levels in uninfected animals. n=2 for biological replicates. n=2 for technical replicates.

3.7   INTRANASAL INOCULATION OF PRAIRIE VOLES WITH THE BETA VARIANT

Due to the lack of clinical symptoms observed in the prairie voles following infection with the WA1/2020 isolate and the UK (α) and Delta variants, we decided to perform an infection study using the Beta variant. Because BALB/c mice are susceptible to this variant (Kant et al., 2021) (as opposed to other variants), we hypothesized that this variant might be more suitable to infect rodents. For this study, we propagated the Beta stock (p1), initially amplified in VeroE6/TMPRSS2 cells, in prairie voles (p2) before infecting the experimental animals to reduce interference with receptor-RBD binding. After the prairie voles were intranasally inoculated with $7*10^4$ PFU (70μL at $1*10^6$ PFU/mL) of the Beta p2 variant, we monitored their body weight and collected tissue samples 3 and 7dpi (Figure 3.9A). Minimal changes in body weight were detected over the 7-day study. However, we detected at least 10^5 PFU/mL in the nasal wash and lung homogenate of the Beta-infected animals 3dpi (Figure 3.9B). These data demonstrate that the prairie voles, like the BALB/c mice, are susceptible to the Beta variant.
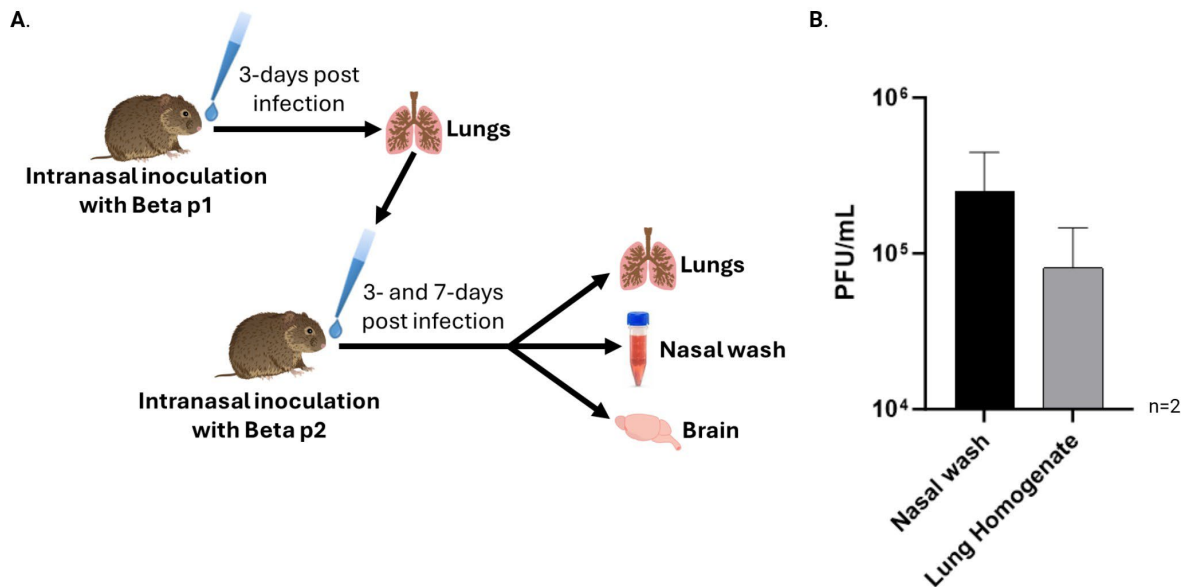
Figure 3.9: Intranasal inoculation of prairie voles with the Beta variant. **A**. Schematic for animal infection. **B**. PFU/mL in nasal wash and lung homogenates of Beta-infected animals 3dpi. n=2 for biological replicates.

3.8   TRANSMISSION OF SARS-CoV-2 FROM INFECTED TO UNINFECTED PRAIRIE VOLES

To assess viral transmission between prairie voles, we infected half of the animals in the study group with 5mL of UK (α) variant at $1*10^6$ PFU/mL using an inhalation exposure system. Immediately following inoculation, we placed the infected prairie voles in a clean cage with an uninfected cage mate (Figure 3.10A). Both animals were monitored over 7 days for loss of weight and reduced physical activity. No changes in body weight or activity levels were observed in either animal group. Viral RNA copies in the tissues and nasal wash of the uninfected animals were detected at 4dpi and increased at 7dpi (data not shown). By 7dpi, the levels of viral RNA copies in the brains and nasal wash of the uninfected animals were comparable or higher, respectively, to those detected in the brains and nasal wash of the infected animals (Figure 3.10B). Lower levels of viral RNA copies in the lungs of the uninfected animals at 7dpi (Figure 3.10B) suggest delayed viral migration to the lower respiratory tract or a change in tissue tropism following transmission. In either case, these results demonstrate SARS-CoV-2 transmission among prairie voles.
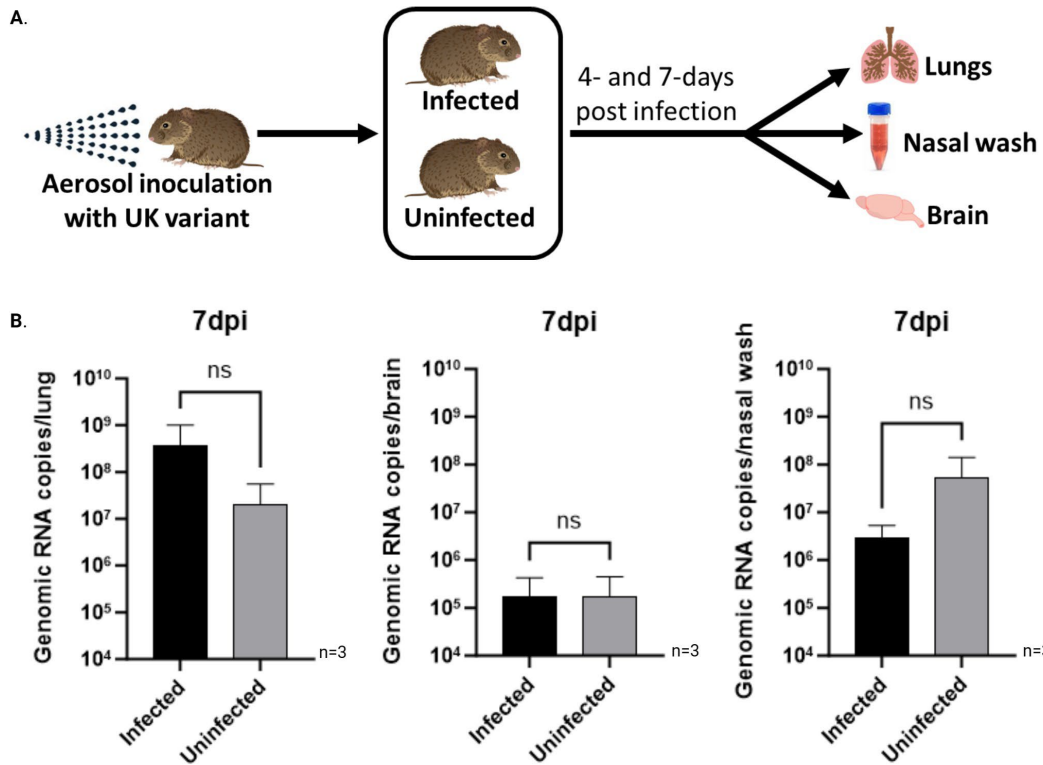
Figure 3.10: Prairie vole UK (α) transmission study. **A**. Schematic for UK (α) variant transmission study. **B**. The number of viral RNA copies detected in the tissues and nasal wash of infected and uninfected animals 7dpi as determined by qRT-PCR. n=3 for biological replicates. n=2 for technical replicates.

3.9 REMDESIVIR TREATMENT OF SARS-COV-2-INFECTED ANIMALS

To explore the potential of the prairie vole as a model to test novel therapeutics, we evaluated the efficacy of remdesivir treatment in these animals following SARS-CoV-2 infection. Remdesivir is a broad-spectrum antiviral that targets the highly conserved virus RNA-dependent RNA polymerase and remains one of the few treatment options available for SARS-CoV-2-infected patients (Gottlieb et al., 2022). Following aerosol inoculation with 5mL of the UK (α) variant at $1*10^6$ PFU/mL, we administered remdesivir or the vehicle control via IP injection at 1 and 2dpi (Figure 3.12A). At 3dpi, we collected tissues and nasal wash samples and compared the levels of viral RNA copies and the viral titers detected in the control group to those of the treatment group. We observed statistically lower levels of viral RNA copies, $TCID_{50}$/mL, and PFU/mL in the lungs of the treatment group (Figure 3.12B-D), confirming that remdesivir reduces the viral titer in the lungs of SARS-CoV-2-infected prairie voles.

In contrast, mice secrete a plasma carboxylesterase 1c (*Ces1c*) that significantly reduces remdesivir half-life in circulation. For this reason, researchers evaluating the therapeutic effectiveness of remdesivir have utilized either genetically altered (*Ces1c-/-* C57BL/6) mice to enhance the drug's therapeutic response or prodrug analogs (Schäfer et al., 2022). Figure 3.12E, which shows that remdesivir treatment failed to reduce the viral titer in the lungs of SARS-CoV-2-Venus-2A-infected mice, confirms the drug's lack of efficacy in mice expressing *Ces1c*. Our findings suggest that prairie voles can be treated with clinical antivirals and more closely approximate drug exposure profiles in humans.
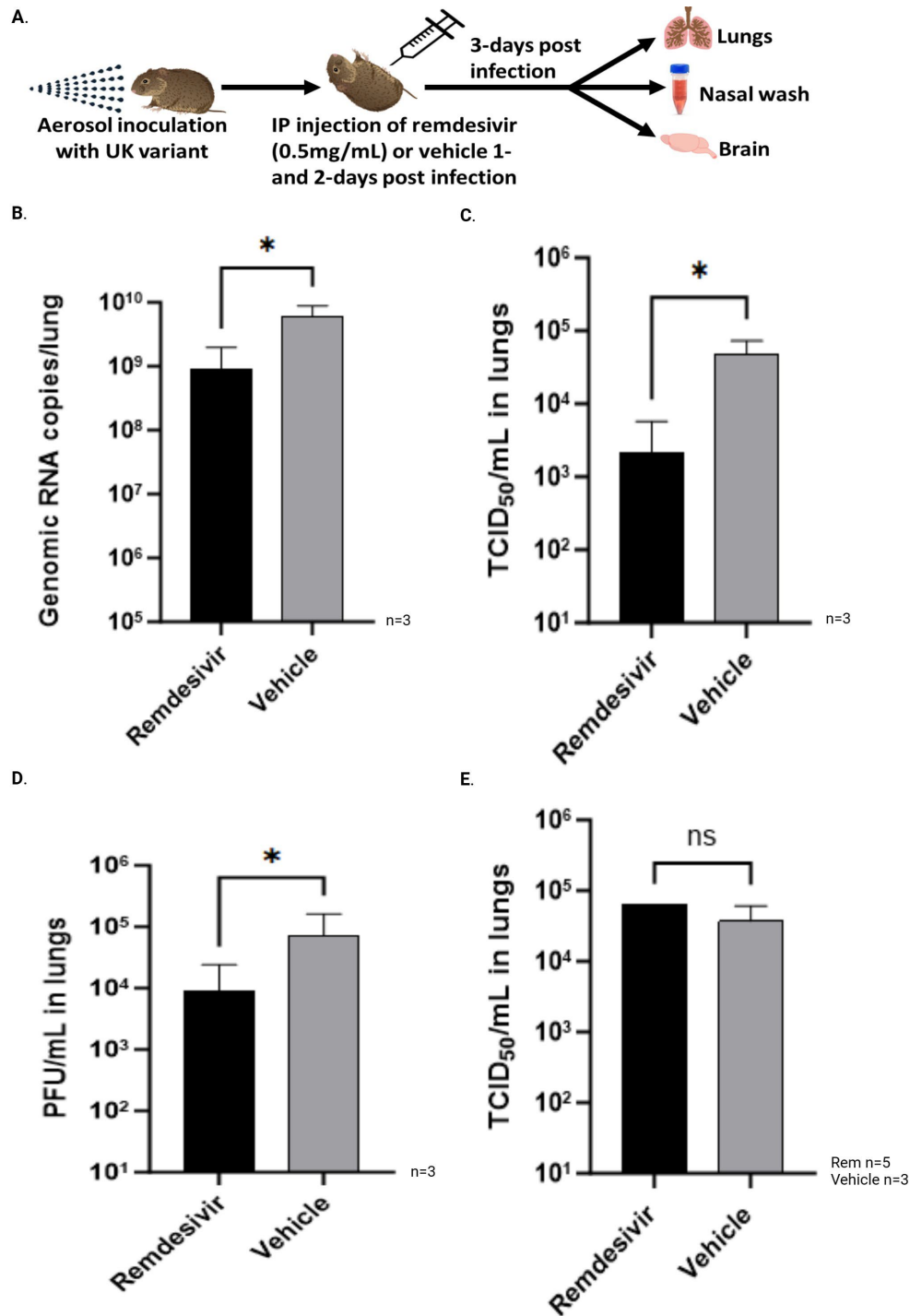
Figure 3.12: Remdesivir treatment of SARS-CoV-2-infected prairie voles. **A**. Schematic for the treatment study. **B-D**. The number of viral RNA copies, $TCID_{50}$/mL, and PFU/mL in the lungs of remdesivir treated and untreated SARS-CoV-2-infected prairie voles at 3dpi as determined by qRT-PCR, $TCID_{50}$ assay, and plaque assay, respectively. n=3 for biological replicates. n=2 for qRT-PCR technical replicates. n=9 for plaque assay technical replicates. **E**. $TCID_{50}$/mL in the lungs of remdesivir treated and untreated SARS-CoV-2-infected transgenic mice at 3dpi. n=5 for treatment group biological replicates. n=3 for vehicle group biological replicates.

3.10 TRANSGENIC MOUSE VS PRAIRIE VOLE INFECTION MODEL

To determine the effectiveness of the prairie vole SARS-CoV-2 infection model, we conducted comparative SARS-CoV-2 infection studies in transgenic mice expressing the hACE2 receptor. In the first of these comparative studies, we subjected the K18hACE2 transgenic mice to intranasal administration of $7*10^4$ PFU ($70\mu L$ at $1*10^6$ PFU/mL) of the UK (α) variant (Figure 3.13A). The results of this study were then compared to those of the prairie vole study involving aerosol delivery of 5mL of the UK (α) variant at $1*10^6$ PFU/mL (Figure 3.14A). In both studies, we collected tissues and nasal wash samples 2, 4, and 7dpi for analysis via qRT-PCR (Figure 3.13A&3.14A). We detected reduced viral RNA copies within the prairie vole tissues and nasal wash 7dpi compared to 2 and 4dpi (Figure 3.14B-D).

Similarly, the number of viral RNA copies detected in the transgenic mouse nasal wash was lower at 7dpi compared to 2 and 4dpi (Figure 3.13D). In contrast, we detected increased levels of viral RNA copies within the transgenic mouse lungs and brains at 4 and 7dpi compared to 2dpi (Figure 3.13B&C). When the results from each study were compared, we determined that the prairie voles had higher levels of viral RNA copies in their lungs at 2 and 4dpi as opposed to the transgenic mice, which had higher levels of viral RNA copies in their lungs at 7dpi (Figure 3.15A). These results imply faster viral clearance in the lungs of the prairie voles compared to the transgenic mice. The transgenic mice also showed statistically higher levels of viral RNA copies in their brains at 4 and 7dpi compared to the prairie voles (Figure 3.15B). The large magnitude of viral RNA copies in the brains of the transgenic mice indicated neurological symptoms and forced an experimental endpoint at 7dpi. After comparing the nasal wash of both models, we found that the transgenic mice also had statistically higher levels of viral RNA copies throughout the study (Figure 3.15C).
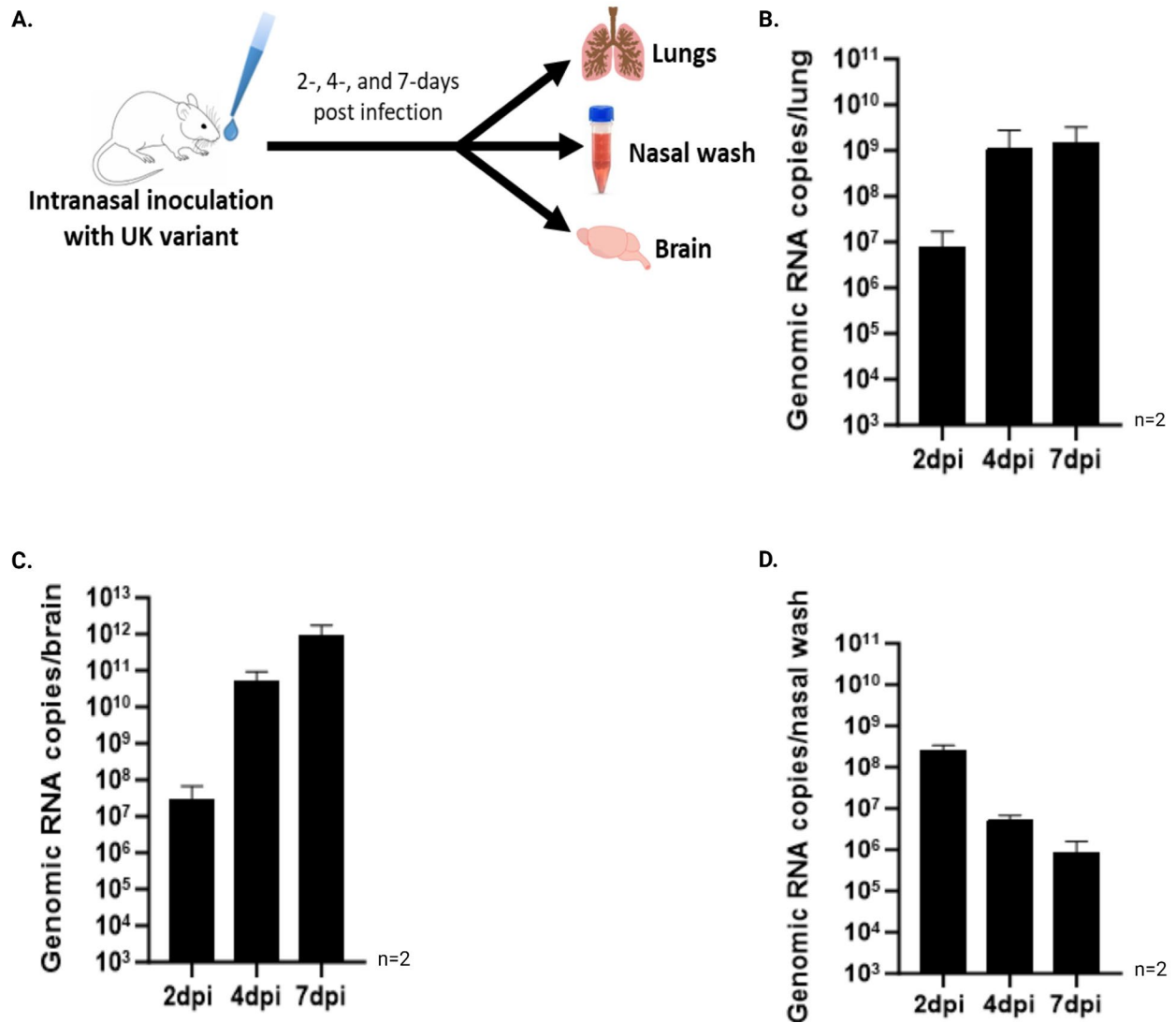
Figure 3.13: Intranasal inoculation of transgenic mice with the UK (α) variant. **A**. Schematic for transgenic mouse infection. **B-D**. The number of viral RNA copies in the lungs, brains, and nasal wash of UK (α)-infected mice 2, 4, and 7dpi as determined via qRT-PCR. n=3 for biological replicates. n=2 for technical replicates.
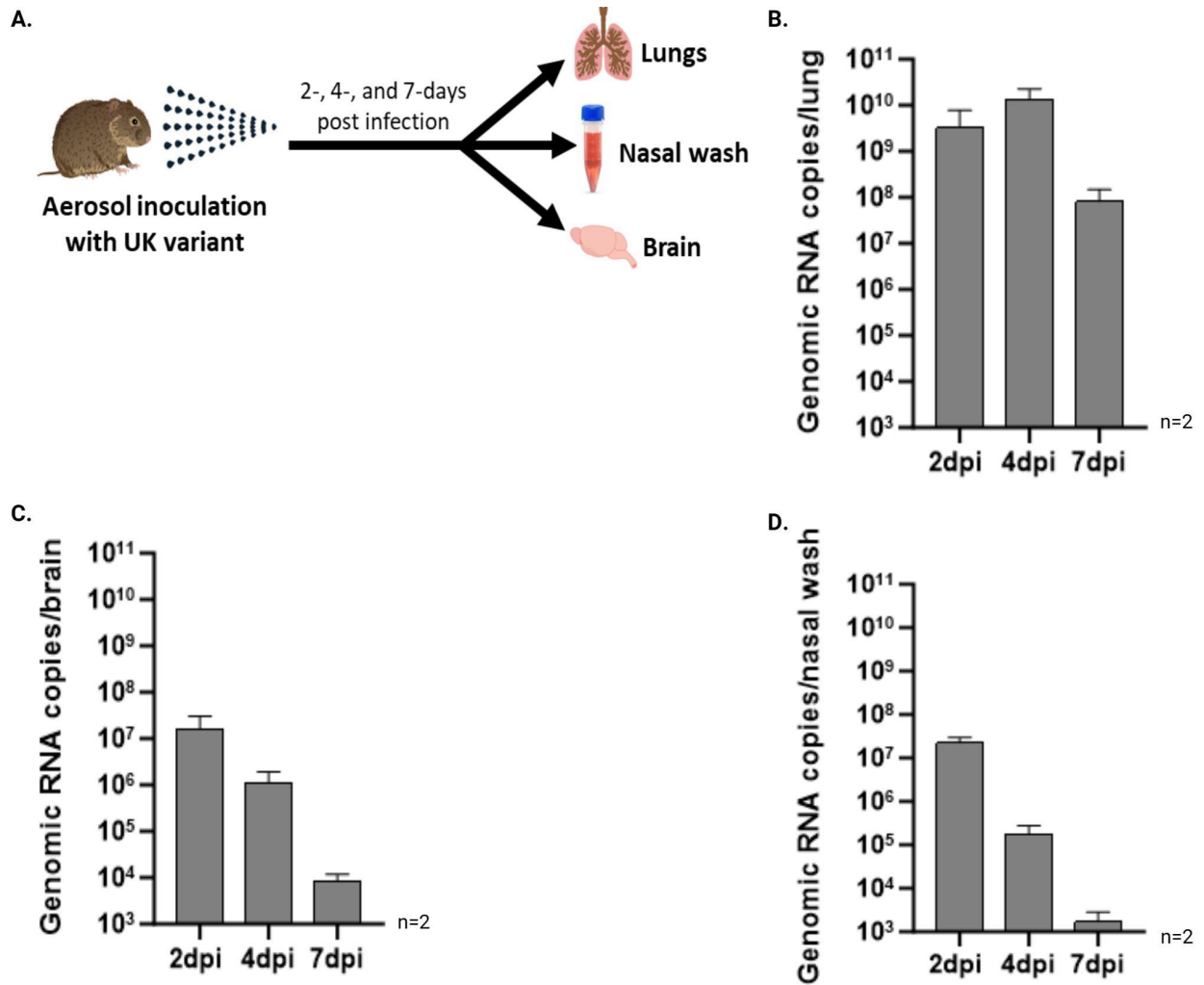
Figure 3.14: Aerosol inoculation of prairie voles with the UK (α) variant. **A**. Schematic for prairie vole infection. **B-D**. The number of viral RNA copies in the lungs, brains, and nasal wash of UK (α)-infected prairie voles 2, 4, 7dpi as determined via qRT-PCR. n=2 for biological replicates. n=2 for technical replicates.
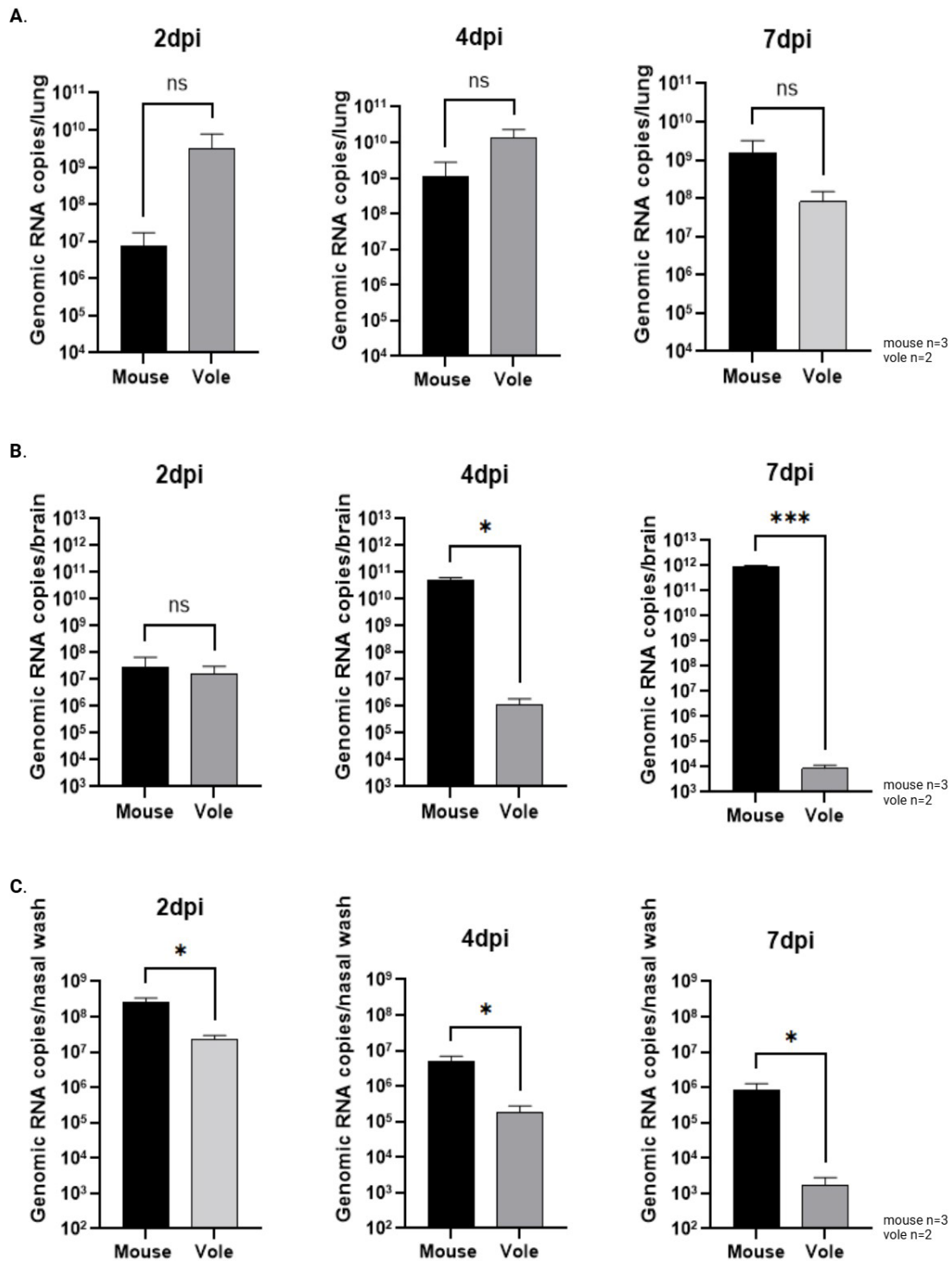
Figure 3.15: UK (α) infection in transgenic mice vs prairie voles. **A**. The number of viral RNA copies in the lungs of UK (α)-infected animals 2, 4, and 7dpi as determined via qRT-PCR. **B**. The number of viral RNA copies in the brains of the UK (α)-infected animals 2, 4, and 7dpi as determined via qRT-PCR. **C**. The number of viral RNA copies in the nasal wash of UK (α)-infected animals 2, 4, and 7dpi as determined via qRT-PCR. n=3 for biological replicates of mice. n=2 for biological replicates of prairie voles. n=2 for technical replicates.

87

For the subsequent comparative investigation, we utilized SARS-CoV-2 expressing fluorescent (Venus-2A) or luciferase expressing (Nluc-2A) reporter genes from the viral nucleocapsid. In this study, the transgenic mice were exposed to 5mL of aerosolized SARS-CoV-2-Venus-2A at $1*10^6$ PFU/mL, while the prairie voles were subjected to intranasal administration of $7*10^4$ PFU (70µL at $1*10^6$ PFU/mL) of SARS-CoV-2-Nluc-2A. The nasal wash from infected animals was collected 3dpi and analyzed for viral titer via plaque assay. We observed a statistically higher viral titer in the nasal wash from the infected prairie voles than in the transgenic mice (Figure 3.16A).

In another study comparing the viral titer in the brains of Venus-2A-infected transgenic mice (aerosol inoculation) at 4dpi and Beta-infected prairie voles (intranasal inoculation) at 3 dpi, we observed a higher PFU/mL in the brains of the transgenic mice (Figure 3.16B). These findings support the qRT-PCR data from the UK (α) infection study, showing higher viral RNA copies in the brains of the transgenic mice than in the brains of the prairie voles. Additionally, in this study, we observed a statistically higher PFU/mL in the lungs of the SARS-CoV-2-Venus-2A-infected mice at 4dpi than the Beta-infected prairie voles at 3dpi (Figure 3.16C). The significant increase in the viral titers in the lungs of infected mice compared to the lungs of infected prairie voles may be due to the difference in the variants used, the difference in collection point, or the difference in expression of the ACE2 receptor within the species.

In the final comparative investigation, we compared Delta infection in the transgenic mice and prairie voles following aerosolized inoculation of the animals with 5mL of $1*10^6$ PFU/mL of the variant. We observed a statistically higher PFU/mL in the nasal wash of prairie voles than in the transgenic mice (Figure 3.16D). Higher viral titers in the nasal wash of the infected prairie

voles indicate viral shedding, which supports our results showing viral transmission between infected and uninfected prairie voles.
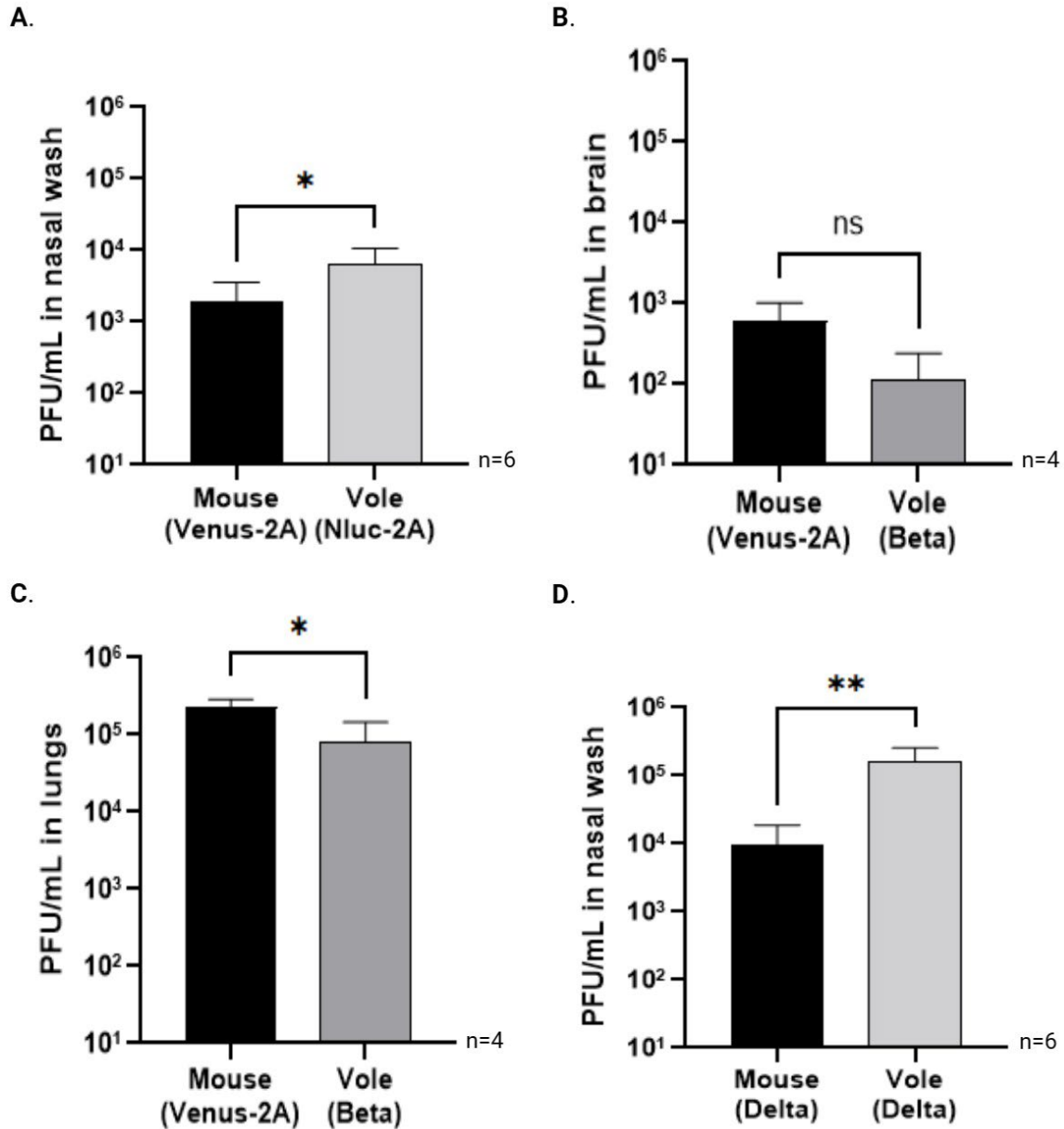
Figure 3.16: Comparison of SARS-CoV-2-infected transgenic mice and prairie voles. **A**. PFU/mL in the nasal wash of SARS-CoV-2-Venus-2A-infected transgenic mice and SARS-CoV-2-Nluc-2A-infected prairie voles at 3dpi. n=6 for biological replicates. **B**. PFU/mL in the brains of SARS-CoV-2-Venus-2A-infected transgenic mice at 4dpi and Beta-infected prairie voles at 3dpi. n=4 for biological replicates. **C**. PFU/mL in the lungs of SARS-CoV-2-Venus-2A-infected mice at 4dpi and Beta-infected prairie voles at 3dpi. n=4 for biological replicates. **D**. PFU/mL in the nasal wash of Delta-infected transgenic mice and prairie voles at 3dpi. n=6 for biological replicates.

3.11   SARS-COV-2-RBD-8-HIS PROTEIN PURIFICATION

The RBD within the S protein of SARS-CoV-2 was purified for use in neutralizing antibody assays. First, the plasmid containing the His-tagged RBD was transfected into Expi293T cells using an Expifectamine 293 transfection kit. Then, the expressed protein was purified via affinity chromatography using a 5mL His Trap purification column. The His-tagged protein was eluted from the column using an elution buffer containing 250mM imidazole in 2.5mL fractions. The elution fractions were analyzed via SDS-PAGE. Based on the SDS-PAGE results in Figure 3.17, elution fractions 3, 4, 5, 6, and 7 contain bands at ~25kDa, corresponding to the RBD. After pooling, concentrating, and dialyzing these elution fractions, the protein yield was determined to be 1.5mg via NanoDrop.
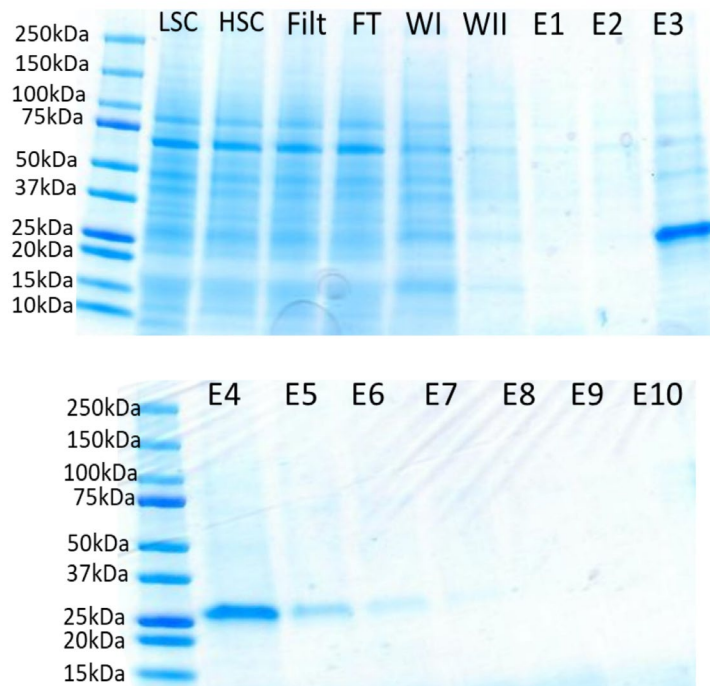
Figure 3.17: Affinity chromatography of RBD-8-His protein. SDS-PAGE was run at 200 volts for 30 minutes with 15μL of samples in each lane. The SDS-PAGE lanes are as follows: LSC – low-speed centrifuge of cell suspension at 1,000rpm; HSC – high-speed centrifuge of supernatant at 8,000rpm; Filt – filtered HSC supernatant; FT – column flow through; WI – column wash I; WII – column wash II; E1-10 – elution fractions 1-10.

3.12 GENERATION OF PRAIRIE VOLE-ADAPTED SARS-CoV-2

Since we used several different SARS-CoV-2 variants throughout our research, we examined which is better suited for infection in the prairie voles as measured by viral titer. For this examination, we compared intranasal inoculation with the Nluc-2A variant to the Beta variant, intranasal inoculation with the UK (α) variant to the Beta variant, and aerosol inoculation with the UK (α) variant to the Delta variant. In the case of intranasal delivery, the Beta-infected prairie voles produced a statistically higher viral titer in their nasal wash than the Nluc-2A-infected prairie voles (Figure 3.18A). Additionally, the Beta-infected prairie voles produced higher viral titers in their nasal wash compared to the UK (α)-infected prairie voles (Figure 3.18B). As for aerosol delivery, we observed a higher viral titer in the nasal wash of the Delta-infected prairie voles compared to the UK (α)-infected prairie voles (Figure 3.18C). These results suggest that intranasally administered Beta and aerosolized Delta are better suited for prairie vole infection than intranasal administration Nluc-2A or aerosolized UK (α).

Considering that the prairie voles showed no signs of clinical symptoms (i.e., loss of body weight) following infection with any of the SARS-CoV-2 variants, we generated a prairie vole-adapted variant via serial passage of the UK (α) variant in the lungs of the animals 15 times. For the first passage, we intranasally inoculated prairie voles with $7*10^4$ PFU (70μL at $1*10^6$ PFU/mL) of the UK (α) variant. The subsequent passages (2-15) were created using the lung homogenate of the previous passage collected at 3dpi. Compared to passage 1 (p1), we observed a statistically significant increase in the viral RNA copies in the lungs of the prairie voles at passage 8 (p8) (Figure 3.19A). Similarly, the lung homogenate from p8 had a statistically higher viral titer than p1 (Figure 3.19B). However, there was no significant increase in the viral titer of the lung homogenates from p8 to 12 or from passage 12 (p12) to 15 (p15) (Figure 3.19C&D).
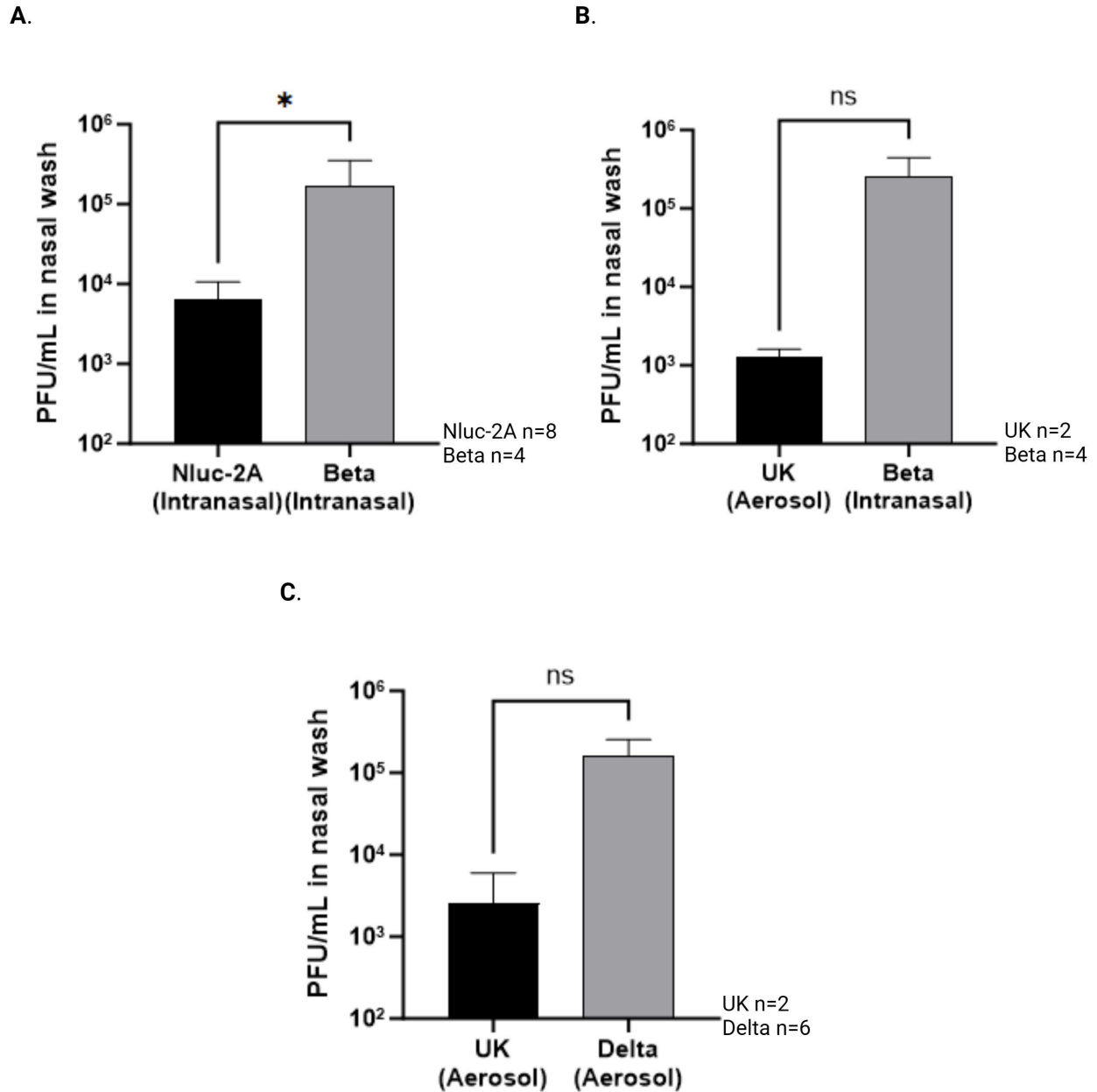
Figure 3.18: Comparison of SARS-CoV-2 infection in prairie voles with different variants. **A.** PFU/mL in the nasal wash of SARS-CoV-2-Nluc-2A-infected prairie voles 4dpi compared to Beta-infected prairie voles 3dpi. n=8 for Nluc-2A-infected biological replicates. n=4 for Beta-infected biological replicates. **B.** PFU/mL in the nasal wash of UK (α)-infected prairie voles at 4dpi compared to Beta-infected prairie voles at 3dpi. n=2 for UK (α)-infected biological replicates. n=4 for Beta-infected biological replicates. **C.** PFU/mL in the nasal wash of UK (α)-infected prairie voles compared to Delta-infected animals. n=2 for UK (α)-infected biological replicates. n=6 for Delta-infected biological replicates.
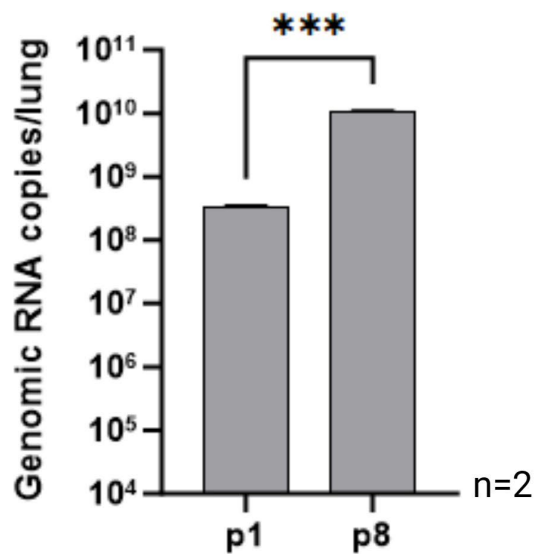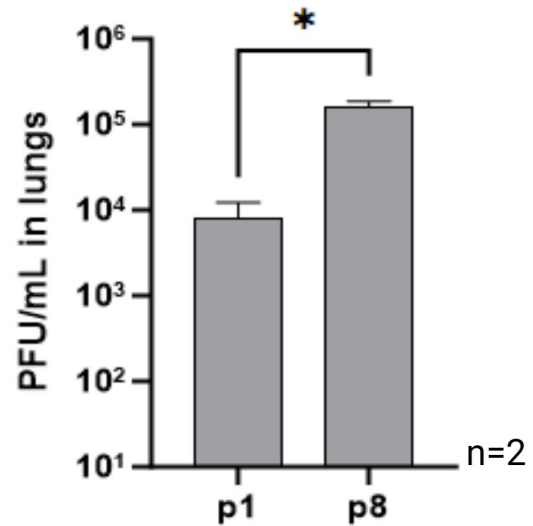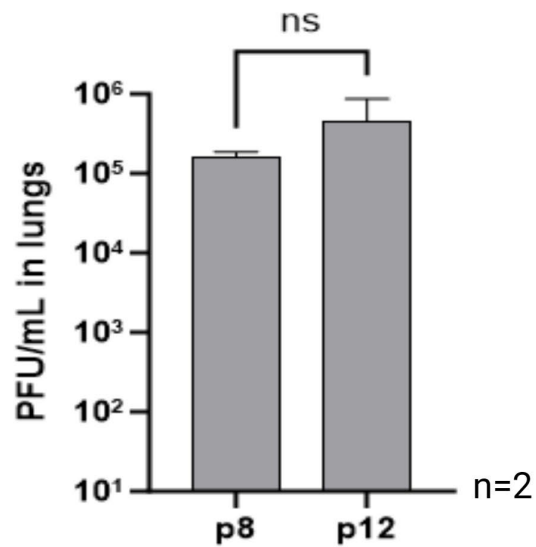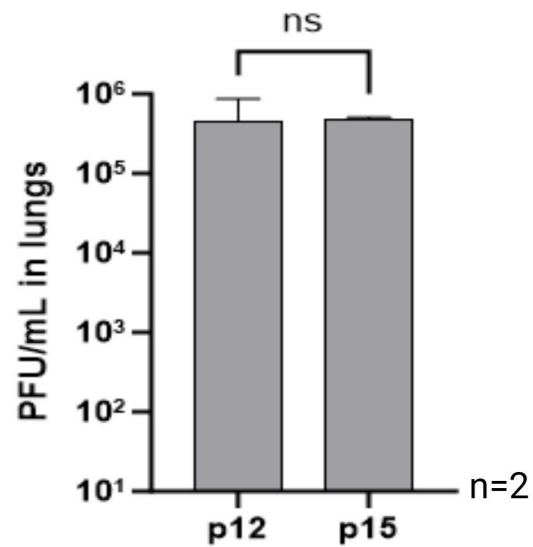
Figure 3.19: Generation of a prairie vole-adapted SARS-CoV-2 variant. **A**. The number of viral RNA copies in the lungs of prairie voles infected with passages 1 and passage 8 determined via qRT-PCR. n=2 for biological replicates and technical replicates. **B**. PFU/mL in the lungs of prairie voles infected with passages 1 and 8. n=2 for biological replicates. **C**. PFU/mL in the lungs of prairie voles infected with passages 8 and 12. n=2 for biological replicates. **D**. PFU/mL in the lungs of prairie voles infected with passages 12 and 15. n=2 for biological replicates.

3.13 ᴵɴᴏᴄᴜʟᴀᴛɪᴏɴ ᴏғ ᴘʀᴀɪʀɪᴇ ᴠᴏʟᴇs ᴡɪᴛʜ ᴛʜᴇ ᴠᴏʟᴇ-ᴀᴅᴀᴘᴛᴇᴅ SARS-CᴏV-2 ᴠᴀʀɪᴀɴᴛ

To determine whether the prairie vole-adapted variant caused measurable symptoms (i.e., weight loss) in the infected prairie voles, the animals were subjected to aerosol inoculation with 5mL of this variant at $1*10^6$ PFU/mL. The prairie voles were monitored for symptoms over fourteen days. Tissue samples were collected 3, 7, and 14dpi, and the viral titer and the number of viral RNA copies per sample were determined via plaque assay and qRT-PCR, respectively. No changes in body weight were observed; however, we observed a statistically higher number of viral RNA copies in the lungs of the infected prairie voles at 3dpi compared to the brain and nasal wash (Figure 3.20A). Additionally, we observed significantly lower numbers of viral RNA copies in the nasal wash of the infected prairie voles at 7 and 14dpi compared to 3dpi (Figure 3.20B). We also observed a significant decrease in the viral titer within the brains of the infected prairie voles compared to their lungs and nasal wash at 3dpi (Figure 3.20C). This data suggests a change in tissue tropism favoring the lungs of the animals following the adaptation of the virus.

Compared to the Beta and Delta variants, we did not see a significant increase in viral titer in the lungs, brains, or nasal wash of the prairie voles following infection with the vole-adapted variant (Figure 3.21A-C).
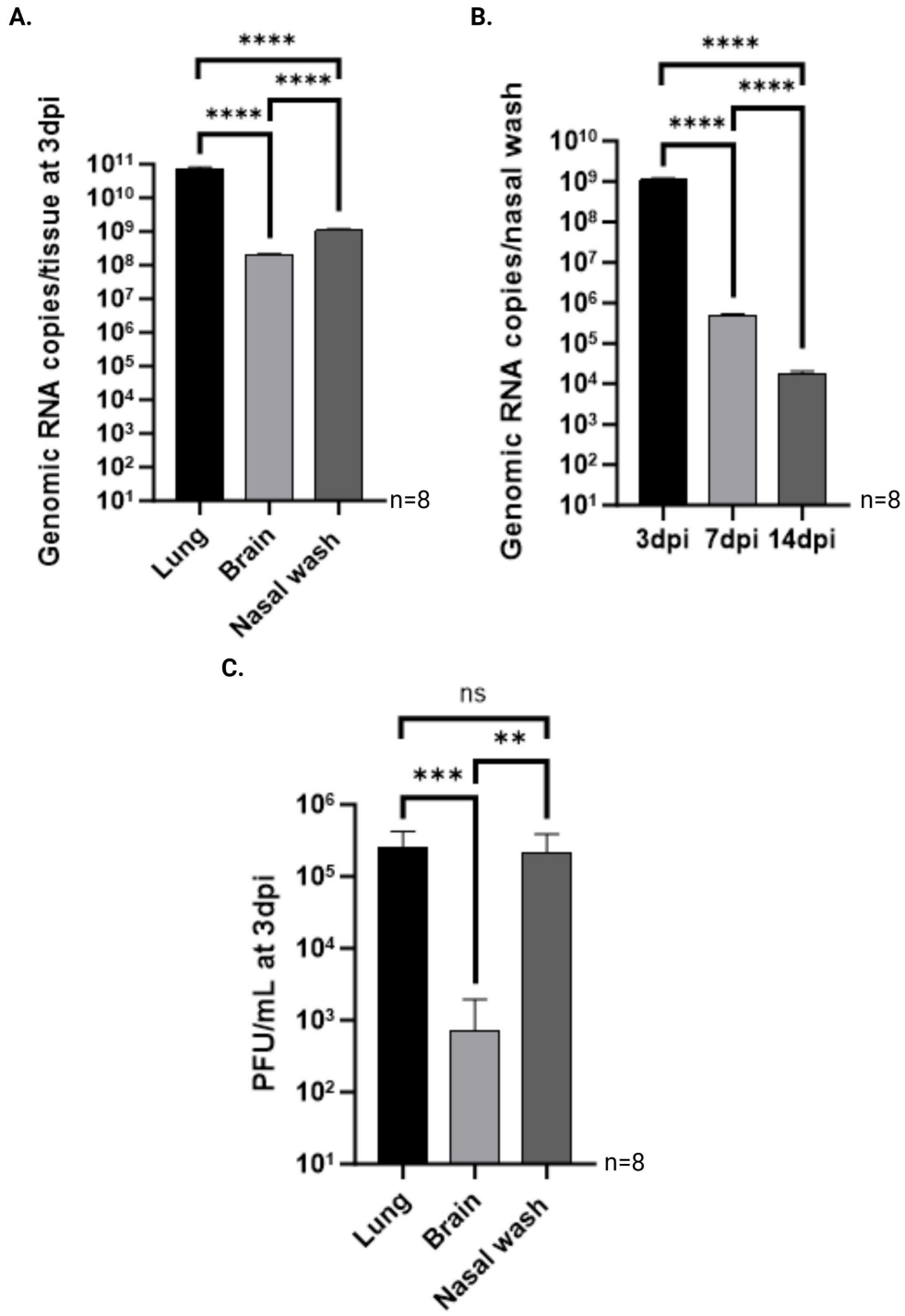
Figure 3.20: Aerosol inoculation of prairie voles with the vole-adapted SARS-CoV-2. **A**. The number of viral RNA copies in the tissues of the infected prairie voles at 3dpi as determined by qRT-PCR. n=8 for biological replicates. n=2 for technical replicates. **B**. The number of viral RNA copies in the nasal wash of infected prairie voles at 3, 7, and 14dpi as determined by qRT-PCR. n=8 for biological replicates. n=2 for technical replicates. **C**. PFU/mL in the tissues of infected prairie voles at 3dpi. n=8 for biological replicates.
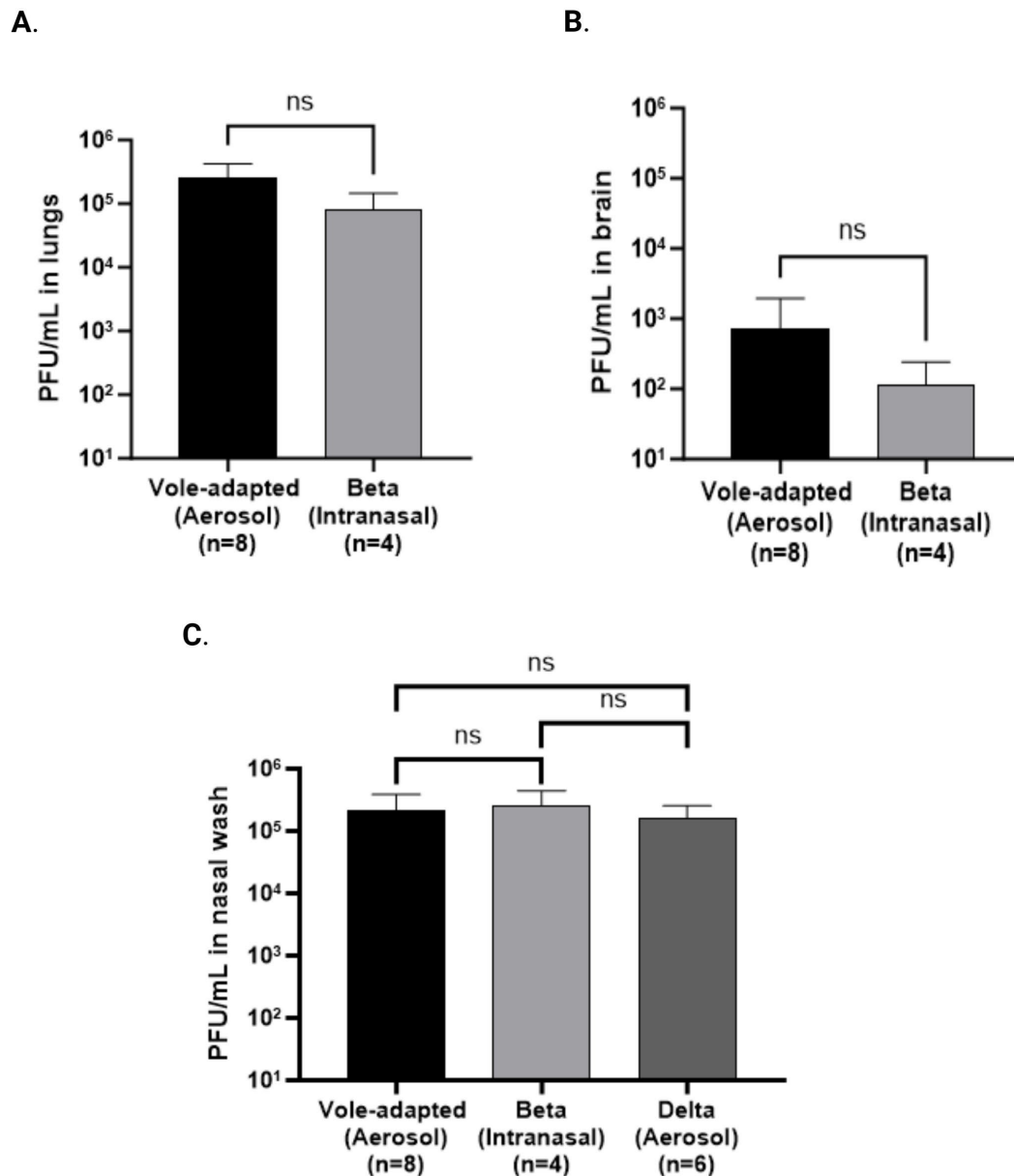
Figure 3.21: Comparison of vole-adapted, Beta, and Delta-infected prairie voles. **A**. Viral titer in the lungs of prairie voles exposed to the aerosolized vole-adapted variant at 3dpi compared to the viral titer in the lungs of Beta-infected prairie voles 3 days following intranasal inoculation. **B**. Viral titer in the brains of prairie voles subjected to aerosol inoculation of the vole-adapted variant at 3dpi compared to the viral titer in the brains of Beta-infected prairie voles 3 days following intranasal inoculation. **C**. Viral titer in the nasal wash of prairie voles 3 days following aerosol administration of the vole-adapted variant compared to the viral titers in Beta-infected and Delta-infected prairie voles, 3 and 4 days following intranasal and aerosol inoculation, respectively. n=8 for biological replicates. n=4 for Beta biological replicates. n=6 for Delta biological replicates.

3.14   CYTOKINE RESPONSE OF PRAIRIE VOLES TO SARS-COV-2 INFECTION

Since none of the variants we tested caused an observable decrease in body weight of the infected prairie voles, we analyzed the host immune response to the virus by measuring the levels of inflammatory cytokines in the lungs of the vole-adapted (aerosol), Beta (intranasal), and Delta (aerosol)-infected prairie voles via qRT-PCR. We detected significantly higher levels of IL-1β and IL-6 (Figure 3.22A&B) in the lungs of Delta-infected prairie voles compared to those infected with the vole-adapted and Beta variants. No significant difference was observed in cytokine levels when comparing the vole-adapted and Beta variants (Figure 3.22A-E). These data suggest that the Delta variant caused a more robust inflammatory response in the lungs of the prairie voles.
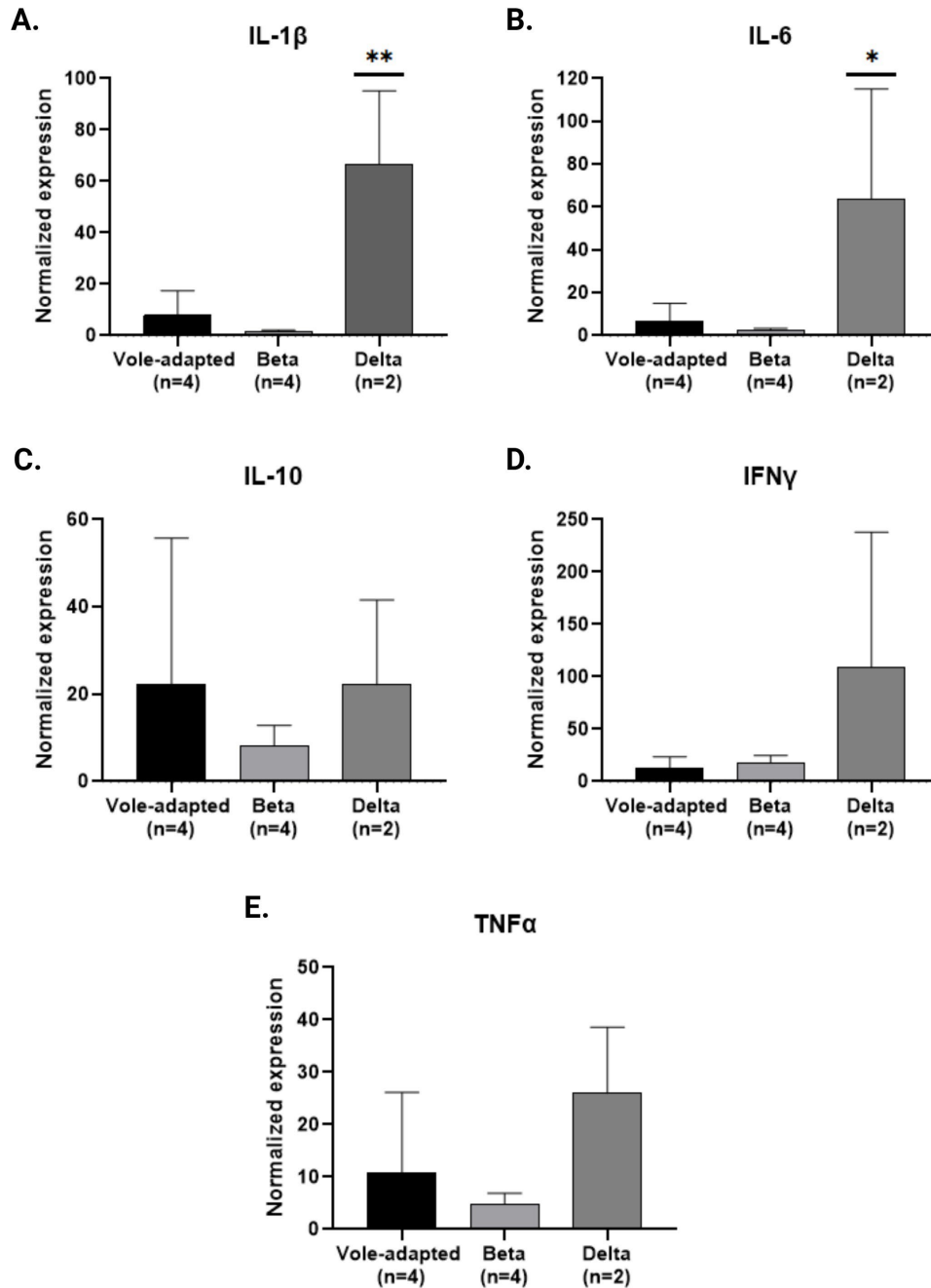
Figure 3.22: Cytokine levels in the lungs of SARS-CoV-2-infected prairie voles. **A**. IL-1β levels within the lungs of vole-adapted, Beta, and Delta-infected prairie voles as determined by qRT-PCR. **B**. IL-6 levels within the lungs of vole-adapted, Beta, and Delta-infected prairie voles as determined by qRT-PCR. **C**. IL-10 levels within the lungs of vole-adapted, Beta, and Delta-infected prairie voles as determined by qRT-PCR. **D**. IFNγ levels within the lungs of vole-adapted, Beta, and Delta-infected prairie voles as determined by qRT-PCR. **E**. TNFα levels within the lungs of vole-adapted, Beta, and Delta-infected prairie voles as determined by qRT-PCR. n=4 for vole-adapted and Beta biological replicates. n=2 for Delta biological replicates. n=2 for technical replicates.

3.15   SEQUENCING OF THE SARS-CoV-2 VOLE-ADAPTED VARIANT

We employed NGS to assess the mutations within the SARS-CoV-2 vole-adapted variant acquired after the adaptation process. Compared to the UK (α) (B.1.1.7) variant, we observed several new mutations not found in the starting variant. We also observed mutations within the Spike protein that indicate a reversal of the variant to the Wuhan variant. Additionally, we observed a mutation that was reported in the Beta variant. Table 3.1 outlines the mutations observed in the vole-adapted variant. Figure 3.23 depicts the mutations within the Spike protein of the UK (α) (B.1.1.7) variant and the vole-adapted variant. Specific mutations we observed in the vole-adapted variant have been reported to play various roles in pathogenesis. For example, the N74K mutation within the Spike protein has been shown to stabilize the Spike protein structure (Hanifa et al., 2022). Additionally, this mutation occurs at the glycosylation site and thus has been reported to affect Spike protein glycosylation (Q. Li et al., 2020). The E484K Spike mutation has been associated with reduced activity of neutralizing antibodies (Jangra et al., 2021).

The F108L mutation observed in Nsp6 has been associated with decreased structural stability of the protein (Suleman et al., 2023). The L260F mutation within Nsp6 was observed in mink-associated SARS-CoV-2 genome sequences (Adney et al., 2022). ORF3a is a viroporin that can function as an ion channel to promote virion release from host cells (Bianchi et al., 2021). It also interacts with the NLRP3 inflammasome through its TRAF3-binding motif, acting as a potent stimulator of IL-1β (Siu et al., 2019). The T223I mutation occurs in the β-barrel domain of the ORF3a, specifically within the connecting loop of β7 and β8, and is predicted to destabilize this domain (Bianchi et al., 2021).

Table 3.2: NGS results of the SARS-CoV-2 vole-adapted genome

Mutation	Genomic region	Comments
G70V	Nsp5	New; not in B.1.1.7
F108L	Nsp6	New; not in B.1.1.7
L260F	Nsp6	New; not in B.1.1.7
D204G	Nsp13	New; not in B.1.1.7
A454V	Nsp13	New; not in B.1.1.7
T63I	Spike	New; not in B.1.1.7
Ins69-70	Spike	Reversal to Wuhan
N74K	Spike	Affects Spike glycosylation
Ins145	Spike	Reversal to Wuhan
E484K	Spike	Seen in Beta
Y501N	Spike	Reversal to Wuhan
A653V	Spike	New; not in B.1.1.7
T223I	ORF3a	New; not in B.1.1.7
V70L	Membrane	New; seen in some B.1.1.7 sub-linages
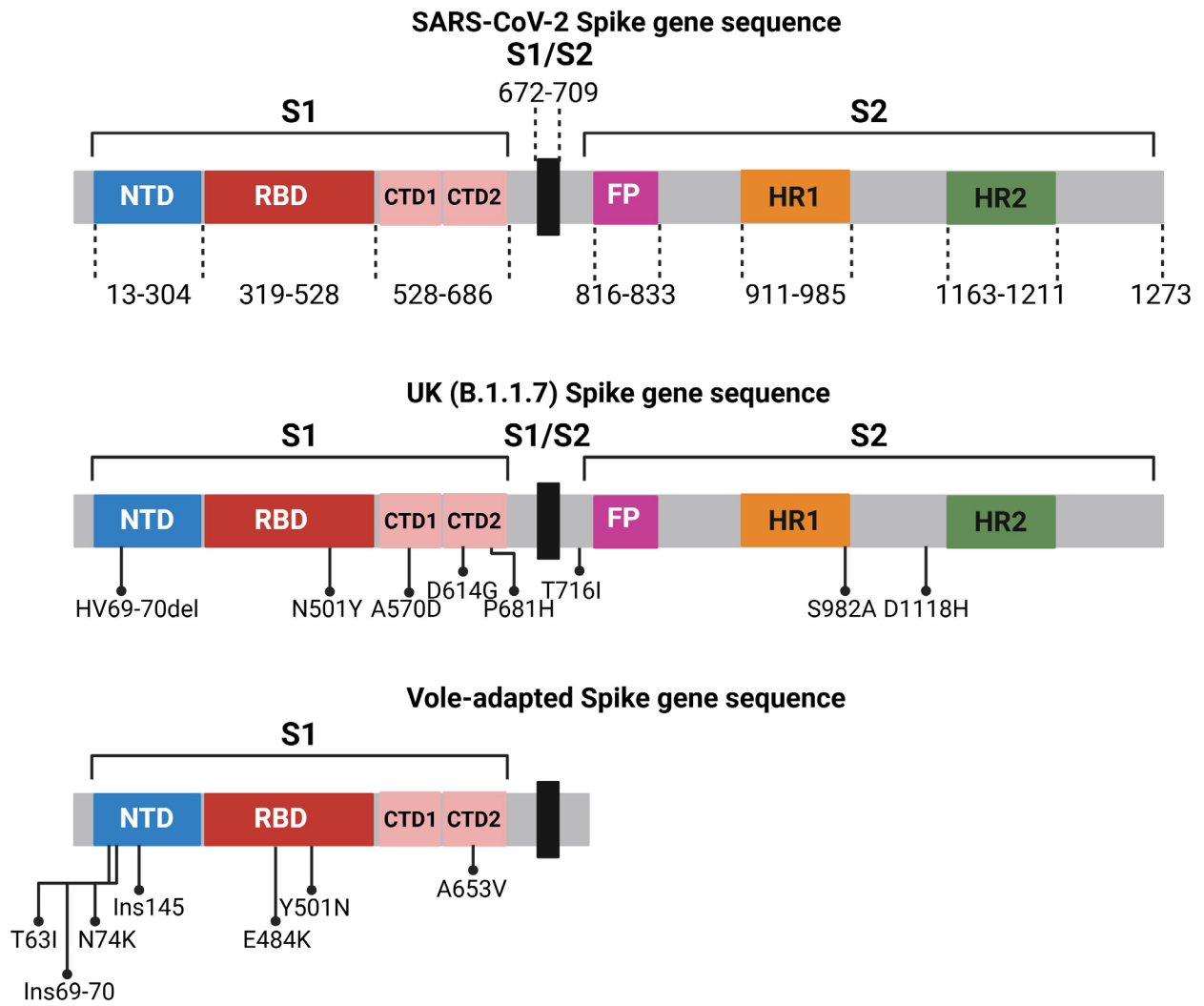
Figure 3.23: Spike gene sequences of the UK and SARS-CoV-2 vole-adapted variants.

Chapter 4: Conclusions

This work demonstrates that prairie voles are susceptible to infection by the WA1/2020 isolate and the UK (α), Beta, and Delta SARS-CoV-2 variants after intranasal and aerosol challenge. Despite their lack of clinical symptoms, infectious particles were recovered from the lung homogenate and nasal wash samples of the prairie voles up to 4dpi, suggesting viral clearance in the prairie voles at 5dpi. However, viral RNA copies were detected in the samples up to 14dpi, the latest time point that vole samples were collected in our studies. This finding is reminiscent of mild SARS-CoV-2 infection in humans that remain PCR positive for prolonged periods after initial infection.

Our *in vivo* comparison of the variants revealed that the Beta variant induced higher viral titers in the nasal wash of the intranasally infected prairie voles, suggesting that it is better suited to infect the animals. Given the lack of noticeable weight loss among the infected prairie voles, we measured the host response to the virus in terms of cytokine levels. We found increased levels of inflammatory cytokines within the infected animals at 3 and 7dpi, with Delta inducing significantly higher levels of IL-1β and IL-6, which are known to play a crucial role in cytokine storm development during human infection.

To increase the signs of symptoms in the SARS-CoV-2-infected prairie voles, we developed a vole-adapted variant through *in vivo* serial passage. However, throughout the 14-day study, the prairie voles failed to show a significant change in body weight following aerosol inoculation with this variant. We observed increased viral titer in the lungs of the prairie voles 3dpi with the vole-adapted variant compared to the intranasally administered Beta variant. Additionally, the significant increase of virus particles in the lungs compared to the brains of the prairie voles infected with the vole-adapted variant suggests that the tropism of this variant has shifted to the

102

lungs. NGS of the vole-adapted variant showed several mutations not found in the UK (α) (B.1.1.7) variant. It also revealed the presence of a mutation found in the Beta variant. Interestingly, we observed three mutations within this vole-adapted variant that indicate a reversal to the Wuhan variant.

Aside from viral detection in the lungs and nasal wash of the infected prairie voles, we detected viral RNA copies and titers in the brain homogenate at 4dpi. By 7dpi, viral RNA copies in the brains of the SARS-CoV-2-infected prairie voles decreased, and infectious particles were no longer recoverable. Although no neurological symptoms were observed in SARS-CoV-2-infected prairie voles throughout our studies, detection of the virus in the brains via qRT-PCR and plaque assay highlights the potential for neuronal effects following SARS-CoV-2 infection. The significance of neuropathology following SARS-CoV-2 infection is even more heightened after observing higher viral titers at 4dpi and increasing numbers of viral RNA copies in the brains of SARS-CoV-2-infected K18hACE transgenic mice.

Our research not only confirms the susceptibility of prairie voles to SARS-CoV-2 infection but also demonstrates the potential for transmission to uninfected cage mates. We observed viral RNA copies in the lungs, brains, and nasal wash of uninfected prairie voles after being housed with an infected cage mate for up to 6 days. Importantly, our study shows that, unlike transgenic mice, prairie voles can be effectively treated with remdesivir. By 3dpi, we observed statistically reduced levels of viral RNA copies and viral titers in the lungs of SARS-CoV-2-infected prairie voles following treatment with IP-administered remdesivir.

Several SARS-CoV-2 infection models showcasing the susceptibility of various species have been utilized to test vaccine and therapeutic efficacy. Our study presents the advantages of a novel animal model for use in viral pathogenesis and drug intervention studies. Compared to

hamsters and other rodent models, prairie voles offer the ability to evaluate disease pathology without the complications associated with sex-related differences. Like ferrets, prairie voles do not show clinical signs of infection in terms of loss of body weight and reduced physical activity, but they are highly susceptible to SARS-CoV-2 infection. After comparing our prairie vole model to the transgenic mouse model, the most striking difference observed was the amount of RNA copies detected in the brains of the mice and the presentation of neurological symptoms exhibited by the SARS-CoV-2-infected mice. These symptoms were so severe that we were forced to humanely end the experiments 7dpi. Unlike the mice, no prairie voles succumbed to disease following infection with a SARS-CoV-2 variant.

The main difficulty associated with a prairie vole model is the limited availability of reagents. However, this issue is also associated with the use of hamster and ferret models. Excessive use of prairie voles in social behavioral studies, which often include neurological components, has illuminated the cross-reactivity of mouse, rat, and hamster antibodies to similar proteins expressed in prairie voles. Another issue with this model is the lack of clinical symptoms regarding body weight loss following aerosol or intranasal inoculation, which makes monitoring disease progression and assessing the efficacy of therapeutics more difficult.

Moreover, the latest time point at which we detected infectious viral particles in the prairie vole tissue and nasal wash samples was 4dpi. However, these findings may be influenced by the viral dose administered. Recent studies have shown a dose-dependent response to viral infection. For instance, a SARS-CoV-2 modeling study revealed that a large inoculum leads to shorter infections with higher viral titer peaks, while a smaller inoculum results in lower viral titer peaks but prolongs the infection (Fain & Dobrovolny, 2020). In another study, researchers demonstrated

that a high dosage (10^{10} genome equivalents (GE) per animal) and a low dosage (10^1 GE per animal) of hepatitis B virus led to prolonged or persistent infection with severe immunopathology.

In contrast, an intermediate dosage ($10^7 - 10^4$ GE per animal) resulted in minimal immunopathology and rapid viral clearance (Asabe et al., 2009). These findings suggest that the lack of symptoms and high viral RNA copies and titers followed by rapid viral clearance observed in the prairie voles could be a result of the amount of initial SARS-CoV-2 inoculum used ($5*10^6$ PFU for aerosol delivery and $7*10^4$ PFU for intranasal delivery). As a result, future work on this project will involve testing the dose-dependent response to infection with the SARS-CoV-2 vole-adapted variant.

Overall, this study found that:

1) Prairie voles are susceptible to intranasal and aerosolized SARS-CoV-2.

2) Virus particles were detected in the lungs and brains of infected prairie voles.

3) Infected prairie voles were able to transmit the virus to uninfected cage mates.

4) Remdesivir treatment reduced viral RNA copies and titers in the lungs of SARS-CoV-2-infected prairie voles.

These findings demonstrate the viability of the prairie vole model system for studying SARS-CoV-2 pathogenesis and drug interventions and highlight its advantages over other models, like mice, in terms of susceptibility and disease presentation. Additionally, thanks to their extensive use and characterization in social behavioral studies, prairie voles offer the ability to assess the effects of SARS-CoV-2 infection on depression and anxiety and to explore the neuropathology associated with SARS-CoV-2 infection. As a result, future work with this model could involve assessing the association between long COVID-19 and depression and mood disorders reported in some patients.

Chapter 5: References

(CDC), C. f. D. C. a. P. (2023). *SARS-CoV-2 Variant Classifications and Definitions*. SARS-CoV-2 Variant Classifications and Definitions (cdc.gov)

AboElkhair, M. A., Ahmed, M. M., Moustapha, A., Zaki, A. M., El Naggar, R. F., Elhamouly, M., & Anis, A. (2023). Monitoring SARS-CoV-2 infection in different animal species and human in Egypt during 2020-2021. *Biologia (Bratisl)*, 1-7. https://doi.org/10.1007/s11756-023-01362-1

Adney, D. R., Lovaglio, J., Schulz, J. E., Yinda, C. K., Avanzato, V. A., Haddock, E.,…Munster, V. J. (2022). Severe acute respiratory disease in American mink experimentally infected with SARS-CoV-2. *JCI Insight*, *7*(22). https://doi.org/10.1172/jci.insight.159573

Aiewsakun, P., Phumiphanjarphak, W., Ludowyke, N., Purwono, P. B., Manopwisedjaroen, S., Srisaowakarn, C.,…Thitithanyanont, A. (2023). Systematic Exploration of SARS-CoV-2 Adaptation to Vero E6, Vero E6/TMPRSS2, and Calu-3 Cells. *Genome Biol Evol*, *15*(4). https://doi.org/10.1093/gbe/evad035

Amraei, R., Xia, C., Olejnik, J., White, M. R., Napoleon, M. A., Lotfollahzadeh, S.,…Rahimi, N. (2022). Extracellular Vimentin Is an Attachment Factor That Facilitates SARS-CoV-2 Entry Into Human Endothelial Cells. *Proceedings of the National Academy of Sciences*. https://doi.org/10.1073/pnas.2113874119

Andersen, K. G., Rambaut, A., Lipkin, W. I., Holmes, E. C., & Garry, R. F. (2020). The proximal origin of SARS-CoV-2. *Nature Medicine*, *26*(4), 450-452. https://doi.org/10.1038/s41591-020-0820-9

Asabe, S., Wieland Stefan, F., Chattopadhyay Pratip, K., Roederer, M., Engle Ronald, E., Purcell Robert, H., & Chisari Francis, V. (2009). The Size of the Viral Inoculum Contributes to the Outcome of Hepatitis B Virus Infection. *Journal of Virology*, *83*(19), 9652-9662. https://doi.org/10.1128/jvi.00867-09

Au, G. G., Marsh, G. A., McAuley, A. J., Lowther, S., Trinidad, L., Edwards, S.,…Vasan, S. S. (2022). Characterisation and natural progression of SARS-CoV-2 infection in ferrets. *Scientific Reports*, *12*(1), 5680. https://doi.org/10.1038/s41598-022-08431-6

B, A., A, J., J, L., & al., e. (2002). *Molecular Biology of the Cell* (4th ed.). Garland Science.

Barton, M. I., MacGowan, S. A., Kutuzov, M. A., Dushek, O., Barton, G. J., & van der Merwe, P. A. (2021). Effects of common mutations in the SARS-CoV-2 Spike RBD and its ligand, the human ACE2 receptor on binding affinity and kinetics. *Elife*, *10*. https://doi.org/10.7554/eLife.70658

Bassett, M., Salemi, M., & Magalis, B. R. (2022). Lessons Learned and Yet-to-Be Learned on the Importance of RNA Structure in SARS-CoV-2 Replication. *Microbiology and Molecular Biology Reviews*. https://doi.org/10.1128/mmbr.00057-21

Becker, J. B., Arnold, A. P., Berkley, K. J., Blaustein, J. D., Eckel, L. A., Hampson, E.,…Young, E. (2005). Strategies and methods for research on sex differences in brain and behavior. *Endocrinology*, *146*(4), 1650-1673. https://doi.org/10.1210/en.2004-1142

Berg, R. E., & Forman, J. (2006). The role of CD8 T cells in innate immunity and in antigen non-specific protection. *Curr Opin Immunol*, *18*(3), 338-343. https://doi.org/10.1016/j.coi.2006.03.010

Bianchi, M., Borsetti, A., Ciccozzi, M., & Pascarella, S. (2021). SARS-Cov-2 ORF3a: Mutability and function. *Int J Biol Macromol*, *170*, 820-826. https://doi.org/10.1016/j.ijbiomac.2020.12.142

Blocker, T. D., & Ophir, A. G. (2016). A preference to bond? Male prairie voles form pair bonds even in the presence of multiple receptive females. *Anim Behav*, *122*, 89-97. https://doi.org/10.1016/j.anbehav.2016.10.007

Blumberg, E. A., Noll, J. H., Tebas, P., Fraietta, J. A., Frank, I., Marshall, A.,…Hexner, E. O. (2022). A phase I trial of cyclosporine for hospitalized patients with COVID-19. *JCI Insight*, *7*(11). https://doi.org/10.1172/jci.insight.155682

Boni, M. F., Lemey, P., Jiang, X., Lam, T. T.-Y., Perry, B. W., Castoe, T. A.,…Robertson, D. L. (2020). Evolutionary origins of the SARS-CoV-2 sarbecovirus lineage responsible for the COVID-19 pandemic. *Nature Microbiology*, *5*(11), 1408-1417. https://doi.org/10.1038/s41564-020-0771-4

Boyton, R. J., & Altmann, D. M. (2021). The immunology of asymptomatic SARS-CoV-2 infection: what are the key questions? *Nature Reviews Immunology*, *21*(12), 762-768. https://doi.org/10.1038/s41577-021-00631-x

Braun, E., & Sauter, D. (2019). Furin-mediated Protein Processing in Infectious Diseases and Cancer. *Clinical & Translational Immunology*. https://doi.org/10.1002/cti2.1073

Bugge, T. H., Antalis, T. M., & Wu, Q. (2009). Type II transmembrane serine proteases. *J Biol Chem*, *284*(35), 23177-23181. https://doi.org/10.1074/jbc.R109.021006

Cao, W., Feng, Q., & Wang, X. (2021). Computational analysis of TMPRSS2 expression in normal and SARS-CoV-2-infected human tissues. *Chem Biol Interact*, *346*, 109583. https://doi.org/10.1016/j.cbi.2021.109583

Caruso Í, P., Sanches, K., Da Poian, A. T., Pinheiro, A. S., & Almeida, F. C. L. (2021). Dynamics of the SARS-CoV-2 nucleoprotein N-terminal domain triggers RNA duplex destabilization. *Biophys J*, *120*(14), 2814-2827. https://doi.org/10.1016/j.bpj.2021.06.003

Castaño-Rodriguez, C., Honrubia, J. M., Gutiérrez-Álvarez, J., DeDiego, M. L., Nieto-Torres, J. L., Jimenez-Guardeño, J. M.,…Enjuanes, L. (2018). Role of Severe Acute Respiratory Syndrome Coronavirus Viroporins E, 3a, and 8a in Replication and Pathogenesis. *mBio*, *9*(3). https://doi.org/10.1128/mBio.02325-17

Chalfin, L., Dayan, M., Levy, D. R., Austad, S. N., Miller, R. A., Iraqi, F. A.,…Kimchi, T. (2014). Mapping ecologically relevant social behaviours by gene knockout in wild mice. *Nature Communications*, *5*(1), 4569. https://doi.org/10.1038/ncomms5569

Challen, R., Brooks-Pollock, E., Read, J. M., Dyson, L., Tsaneva-Atanasova, K., & Danon, L. (2021). Risk of mortality in patients infected with SARS-CoV-2 variant of concern 202012/1: matched cohort study. *BMJ*, *372*, n579. https://doi.org/10.1136/bmj.n579

Chaturvedi, R., Lui, B., Aaronson, J. A., White, R. S., & Samuels, J. D. (2022). COVID-19 complications in males and females: recent developments. *J Comp Eff Res*, *11*(9), 689-698. https://doi.org/10.2217/cer-2022-0027

Chen, J., Wang, R., Wang, M., & Wei, G. W. (2020). Mutations Strengthened SARS-CoV-2 Infectivity. *J Mol Biol*, *432*(19), 5212-5226. https://doi.org/10.1016/j.jmb.2020.07.009

Chen, K., Xiao, F., Hu, D., Ge, W., Tian, M., Wang, W.,…Wu, J. (2020). SARS-CoV-2 Nucleocapsid Protein Interacts with RIG-I and Represses RIG-Mediated IFN-β Production. *Viruses*, *13*(1). https://doi.org/10.3390/v13010047

Chen, Y., Cai, H., Pan, J., Xiang, N., Tien, P., Ahola, T., & Guo, D. (2009). Functional screen reveals SARS coronavirus nonstructural protein nsp14 as a novel cap N7 methyltransferase. *Proc Natl Acad Sci U S A*, *106*(9), 3484-3489. https://doi.org/10.1073/pnas.0808790106

Chen, Y., Su, C., Ke, M., Jin, X., Xu, L., Zhang, Z.,…Guo, D. (2011). Biochemical and structural insights into the mechanisms of SARS coronavirus RNA ribose 2'-O-methylation by nsp16/nsp10 protein complex. *PLoS Pathog*, *7*(10), e1002294. https://doi.org/10.1371/journal.ppat.1002294

Corbett, K. S., Flynn, B., Foulds, K. E., Francica, J. R., Boyoglu-Barnum, S., Werner, A. P.,…Graham, B. S. (2020). Evaluation of the mRNA-1273 Vaccine against SARS-CoV-2 in Nonhuman Primates. *N Engl J Med*, *383*(16), 1544-1555. https://doi.org/10.1056/NEJMoa2024671

Corso, C. M., Marchisio, P., Agostoni, C., Casazza, G., Costantino, G., & Milani, G. P. (2022). Frequency of SARS-CoV-2 Positivity Among Children Presenting With Gastroenteritis in Emergency Department. *The Pediatric Infectious Disease Journal*. https://doi.org/10.1097/inf.0000000000003733

Crotty, S. (2014). T follicular helper cell differentiation, function, and roles in disease. *Immunity*, *41*(4), 529-542. https://doi.org/10.1016/j.immuni.2014.10.004

Cui, Z., Zeng, C., Huang, F., Yuan, F., Yan, J., Zhao, Y.,…Wang, Q. (2022). Cas13d knockdown of lung protease Ctsl prevents and treats SARS-CoV-2 infection. *Nat Chem Biol*, *18*(10), 1056-1064. https://doi.org/10.1038/s41589-022-01094-4

D'Angelo, D., Quarta, E., Glieca, S., Varacca, G., Flammini, L., Bertoni, S.,…Buttini, F. (2023). An Enhanced Dissolving Cyclosporin-A Inhalable Powder Efficiently Reduces SARS-CoV-2 Infection In Vitro. *Pharmaceutics*, *15*(3). https://doi.org/10.3390/pharmaceutics15031023

Devaux, C. A., Melenotte, C., Piercecchi-Marti, M. D., Delteil, C., & Raoult, D. (2021). Cyclosporin A: A Repurposable Drug in the Treatment of COVID-19? *Front Med (Lausanne)*, *8*, 663708. https://doi.org/10.3389/fmed.2021.663708

Dhama, K., Patel, S. K., Sharun, K., Pathak, M., Tiwari, R., Yatoo, M. I.,…Rodriguez-Morales, A. J. (2020). SARS-CoV-2 jumping the species barrier: Zoonotic lessons from SARS, MERS and recent advances to combat this pandemic virus. *Travel Med Infect Dis*, *37*, 101830. https://doi.org/10.1016/j.tmaid.2020.101830

Diamond, M. S., & Kanneganti, T. D. (2022). Innate immunity: the first line of defense against SARS-CoV-2. *Nat Immunol*, *23*(2), 165-176. https://doi.org/10.1038/s41590-021-01091-0

Dixon, B. E., Wools-Kaloustian, K., Fadel, W. F., Duszynski, T. J., Yiannoutsos, C., Halverson, P. K., & Menachemi, N. (2020). Symptoms and symptom clusters associated with SARS-CoV-2 infection in community-based populations: Results from a statewide epidemiological study. *medRxiv*. https://doi.org/10.1101/2020.10.11.20210922

Dluzen, D. E., Ramirez, V. D., Carter, C. S., & Getz, L. L. (1981). Male vole urine changes luteinizing hormone-releasing hormone and norepinephrine in female olfactory bulb. *Science*, *212*(4494), 573-575. https://doi.org/10.1126/science.7010608

Drożdżal, S., Rosik, J., Lechowicz, K., Machaj, F., Szostak, B., Przybyciński, J.,…Łos, M. J. (2021). An update on drugs with therapeutic potential for SARS-CoV-2 (COVID-19) treatment. *Drug Resist Updat*, *59*, 100794. https://doi.org/10.1016/j.drup.2021.100794

Emlen, S. T., & Oring, L. W. (1977). Ecology, Sexual Selection, and the Evolution of Mating Systems. *Science*, *197*(4300), 215-223. https://doi.org/10.1126/science.327542

Esakandari, H., Nabi-Afjadi, M., Fakkari-Afjadi, J., Farahmandian, N., Miresmaeili, S. M., & Bahreini, E. (2020). A comprehensive review of COVID-19 characteristics. *Biol Proced Online*, *22*, 19. https://doi.org/10.1186/s12575-020-00128-2

Everett, H. E., Lean, F. Z. X., Byrne, A. M. P., van Diemen, P. M., Rhodes, S., James, J.,…Brookes, S. M. (2021). Intranasal Infection of Ferrets with SARS-CoV-2 as a Model for Asymptomatic Human Infection. *Viruses*, *13*(1). https://doi.org/10.3390/v13010113

Fain, B., & Dobrovolny, H. M. (2020). Initial Inoculum and the Severity of COVID-19: A Mathematical Modeling Study of the Dose-Response of SARS-CoV-2 Infections. *Epidemiologia (Basel)*, *1*(1), 5-15. https://doi.org/10.3390/epidemiologia1010003

Falcone, M., Tiseo, G., Valoriani, B., Barbieri, C., Occhineri, S., Mazzetti, P.,…Menichetti, F. (2021). Efficacy of Bamlanivimab/Etesevimab and Casirivimab/Imdevimab in Preventing Progression to Severe COVID-19 and Role of Variants of Concern. *Infect Dis Ther*, *10*(4), 2479-2488. https://doi.org/10.1007/s40121-021-00525-4

Fenizia, C., Galbiati, S., Vanetti, C., Vago, R., Clerici, M., Tacchetti, C., & Daniele, T. (2022). Cyclosporine A Inhibits Viral Infection and Release as Well as Cytokine Production in Lung Cells by Three SARS-CoV-2 Variants. *Microbiol Spectr*, *10*(1), e0150421. https://doi.org/10.1128/spectrum.01504-21

Finkel, Y., Gluck, A., Nachshon, A., Winkler, R., Fisher, T., Rozman, B.,…Stern-Ginossar, N. (2021). SARS-CoV-2 uses a multipronged strategy to impede host protein synthesis. *Nature*, *594*(7862), 240-245. https://doi.org/10.1038/s41586-021-03610-3

Fischer, T. R., Meidner, L., Schwickert, M., Weber, M., Zimmermann, R. A., Kersten, C.,…Helm, M. (2022). Chemical biology and medicinal chemistry of RNA methyltransferases. *Nucleic Acids Res*, *50*(8), 4216-4245. https://doi.org/10.1093/nar/gkac224

Fraser, B. J., Beldar, S., Seitova, A., Hutchinson, A., Mannar, D., Li, Y.,…Bénard, F. (2022). Structure and activity of human TMPRSS2 protease implicated in SARS-CoV-2 activation. *Nature Chemical Biology*, *18*(9), 963-971. https://doi.org/10.1038/s41589-022-01059-7

Frazier, M. N., Dillard, L. B., Krahn, J. M., Perera, L., Williams, J. G., Wilson, I. M.,…Stanley, R. E. (2021). Characterization of SARS2 Nsp15 nuclease activity reveals it's mad about U. *Nucleic Acids Res*, *49*(17), 10136-10149. https://doi.org/10.1093/nar/gkab719

Freitas, R. S., Crum, T. F., & Parvatiyar, K. (2021). SARS-CoV-2 Spike Antagonizes Innate Antiviral Immunity by Targeting Interferon Regulatory Factor 3. *Front Cell Infect Microbiol*, *11*, 789462. https://doi.org/10.3389/fcimb.2021.789462

Fu, Y. Z., Wang, S. Y., Zheng, Z. Q., Yi, H., Li, W. W., Xu, Z. S., & Wang, Y. Y. (2021). SARS-CoV-2 membrane glycoprotein M antagonizes the MAVS-mediated innate antiviral response. *Cell Mol Immunol*, *18*(3), 613-620. https://doi.org/10.1038/s41423-020-00571-x

Gao, Y., Yan, L., Huang, Y., Liu, F., Zhao, Y., Cao, L.,…Rao, Z. (2020). Structure of the RNA-dependent RNA polymerase from COVID-19 virus. *Science*, *368*(6492), 779-782. https://doi.org/10.1126/science.abb7498

Generali, D., Bosio, G., Malberti, F., Cuzzoli, A., Testa, S., Romanini, L.,…Pan, A. (2021). Canakinumab as treatment for COVID-19-related pneumonia: A prospective case-control study. *Int J Infect Dis*, *104*, 433-440. https://doi.org/10.1016/j.ijid.2020.12.073

Getz, L. L., Carter, C. S., & Gavish, L. (1981). The mating system of the prairie vole, Microtus ochrogaster: Field and laboratory evidence for pair-bonding. *Behavioral Ecology and Sociobiology*, *8*(3), 189-194. https://doi.org/10.1007/BF00299829

Getz, L. L., & Carter, S. C. (1996). Prairie-Vole Partnerships. *American Scientist*, *84(1)*, 56-62.

Getz, L. L., McGuire, B., Pizzuto, T., Hofmann, J. E., & Frase, B. (1993). Social Organization of the Prairie Vole (Microtus ochrogaster). *Journal of Mammalogy*, *74*(1), 44-58. https://doi.org/10.2307/1381904

Gheblawi, M., Wang, K., Viveiros, A., Nguyen, Q., Zhong, J. C., Turner, A. J.,…Oudit, G. Y. (2020). Angiotensin-Converting Enzyme 2: SARS-CoV-2 Receptor and Regulator of the Renin-Angiotensin System: Celebrating the 20th Anniversary of the Discovery of ACE2. *Circ Res*, *126*(10), 1456-1474. https://doi.org/10.1161/circresaha.120.317015

Gomes, C. P., Fernandes, D. E., Casimiro, F., da Mata, G. F., Passos, M. T., Varela, P.,…Pesquero, J. B. (2020). Cathepsin L in COVID-19: From Pharmacological Evidences to Genetics. *Front Cell Infect Microbiol*, *10*, 589505. https://doi.org/10.3389/fcimb.2020.589505

Gorbalenya, A. E., Baker, S. C., Baric, R. S., de Groot, R. J., Drosten, C., Gulyaeva, A. A.,…Coronaviridae Study Group of the International Committee on Taxonomy of, V. (2020). The species Severe acute respiratory syndrome-related coronavirus: classifying 2019-nCoV and naming it SARS-CoV-2. *Nature Microbiology*, *5*(4), 536-544. https://doi.org/10.1038/s41564-020-0695-z

Gori Savellini, G., Anichini, G., Gandolfo, C., & Cusi, M. G. (2021). SARS-CoV-2 N Protein Targets TRIM25-Mediated RIG-I Activation to Suppress Innate Immunity. *Viruses*, *13*(8). https://doi.org/10.3390/v13081439

Gottlieb, R. L., Vaca, C. E., Paredes, R., Mera, J., Webb, B. J., Perez, G.,…Hill, J. A. (2022). Early Remdesivir to Prevent Progression to Severe Covid-19 in Outpatients. *N Engl J Med*, *386*(4), 305-315. https://doi.org/10.1056/NEJMoa2116846

Govind Kumar, V., Ogden, D. S., Isu, U. H., Polasa, A., Losey, J., & Moradi, M. (2022). Prefusion spike protein conformational changes are slower in SARS-CoV-2 than in SARS-CoV-1. *J Biol Chem*, *298*(4), 101814. https://doi.org/10.1016/j.jbc.2022.101814

Grifoni, A., Weiskopf, D., Ramirez, S. I., Mateus, J., Dan, J. M., Moderbacher, C. R.,…Sette, A. (2020). Targets of T Cell Responses to SARS-CoV-2 Coronavirus in Humans with COVID-19 Disease and Unexposed Individuals. *Cell*, *181*(7), 1489-1501.e1415. https://doi.org/10.1016/j.cell.2020.05.015

Gruder-Adams, S., & Getz, L. L. (1985). Comparison of the Mating System and Paternal Behavior in Microtus ochrogaster and M. pennsylvanicus. *Journal of Mammalogy*, *66(1)*, 165-167.

Gu, H., Chen, Q., Yang, G., He, L., Fan, H., Deng, Y. Q.,…Zhou, Y. (2020). Adaptation of SARS-CoV-2 in BALB/c mice for testing vaccine efficacy. *Science*, *369*(6511), 1603-1607. https://doi.org/10.1126/science.abc4730

Guo, W., Porter, L. M., Crozier, T. W., Coates, M., Jha, A., McKie, M.,…McCaughan, F. (2022). Topical TMPRSS2 inhibition prevents SARS-CoV-2 infection in differentiated human airway cultures. *Life Sci Alliance*, *5*(4). https://doi.org/10.26508/lsa.202101116

Hamming, I., Timens, W., Bulthuis, M. L., Lely, A. T., Navis, G., & van Goor, H. (2004). Tissue distribution of ACE2 protein, the functional receptor for SARS coronavirus. A first step in understanding SARS pathogenesis. *J Pathol*, *203*(2), 631-637. https://doi.org/10.1002/path.1570

Hanifa, M., Salman, M., Fatima, M., Mukhtar, N., Almajhdi, F. N., Zaman, N.,…Khan, A. (2022). Mutational analysis of the spike protein of SARS-COV-2 isolates revealed atomistic features responsible for higher binding and infectivity. *Front Cell Dev Biol*, *10*, 940863. https://doi.org/10.3389/fcell.2022.940863

Harvey, W. T., Carabelli, A. M., Jackson, B., Gupta, R. K., Thomson, E. C., Harrison, E. M.,…Robertson, D. L. (2021). SARS-CoV-2 variants, spike mutations and immune escape. *Nat Rev Microbiol*, *19*(7), 409-424. https://doi.org/10.1038/s41579-021-00573-0

Hawkley, L. C., & Capitanio, J. P. (2015). Perceived social isolation, evolutionary fitness and health outcomes: a lifespan approach. *Philos Trans R Soc Lond B Biol Sci*, *370*(1669). https://doi.org/10.1098/rstb.2014.0114

Hayashi, T., Abiko, K., Mandai, M., Yaegashi, N., & Konishi, I. (2020). Highly conserved binding region of ACE2 as a receptor for SARS-CoV-2 between humans and mammals. *Vet Q*, *40*(1), 243-249. https://doi.org/10.1080/01652176.2020.1823522

He, J., Tao, H., Yan, Y., Huang, S. Y., & Xiao, Y. (2020). Molecular Mechanism of Evolution and Human Infection With SARS-CoV-2. *Viruses*. https://doi.org/10.3390/v12040428

Helms, J., Kremer, S., Merdji, H., Clere-Jehl, R., Schenck, M., Kummerlen, C.,…Meziani, F. (2020). Neurologic Features in Severe SARS-CoV-2 Infection. *New England Journal of Medicine*, *382*(23), 2268-2270. https://doi.org/10.1056/NEJMc2008597

Hicks, J., Klumpp-Thomas, C., Kalish, H., Shunmugavel, A., Mehalko, J., Denson, J. P.,…Sadtler, K. (2021). Serologic Cross-Reactivity of SARS-CoV-2 with Endemic and Seasonal Betacoronaviruses. *J Clin Immunol*, *41*(5), 906-913. https://doi.org/10.1007/s10875-021-00997-6

Hoffmann, M., Hofmann-Winkler, H., Smith, J. C., Krüger, N., Sørensen, L. K., Søgaard, O. S.,…Pöhlmann, S. (2020). Camostat mesylate inhibits SARS-CoV-2 activation by TMPRSS2-related proteases and its metabolite GBPA exerts antiviral activity. *bioRxiv*. https://doi.org/10.1101/2020.08.05.237651

Hoffmann, M., Kleine-Weber, H., Schroeder, S., Krüger, N., Herrler, T., Erichsen, S.,…Pöhlmann, S. (2020). SARS-CoV-2 Cell Entry Depends on ACE2 and TMPRSS2 and Is Blocked by a Clinically Proven Protease Inhibitor. *Cell*, *181*(2), 271-280.e278. https://doi.org/https://doi.org/10.1016/j.cell.2020.02.052

Hofmann, J. E., Getz, L., & Gavish, L. (1984). Home Range Overlap and Nest Cohabitation of Male and Female Prairie Voles. *The American Midland Naturalist*, *112 (2)*, *315-319*.

Hu, B., Guo, H., Zhou, P., & Shi, Z.-L. (2021). Characteristics of SARS-CoV-2 and COVID-19. *Nature Reviews Microbiology*, *19*(3), 141-154. https://doi.org/10.1038/s41579-020-00459-7

Hu, J., Igarashi, A., Kamata, M., & Nakagawa, H. (2001). Angiotensin-converting enzyme degrades Alzheimer amyloid beta-peptide (A beta); retards A beta aggregation, deposition, fibril formation; and inhibits cytotoxicity. *J Biol Chem*, *276*(51), 47863-47868. https://doi.org/10.1074/jbc.M104068200

Imai, M., Iwatsuki-Horimoto, K., Hatta, M., Loeber, S., Halfmann, P. J., Nakajima, N.,…Kawaoka, Y. (2020). Syrian hamsters as a small animal model for SARS-CoV-2 infection and countermeasure development. *Proc Natl Acad Sci U S A*, *117*(28), 16587-16595. https://doi.org/10.1073/pnas.2009799117

Insel, T. R., & Shapiro, L. E. (1992). Oxytocin receptor distribution reflects social organization in monogamous and polygamous voles. *Proc Natl Acad Sci U S A*, *89*(13), 5981-5985. https://doi.org/10.1073/pnas.89.13.5981

Insel, T. R., Wang, Z. X., & Ferris, C. F. (1994). Patterns of brain vasopressin receptor distribution associated with social organization in microtine rodents. *J Neurosci*, *14*(9), 5381-5392. https://doi.org/10.1523/jneurosci.14-09-05381.1994

Iyer, A. S., Jones, F. K., Nodoushani, A., Kelly, M., Becker, M., Slater, D.,…Charles, R. C. (2020). Persistence and decay of human antibody responses to the receptor binding domain of SARS-CoV-2 spike protein in COVID-19 patients. *Sci Immunol*, *5*(52). https://doi.org/10.1126/sciimmunol.abe0367

Jackson, C. B., Farzan, M., Chen, B., & Choe, H. (2022). Mechanisms of SARS-CoV-2 entry into cells. *Nature Reviews Molecular Cell Biology*, *23*(1), 3-20. https://doi.org/10.1038/s41580-021-00418-x

Jangra, S., Ye, C., Rathnasinghe, R., Stadlbauer, D., Krammer, F., Simon, V.,…Schotsaert, M. (2021). The E484K mutation in the SARS-CoV-2 spike protein reduces but does not abolish neutralizing activity of human convalescent and post-vaccination sera. *medRxiv*. https://doi.org/10.1101/2021.01.26.21250543

Johnson, B. A., Xie, X., Bailey, A. L., Kalveram, B., Lokugamage, K. G., Muruato, A.,…Menachery, V. D. (2021). Loss of furin cleavage site attenuates SARS-CoV-2 pathogenesis. *Nature*, *591*(7849), 293-299. https://doi.org/10.1038/s41586-021-03237-4

Johnson, Z. V., & Young, L. J. (2015). Neurobiological mechanisms of social attachment and pair bonding. *Curr Opin Behav Sci*, *3*, 38-44. https://doi.org/10.1016/j.cobeha.2015.01.009

Kant, R., Kareinen, L., Smura, T., Freitag, T. L., Jha, S. K., Alitalo, K.,…Vapalahti, O. (2021). Common Laboratory Mice Are Susceptible to Infection with the SARS-CoV-2 Beta Variant. *Viruses*, *13*(11). https://doi.org/10.3390/v13112263

Karki, R., & Kanneganti, T. D. (2022). Innate immunity, cytokine storm, and inflammatory cell death in COVID-19. *J Transl Med*, *20*(1), 542. https://doi.org/10.1186/s12967-022-03767-z

Karki, R., Sharma, B. R., Tuladhar, S., Williams, E. P., Zalduondo, L., Samir, P.,…Kanneganti, T. D. (2021). Synergism of TNF-α and IFN-γ Triggers Inflammatory Cell Death, Tissue Damage, and Mortality in SARS-CoV-2 Infection and Cytokine Shock Syndromes. *Cell*, *184*(1), 149-168.e117. https://doi.org/10.1016/j.cell.2020.11.025

Kato, H., Takeuchi, O., Mikamo-Satoh, E., Hirai, R., Kawai, T., Matsushita, K.,…Akira, S. (2008). Length-dependent recognition of double-stranded ribonucleic acids by retinoic acid-inducible gene-I and melanoma differentiation-associated gene 5. *J Exp Med*, *205*(7), 1601-1610. https://doi.org/10.1084/jem.20080091

Kawasaki, T., & Kawai, T. (2014). Toll-like receptor signaling pathways. *Front Immunol*, *5*, 461. https://doi.org/10.3389/fimmu.2014.00461

Kenkel, W. M., Gustison, M. L., & Beery, A. K. (2021). A Neuroscientist's Guide to the Vole. *Curr Protoc*, *1*(6), e175. https://doi.org/10.1002/cpz1.175

Kim, Y.-I., Kim, S.-G., Kim, S.-M., Kim, E.-H., Park, S.-J., Yu, K.-M.,…Choi, Y. K. (2020). Infection and Rapid Transmission of SARS-CoV-2 in Ferrets. *Cell Host & Microbe*, *27*(5), 704-709.e702. https://doi.org/https://doi.org/10.1016/j.chom.2020.03.023

Kim, Y.-M., & Shin, E.-C. (2021). Type I and III interferon responses in SARS-CoV-2 infection. *Experimental & Molecular Medicine*, *53*(5), 750-760. https://doi.org/10.1038/s12276-021-00592-0

Kinoshita, T., Shinoda, M., Nishizaki, Y., Shiraki, K., Hirai, Y., Kichikawa, Y.,…Kadota, J. (2022). A multicenter, double-blind, randomized, parallel-group, placebo-controlled study to evaluate the efficacy and safety of camostat mesilate in patients with COVID-19 (CANDLE study). *BMC Medicine*, *20*(1), 342. https://doi.org/10.1186/s12916-022-02518-7

Kitano, K., Yamagishi, A., Horie, K., Nishimori, K., & Sato, N. (2022). Helping behavior in prairie voles: A model of empathy and the importance of oxytocin. *iScience*, *25*(4), 103991. https://doi.org/10.1016/j.isci.2022.103991

Klaser, K., Thompson, E. J., Nguyen, L. H., Sudre, C. H., Antonelli, M., Murray, B.,…Steves, C. J. (2021). Anxiety and depression symptoms after COVID-19 infection: results from the COVID Symptom Study app. *medRxiv*. https://doi.org/10.1101/2021.07.07.21260137

Koch, J., Uckeley, Z. M., Doldan, P., Stanifer, M., Boulant, S., & Lozach, P. Y. (2021). TMPRSS2 expression dictates the entry route used by SARS-CoV-2 to infect host cells. *Embo j*, *40*(16), e107821. https://doi.org/10.15252/embj.2021107821

Kumavath, R., Barh, D., Andrade, B. S., Imchen, M., Aburjaile, F. F., Ch, A.,…Azevedo, V. (2021). The Spike of SARS-CoV-2: Uniqueness and Applications. *Front Immunol*, *12*, 663912. https://doi.org/10.3389/fimmu.2021.663912

Lau, E. H. Y., Tsang, O. T. Y., Hui, D. S. C., Kwan, M. Y. W., Chan, W. H., Chiu, S. S.,…Peiris, M. (2021). Neutralizing antibody titres in SARS-CoV-2 infections. *Nat Commun*, *12*(1), 63. https://doi.org/10.1038/s41467-020-20247-4

Lee, N. S., Goodwin, N. L., Freitas, K. E., & Beery, A. K. (2019). Affiliation, Aggression, and Selectivity of Peer Relationships in Meadow and Prairie Voles. *Front Behav Neurosci*, *13*, 52. https://doi.org/10.3389/fnbeh.2019.00052

Li, F. (2013). Receptor recognition and cross-species infections of SARS coronavirus. *Antiviral research*, *100*(1), 246-254. https://doi.org/10.1016/j.antiviral.2013.08.014

Li, H., Liu, S.-M., Yu, X.-H., Tang, S.-L., & Tang, C.-K. (2020). Coronavirus disease 2019 (COVID-19): current status and future perspectives. *International journal of antimicrobial agents*, 105951-105951. https://doi.org/10.1016/j.ijantimicag.2020.105951

Li, L., Wang, J., Ma, X., Sun, X., Li, J., Yang, X.,…Duan, Z. (2021). A Novel SARS-CoV-2 Related Coronavirus With Complex Recombination Isolated From Bats in Yunnan Province, China. *Emerging Microbes & Infections*. https://doi.org/10.1080/22221751.2021.1964925

Li, M.-Y., Li, L., Zhang, Y., & Wang, X.-S. (2020). Expression of the SARS-CoV-2 cell receptor gene ACE2 in a wide variety of human tissues. *Infectious Diseases of Poverty*, *9*(1), 45. https://doi.org/10.1186/s40249-020-00662-x

Li, Q., Wu, J., Nie, J., Zhang, L., Hao, H., Liu, S.,…Wang, Y. (2020). The Impact of Mutations in SARS-CoV-2 Spike on Viral Infectivity and Antigenicity. *Cell*, *182*(5), 1284-1294.e1289. https://doi.org/10.1016/j.cell.2020.07.012

Li, W., Wong, S.-K., Li, F., Kuhn, J. H., Huang, I. C., Choe, H., & Farzan, M. (2006). Animal origins of the severe acute respiratory syndrome coronavirus: insight from ACE2-S-protein interactions. *Journal of virology*, *80*(9), 4211-4219. https://doi.org/10.1128/jvi.80.9.4211-4219.2006

Li, X. N., Huang, Y., Wang, W., Jing, Q. L., Zhang, C. H., Qin, P. Z.,…Zhong, N. S. (2021). Effectiveness of inactivated SARS-CoV-2 vaccines against the Delta variant infection in Guangzhou: a test-negative case-control real-world study. *Emerg Microbes Infect*, *10*(1), 1751-1759. https://doi.org/10.1080/22221751.2021.1969291

Lin, B., Ferguson, C., White, J. T., Wang, S., Vessella, R., True, L. D.,…Nelson, P. S. (1999). Prostate-localized and androgen-regulated expression of the membrane-bound serine protease TMPRSS2. *Cancer Res*, *59*(17), 4180-4184.

Lin, H. X. J., Cho, S., Meyyur Aravamudan, V., Sanda, H. Y., Palraj, R., Molton, J. S., & Venkatachalam, I. (2021). Remdesivir in Coronavirus Disease 2019 (COVID-19)

treatment: a review of evidence. *Infection*, *49*(3), 401-410.
https://doi.org/10.1007/s15010-020-01557-7

Liu, G., Lee, J. H., Parker, Z. M., Acharya, D., Chiang, J. J., van Gent, M.,…Gack, M. U. (2021). ISG15-dependent activation of the sensor MDA5 is antagonized by the SARS-CoV-2 papain-like protease to evade host innate immunity. *Nat Microbiol*, *6*(4), 467-478. https://doi.org/10.1038/s41564-021-00884-1

Liu, Y., Liu, J., Plante, K. S., Plante, J. A., Xie, X., Zhang, X.,…Weaver, S. C. (2022). The N501Y spike substitution enhances SARS-CoV-2 infection and transmission. *Nature*, *602*(7896), 294-299. https://doi.org/10.1038/s41586-021-04245-0

Liu, Y., Qin, C., Rao, Y., Ngo, C., Feng, J. J., Zhao, J.,…Feng, P. (2021). SARS-CoV-2 Nsp5 Demonstrates Two Distinct Mechanisms Targeting RIG-I and MAVS To Evade the Innate Immune Response. *mBio*, *12*(5), e0233521. https://doi.org/10.1128/mBio.02335-21

Lovato, A., & Filippis, C. d. (2020). Clinical Presentation of COVID-19: A Systematic Review Focusing on Upper Airway Symptoms. *Ear Nose & Throat Journal*. https://doi.org/10.1177/0145561320920762

Lu, S., Zhao, Y., Yu, W., Yang, Y., Gao, J., Wang, J.,…Peng, X. (2020). Comparison of SARS-CoV-2 infections among 3 species of non-human primates. *bioRxiv*, 2020.2004.2008.031807. https://doi.org/10.1101/2020.04.08.031807

Ma, C., & Gong, C. (2021). ACE2 models of frequently contacted animals provide clues of their SARS-CoV-2 S protein affinity and viral susceptibility. *J Med Virol*, *93*(7), 4469-4479. https://doi.org/10.1002/jmv.26953

Mandala, V. S., McKay, M. J., Shcherbakov, A. A., Dregni, A. J., Kolocouris, A., & Hong, M. (2020). Structure and drug binding of the SARS-CoV-2 envelope protein transmembrane domain in lipid bilayers. *Nature Structural & Molecular Biology*, *27*(12), 1202-1208. https://doi.org/10.1038/s41594-020-00536-8

Mantovani, S., Oliviero, B., Varchetta, S., Renieri, A., & Mondelli, M. U. (2023). TLRs: Innate Immune Sentries against SARS-CoV-2 Infection. *Int J Mol Sci*, *24*(9). https://doi.org/10.3390/ijms24098065

Masiá, M., Padilla, S., García, J. A., García-Abellán, J., Navarro, A., Guillén, L.,…Gutiérrez, F. (2021). Impact of the Addition of Baricitinib to Standard of Care Including Tocilizumab and Corticosteroids on Mortality and Safety in Severe COVID-19. *Front Med (Lausanne)*, *8*, 749657. https://doi.org/10.3389/fmed.2021.749657

Matsuyama, S., Nao, N., Shirato, K., Kawase, M., Saito, S., Takayama, I.,…Takeda, M. (2020). Enhanced Isolation of SARS-CoV-2 by TMPRSS2-expressing Cells. *Proceedings of the National Academy of Sciences*. https://doi.org/10.1073/pnas.2002589117

McGraw, L. A., & Young, L. J. (2010). The prairie vole: an emerging model organism for understanding the social brain. *Trends in neurosciences*, *33*(2), 103-109. https://doi.org/10.1016/j.tins.2009.11.006

McGuire, B., & Getz, L. L. (2010). Alternative male reproductive tactics in a natural population of prairie voles Microtus ochrogaster. *Acta Theriologica*, *55*(3), 261-270. https://doi.org/10.4098/j.at.0001-7051.077.2009

McLean, A. C., Valenzuela, N., Fai, S., & Bennett, S. A. (2012). Performing vaginal lavage, crystal violet staining, and vaginal cytological evaluation for mouse estrous cycle staging identification. *J Vis Exp*(67), e4389. https://doi.org/10.3791/4389

Meekins, D. A., Gaudreault, N. N., & Richt, J. A. (2021). Natural and Experimental SARS-CoV-2 Infection in Domestic and Wild Animals. *Viruses*, *13*(10). https://doi.org/10.3390/v13101993

Meyer, D., Sielaff, F., Hammami, M. M., Böttcher-Friebertshäuser, E., Garten, W., & Steinmetzer, T. (2013). Identification of the First Synthetic Inhibitors of the Type II Transmembrane Serine Protease TMPRSS2 Suitable for Inhibition of Influenza Virus Activation. *Biochemical Journal*. https://doi.org/10.1042/bj20130101

Miller, A. K., Mifsud, J. C. O., Costa, V. A., Grimwood, R. M., Kitson, J., Baker, C. F.,…Geoghegan, J. L. (2021). Slippery When Wet: Cross-Species Transmission of Divergent Coronaviruses in Bony and Jawless Fish and the Evolutionary History of the <i>Coronaviridae</I>. *Virus Evolution*. https://doi.org/10.1093/ve/veab050

Minkoff, J. M., & tenOever, B. (2023). Innate immune evasion strategies of SARS-CoV-2. *Nat Rev Microbiol*, *21*(3), 178-194. https://doi.org/10.1038/s41579-022-00839-1

Mora, S., Dussaubat, N., & Díaz-Véliz, G. (1996). Effects of the estrous cycle and ovarian hormones on behavioral indices of anxiety in female rats. *Psychoneuroendocrinology*, *21*(7), 609-620. https://doi.org/10.1016/s0306-4530(96)00015-7

Mousavizadeh, L., & Ghasemi, S. (2020). Genotype and phenotype of COVID-19: Their roles in pathogenesis. *Journal of microbiology, immunology, and infection = Wei mian yu gan ran za zhi*, S1684-1182(1620)30082-30087. https://doi.org/10.1016/j.jmii.2020.03.022

Nakayama, K. (1997). Furin: A Mammalian Subtilisin/Kex2p-Like Endoprotease Involved in Processing of a Wide Variety of Precursor Proteins. *Biochemical Journal*. https://doi.org/10.1042/bj3270625

Nencka, R., Silhan, J., Klima, M., Otava, T., Kocek, H., Krafcikova, P., & Boura, E. (2022). Coronaviral RNA-methyltransferases: function, structure and inhibition. *Nucleic Acids Research*, *50*(2), 635-650. https://doi.org/10.1093/nar/gkab1279

Ng, K. W., Faulkner, N., Cornish, G. H., Rosa, A., Harvey, R., Hussain, S.,…Kassiotis, G. (2020). Preexisting and de novo humoral immunity to SARS-CoV-2 in humans. *Science*, *370*(6522), 1339-1343. https://doi.org/10.1126/science.abe1107

Nicola, M., Alsafi, Z., Sohrabi, C., Kerwan, A., Al-Jabir, A., Iosifidis, C.,…Agha, R. (2020). The Socio-Economic Implications of the Coronavirus and COVID-19 Pandemic: A Review. *International journal of surgery (London, England)*, S1743-9191(1720)30316-30312. https://doi.org/10.1016/j.ijsu.2020.04.018

Nieva, J. L., Madan, V., & Carrasco, L. (2012). Viroporins: structure and biological functions. *Nature Reviews Microbiology*, *10*(8), 563-574. https://doi.org/10.1038/nrmicro2820

Ong, S. W. X., Tan, Y. K., Chia, P. Y., Lee, T. H., Ng, O. T., Wong, M., & Marimuthu, K. (2020). Air, Surface Environmental, and Personal Protective Equipment Contamination by Severe Acute Respiratory Syndrome Coronavirus 2 (SARS-CoV-2) From a Symptomatic Patient. *Jama*. https://doi.org/10.1001/jama.2020.3227

Ou, X., Liu, Y., Lei, X., Li, P., Mi, D., Ren, L.,…Qian, Z. (2020). Characterization of spike glycoprotein of SARS-CoV-2 on virus entry and its immune cross-reactivity with SARS-CoV. *Nat Commun*, *11*(1), 1620. https://doi.org/10.1038/s41467-020-15562-9

Pal, M., Berhanu, G., Desalegn, C., & Kandi, V. (2020). Severe Acute Respiratory Syndrome Coronavirus-2 (SARS-CoV-2): An Update. *Cureus*. https://doi.org/10.7759/cureus.7423

Pan, T., Chen, R., He, X., Yuan, Y., Deng, X., Li, R.,…Zhang, H. (2021). Infection of wild-type mice by SARS-CoV-2 B.1.351 variant indicates a possible novel cross-species

transmission route. *Signal Transduction and Targeted Therapy*, *6*(1), 420. https://doi.org/10.1038/s41392-021-00848-1

Paterson, R. W., Brown, R. L., Benjamin, L., Nortley, R., Wiethoff, S., Bharucha, T.,…for the, U. C. L. Q. S. N. H. f. N. a. N. C.-S. G. (2020). The emerging spectrum of COVID-19 neurology: clinical, radiological and laboratory findings. *Brain*, *143*(10), 3104-3120. https://doi.org/10.1093/brain/awaa240

Peacock, T. P., Goldhill, D. H., Zhou, J., Baillon, L., Frise, R., Swann, O. C.,…Barclay, W. S. (2021). The furin cleavage site in the SARS-CoV-2 spike protein is required for transmission in ferrets. *Nature Microbiology*, *6*(7), 899-909. https://doi.org/10.1038/s41564-021-00908-w

Perez-Gomez, R. (2021). The Development of SARS-CoV-2 Variants: The Gene Makes the Disease. *J Dev Biol*, *9*(4). https://doi.org/10.3390/jdb9040058

Pires De Souza, G. A., Le Bideau, M., Boschi, C., Wurtz, N., Colson, P., Aherfi, S.,…La Scola, B. (2022). Choosing a cellular model to study SARS-CoV-2. *Front Cell Infect Microbiol*, *12*, 1003608. https://doi.org/10.3389/fcimb.2022.1003608

Pitol, A. K., & Julian, T. R. (2021). Community Transmission of SARS-CoV-2 by Surfaces: Risks and Risk Reduction Strategies. *Environmental Science & Technology Letters*. https://doi.org/10.1021/acs.estlett.0c00966

Prasad, K., Ahamad, S., Kanipakam, H., Gupta, D., & Kumar, V. (2021). Simultaneous Inhibition of SARS-CoV-2 Entry Pathways by Cyclosporine. *ACS Chemical Neuroscience*, *12*(5), 930-944. https://doi.org/10.1021/acschemneuro.1c00019

Primorac, D., Vrdoljak, K., Brlek, P., Pavelić, E., Molnar, V., Matišić, V.,…Parčina, M. (2022). Adaptive Immune Responses and Immunity to SARS-CoV-2. *Front Immunol*, *13*, 848582. https://doi.org/10.3389/fimmu.2022.848582

Rabaan, A. A., Al-Ahmed, S. H., Muhammad, J., Khan, A., Sule, A. A., Tirupathi, R.,…Dhama, K. (2021). Role of Inflammatory Cytokines in COVID-19 Patients: A Review on Molecular Mechanisms, Immune Functions, Immunopathology and Immunomodulatory Drugs to Counter Cytokine Storm. *Vaccines (Basel)*, *9*(5). https://doi.org/10.3390/vaccines9050436

Rashid, F., Xie, Z., Suleman, M., Shah, A., Khan, S., & Luo, S. (2022). Roles and functions of SARS-CoV-2 proteins in host immune evasion. *Front Immunol*, *13*, 940756. https://doi.org/10.3389/fimmu.2022.940756

Rastogi, I., Jeon, D., Moseman, J. E., Muralidhar, A., Potluri, H. K., & McNeel, D. G. (2022). Role of B cells as antigen presenting cells. *Front Immunol*, *13*, 954936. https://doi.org/10.3389/fimmu.2022.954936

Reikine, S., Nguyen, J. B., & Modis, Y. (2014). Pattern Recognition and Signaling Mechanisms of RIG-I and MDA5. *Front Immunol*, *5*, 342. https://doi.org/10.3389/fimmu.2014.00342

Rodda, L. B., Netland, J., Shehata, L., Pruner, K. B., Morawski, P. A., Thouvenel, C. D.,…Pepper, M. (2021). Functional SARS-CoV-2-Specific Immune Memory Persists after Mild COVID-19. *Cell*, *184*(1), 169-183.e117. https://doi.org/10.1016/j.cell.2020.11.029

Ross, H. E., Freeman, S. M., Spiegel, L. L., Ren, X., Terwilliger, E. F., & Young, L. J. (2009). Variation in oxytocin receptor density in the nucleus accumbens has differential effects on affiliative behaviors in monogamous and polygamous voles. *J Neurosci*, *29*(5), 1312-1318. https://doi.org/10.1523/jneurosci.5039-08.2009

Rosshart, S. P., Herz, J., Vassallo, B. G., Hunter, A., Wall, M. K., Badger, J. H.,…Rehermann, B. (2019). Laboratory mice born to wild mice have natural microbiota and model human immune responses. *Science*, *365*(6452), eaaw4361. https://doi.org/10.1126/science.aaw4361

Rossi Á, D., de Araújo, J. L. F., de Almeida, T. B., Ribeiro-Alves, M., de Almeida Velozo, C., Almeida, J. M.,…Cardoso, C. C. (2021). Association between ACE2 and TMPRSS2 nasopharyngeal expression and COVID-19 respiratory distress. *Sci Rep*, *11*(1), 9658. https://doi.org/10.1038/s41598-021-88944-8

Rydyznski Moderbacher, C., Ramirez, S. I., Dan, J. M., Grifoni, A., Hastie, K. M., Weiskopf, D.,…Crotty, S. (2020). Antigen-Specific Adaptive Immunity to SARS-CoV-2 in Acute COVID-19 and Associations with Age and Disease Severity. *Cell*, *183*(4), 996-1012.e1019. https://doi.org/10.1016/j.cell.2020.09.038

Sacchetto, L., Chaves, B. A., Costa, E. R., Medeiros, A. S. d. M., Gordo, M., Araújo, D. B.,…Nogueira, M. L. (2021). Lack of Evidence of Severe Acute Respiratory Syndrome Coronavirus 2 (SARS-CoV-2) Spillover in Free-Living Neotropical Non-Human Primates, Brazil. *Viruses*. https://doi.org/10.3390/v13101933

Salonen, A., Ahola, T., & Kääriäinen, L. (2005). Viral RNA replication in association with cellular membranes. *Curr Top Microbiol Immunol*, *285*, 139-173. https://doi.org/10.1007/3-540-26764-6_5

Samavati, L., & Uhal, B. D. (2020). ACE2, Much More Than Just a Receptor for SARS-COV-2. *Front Cell Infect Microbiol*, *10*, 317. https://doi.org/10.3389/fcimb.2020.00317

Samir, P., Malireddi, R. K. S., & Kanneganti, T. D. (2020). The PANoptosome: A Deadly Protein Complex Driving Pyroptosis, Apoptosis, and Necroptosis (PANoptosis). *Front Cell Infect Microbiol*, *10*, 238. https://doi.org/10.3389/fcimb.2020.00238

Sawicki, S. G., & Sawicki, D. L. (1995). Coronaviruses use discontinuous extension for synthesis of subgenome-length negative strands. *Adv Exp Med Biol*, *380*, 499-506. https://doi.org/10.1007/978-1-4615-1899-0_79

Schmithausen, R. M., Döhla, M., Schößler, H., Diegmann, C., Schulte, B., Richter, E.,…Streeck, H. (2020). Characteristic Temporary Loss of Taste and Olfactory Senses in SARS-CoV-2-positive-Individuals With Mild Symptoms. *Pathogens and Immunity*. https://doi.org/10.20411/pai.v5i1.374

Schäfer, A., Martinez, D. R., Won, J. J., Meganck, R. M., Moreira, F. R., Brown, A. J.,…Sheahan, T. P. (2022). Therapeutic treatment with an oral prodrug of the remdesivir parental nucleoside is protective against SARS-CoV-2 pathogenesis in mice. *Sci Transl Med*, *14*(643), eabm3410. https://doi.org/10.1126/scitranslmed.abm3410

Sette, A., & Crotty, S. (2021). Adaptive immunity to SARS-CoV-2 and COVID-19. *Cell*, *184*(4), 861-880. https://doi.org/10.1016/j.cell.2021.01.007

Setti, L., Passarini, F., Gennaro, G. d., Barbieri, P., Perrone, M. G., Borelli, M.,…Miani, A. (2020). Airborne Transmission Route of COVID-19: Why 2 Meters/6 Feet of Inter-Personal Distance Could Not Be Enough. *International Journal of Environmental Research and Public Health*. https://doi.org/10.3390/ijerph17082932

Shang, C., Liu, Z., Zhu, Y., Lu, J., Ge, C., Zhang, C.,…Li, X. (2021). SARS-CoV-2 Causes Mitochondrial Dysfunction and Mitophagy Impairment. *Front Microbiol*, *12*, 780768. https://doi.org/10.3389/fmicb.2021.780768

Shemesh, M., Aktepe, T. E., Deerain, J. M., McAuley, J. L., Audsley, M. D., David, C. T.,…Harari, D. (2021). SARS-CoV-2 suppresses IFNβ production mediated by NSP1, 5,

6, 15, ORF6 and ORF7b but does not suppress the effects of added interferon. *PLoS Pathog*, *17*(8), e1009800. https://doi.org/10.1371/journal.ppat.1009800

Shen, J., Fan, J., Zhao, Y., Jiang, D., Niu, Z., Zhang, Z., & Cao, G. (2023). Innate and adaptive immunity to SARS-CoV-2 and predisposing factors. *Front Immunol*, *14*, 1159326. https://doi.org/10.3389/fimmu.2023.1159326

Shi, J., Wen, Z., Zhong, G., Yang, H., Wang, C., Huang, B.,…Bu, Z. (2020). Susceptibility of ferrets, cats, dogs, and other domesticated animals to SARS-coronavirus 2. *Science*, *368*(6494), 1016-1020. https://doi.org/10.1126/science.abb7015

Sia, S. F., Yan, L.-M., Chin, A. W. H., Fung, K., Choy, K.-T., Wong, A. Y. L.,…Yen, H.-L. (2020). Pathogenesis and transmission of SARS-CoV-2 in golden hamsters. *Nature*, *583*(7818), 834-838. https://doi.org/10.1038/s41586-020-2342-5

Singh, A., Singh, R. S., Sarma, P., Batra, G., Joshi, R., Kaur, H.,…Medhi, B. (2020). A Comprehensive Review of Animal Models for Coronaviruses: SARS-CoV-2, SARS-CoV, and MERS-CoV. *Virol Sin*, *35*(3), 290-304. https://doi.org/10.1007/s12250-020-00252-z

Siu, K. L., Yuen, K. S., Castaño-Rodriguez, C., Ye, Z. W., Yeung, M. L., Fung, S. Y.,…Jin, D. Y. (2019). Severe acute respiratory syndrome coronavirus ORF3a protein activates the NLRP3 inflammasome by promoting TRAF3-dependent ubiquitination of ASC. *Faseb j*, *33*(8), 8865-8877. https://doi.org/10.1096/fj.201802418R

Sola, I., Almazán, F., Zúñiga, S., & Enjuanes, L. (2015). Continuous and Discontinuous RNA Synthesis in Coronaviruses. *Annu Rev Virol*, *2*(1), 265-288. https://doi.org/10.1146/annurev-virology-100114-055218

Sosa-Hernández, V. A., Torres-Ruíz, J., Cervantes-Díaz, R., Romero-Ramírez, S., Páez-Franco, J. C., Meza-Sánchez, D. E.,…Maravillas-Montero, J. L. (2020). B Cell Subsets as Severity-Associated Signatures in COVID-19 Patients. *Front Immunol*, *11*, 611004. https://doi.org/10.3389/fimmu.2020.611004

Suleman, M., Ishaq, I., Khan, H., Ullah Khan, S., Masood, R., Albekairi, N. A.,…Crovella, S. (2023). Elucidating the binding mechanism of SARS-CoV-2 NSP6-TBK1 and structure-based designing of phytocompounds inhibitors for instigating the host immune response. *Front Chem*, *11*, 1346796. https://doi.org/10.3389/fchem.2023.1346796

Sulimov, A., Kutov, D., Ilin, I., Xiao, Y., Jiang, S., & Sulimov, V. (2022). Novel Inhibitors of 2'-O-Methyltransferase of the SARS-CoV-2 Coronavirus. *Molecules*, *27*(9). https://doi.org/10.3390/molecules27092721

Süzgün, M. A., Kızılkılıç, E. K., Bostan, B. U., Tütüncü, M., & Kızıltan, G. (2023). Parainfectious Autoimmune Encephalitis Related to SARS-CoV-2 Infection, Presenting With Catatonia. *The International Journal of Psychiatry in Medicine*. https://doi.org/10.1177/00912174231161393

Takeda, M. (2022). Proteolytic activation of SARS-CoV-2 spike protein. *Microbiol Immunol*, *66*(1), 15-23. https://doi.org/10.1111/1348-0421.12945

Takeuchi, A., & Saito, T. (2017). CD4 CTL, a Cytotoxic Subset of CD4(+) T Cells, Their Differentiation and Function. *Front Immunol*, *8*, 194. https://doi.org/10.3389/fimmu.2017.00194

Tan, A. T., Linster, M., Tan, C. W., Le Bert, N., Chia, W. N., Kunasegaran, K.,…Bertoletti, A. (2021). Early induction of functional SARS-CoV-2-specific T cells associates with rapid viral clearance and mild disease in COVID-19 patients. *Cell Rep*, *34*(6), 108728. https://doi.org/10.1016/j.celrep.2021.108728

Thakur, S., Sasi, S., Pillai, S. G., Nag, A., Shukla, D., Singhal, R.,…Velu, G. S. K. (2022). SARS-CoV-2 Mutations and Their Impact on Diagnostics, Therapeutics and Vaccines. *Front Med (Lausanne)*, *9*, 815389. https://doi.org/10.3389/fmed.2022.815389

Thomas, S. (2020). The Structure of the Membrane Protein of SARS-CoV-2 Resembles the Sugar Transporter semiSWEET. https://doi.org/10.20944/preprints202004.0512.v4

Tian, Y., & Zhou, L. Q. (2021). Evaluating the impact of COVID-19 on male reproduction. *Reproduction*, *161*(2), R37-r44. https://doi.org/10.1530/rep-20-0523

Tobback, E., Degroote, S., Buysse, S., Delesie, L., Van Dooren, L., Vanherrewege, S.,…De Scheerder, M. A. (2022). Efficacy and safety of camostat mesylate in early COVID-19 disease in an ambulatory setting: a randomized placebo-controlled phase II trial. *Int J Infect Dis*, *122*, 628-635. https://doi.org/10.1016/j.ijid.2022.06.054

Tokarz, R., Sameroff, S., Hesse, R., Hause, B. M., Desai, A., Jain, K., & Lipkin, W. I. (2015). Discovery of a Novel Nidovirus in Cattle With Respiratory Disease. *Journal of General Virology*. https://doi.org/10.1099/vir.0.000166

Turner, A. J. (2015). ACE2 Cell Biology, Regulation, and Physiological Functions. In *The Protective Arm of the Renin Angiotensin System (RAS)* (pp. 185-189). Copyright © 2015 Elsevier Inc. All rights reserved. https://doi.org/10.1016/b978-0-12-801364-9.00025-0

Vidricaire, G., Denault, J. B., & Leduc, R. (1993). Characterization of a secreted form of human furin endoprotease. *Biochem Biophys Res Commun*, *195*(2), 1011-1018. https://doi.org/10.1006/bbrc.1993.2145

V'kovski, P., Kratzel, A., Steiner, S., Stalder, H., & Thiel, V. (2021). Coronavirus biology and replication: implications for SARS-CoV-2. *Nature Reviews Microbiology*, *19*(3), 155-170. https://doi.org/10.1038/s41579-020-00468-6

Wahl, A., Gralinski, L. E., Johnson, C. E., Yao, W., Kovarova, M., Dinnon, K. H.,…Garcia, J. V. (2021). SARS-CoV-2 infection is effectively treated and prevented by EIDD-2801. *Nature*, *591*(7850), 451-457. https://doi.org/10.1038/s41586-021-03312-w

Wan, Y., Shang, J., Graham, R., Baric, R. S., & Li, F. (2020). Receptor Recognition by the Novel Coronavirus from Wuhan: an Analysis Based on Decade-Long Structural Studies of SARS Coronavirus. *J Virol*, *94*(7). https://doi.org/10.1128/jvi.00127-20

Wang, P., Li, W., Yang, Y., Cheng, N., Zhang, Y., Zhang, N.,…Luo, J. (2022). A polypeptide inhibitor of calcineurin blocks the calcineurin-NFAT signalling pathway in vivo and in vitro. *J Enzyme Inhib Med Chem*, *37*(1), 202-210. https://doi.org/10.1080/14756366.2021.1998024

Weis, N., Bollerup, S., Sund, J. D., Glamann, J. B., Vinten, C., Jensen, L. R.,…Rosenkilde, M. M. (2023). Amantadine for COVID-19 treatment (ACT) study: a randomized, double-blinded, placebo-controlled clinical trial. *Clin Microbiol Infect*, *29*(10), 1313-1319. https://doi.org/10.1016/j.cmi.2023.06.023

WHO. (2021). *WHO Coronavirus (Covid19) Dashboard*. https://covid19.who.int

Winkler, E. S., Bailey, A. L., Kafai, N. M., Nair, S., McCune, B. T., Yu, J.,…Diamond, M. S. (2020). SARS-CoV-2 infection of human ACE2-transgenic mice causes severe lung inflammation and impaired function. *Nature Immunology*, *21*(11), 1327-1335. https://doi.org/10.1038/s41590-020-0778-2

Wong, J., Layton, D., Wheatley, A. K., & Kent, S. J. (2019). Improving immunological insights into the ferret model of human viral infectious disease. *Influenza Other Respir Viruses*, *13*(6), 535-546. https://doi.org/10.1111/irv.12687

Woolsey, C., Borisevich, V., Prasad, A. N., Agans, K. N., Deer, D. J., Dobias, N. S.,…Cross, R. W. (2021). Establishment of an African green monkey model for COVID-19 and protection against re-infection. *Nature Immunology*, *22*(1), 86-98. https://doi.org/10.1038/s41590-020-00835-8

Wrapp, D., Wang, N., Corbett, K. S., Goldsmith, J. A., Hsieh, C.-L., Abiona, O.,…McLellan, J. S. (2020). Cryo-EM structure of the 2019-nCoV spike in the prefusion conformation. *Science*, *367*(6483), 1260. https://doi.org/10.1126/science.abb2507

Wruck, W., & Adjaye, J. (2020). SARS-CoV-2 receptor ACE2 is co-expressed with genes related to transmembrane serine proteases, viral entry, immunity and cellular stress. *Sci Rep*, *10*(1), 21415. https://doi.org/10.1038/s41598-020-78402-2

Wu, A., Peng, Y., Huang, B., Ding, X., Wang, X., Niu, P.,…Wang, J. (2020). Genome composition and divergence of the novel coronavirus (2019-nCoV) originating in China. *Cell host & microbe*, *27*(3), 325-328.

Wu, C., Liu, Y., Yang, Y., Zhang, P., Zhong, W., Wang, Y.,…Li, H. (2020). Analysis of Therapeutic Targets for SARS-CoV-2 and Discovery of Potential Drugs by Computational Methods. *Acta Pharmaceutica Sinica B*. https://doi.org/10.1016/j.apsb.2020.02.008

Xia, H., Cao, Z., Xie, X., Zhang, X., Chen, J. Y., Wang, H.,…Shi, P. Y. (2020). Evasion of Type I Interferon by SARS-CoV-2. *Cell Rep*, *33*(1), 108234. https://doi.org/10.1016/j.celrep.2020.108234

Xiao, L., Sakagami, H., & Miwa, N. (2020). ACE2: The key Molecule for Understanding the Pathophysiology of Severe and Critical Conditions of COVID-19: Demon or Angel? *Viruses*, *12*(5). https://doi.org/10.3390/v12050491

Xu, J., Zhao, S., Teng, T., Abdalla, A. E., Zhu, W., Xie, L.,…Guo, X. (2020). Systematic Comparison of Two Animal-to-Human Transmitted Human Coronaviruses: SARS-CoV-2 and SARS-CoV. *Viruses*. https://doi.org/10.3390/v12020244

Yadati, T., Houben, T., Bitorina, A., & Shiri-Sverdlov, R. (2020). The Ins and Outs of Cathepsins: Physiological Function and Role in Disease Management. *Cells*, *9*(7). https://doi.org/10.3390/cells9071679

Yamada, T., & Takaoka, A. (2023). Innate immune recognition against SARS-CoV-2. *Inflamm Regen*, *43*(1), 7. https://doi.org/10.1186/s41232-023-00259-5

Yang, H., & Rao, Z. (2021). Structural biology of SARS-CoV-2 and implications for therapeutic development. *Nature Reviews Microbiology*, *19*(11), 685-700. https://doi.org/10.1038/s41579-021-00630-8

Yee, J. R., Kenkel, W. M., Kulkarni, P., Moore, K., Perkeybile, A. M., Toddes, S.,…Ferris, C. F. (2016). BOLD fMRI in awake prairie voles: A platform for translational social and affective neuroscience. *Neuroimage*, *138*, 221-232. https://doi.org/10.1016/j.neuroimage.2016.05.046

Young, K. A., Gobrogge, K. L., Liu, Y., & Wang, Z. (2011). The neurobiology of pair bonding: insights from a socially monogamous rodent. *Front Neuroendocrinol*, *32*(1), 53-69. https://doi.org/10.1016/j.yfrne.2010.07.006

Yu, J., Tostanoski, L. H., Peter, L., Mercado, N. B., McMahan, K., Mahrokhian, S. H.,…Barouch, D. H. (2020). DNA vaccine protection against SARS-CoV-2 in rhesus macaques. *Science*, *369*(6505), 806-811. https://doi.org/10.1126/science.abc6284

Yuki, K., Fujiogi, M., & Koutsogiannaki, S. (2020). COVID-19 pathophysiology: A review. *Clinical immunology (Orlando, Fla.)*, *215*, 108427-108427. https://doi.org/10.1016/j.clim.2020.108427

Zaliani, A., Vangeel, L., Reinshagen, J., Iaconis, D., Kuzikov, M., Keminer, O.,…Leyssen, P. (2022). Cytopathic SARS-CoV-2 screening on VERO-E6 cells in a large-scale repurposing effort. *Scientific Data*, *9*(1), 405. https://doi.org/10.1038/s41597-022-01532-x

Zayet, S., Gendrin, V., Gay, C., Selles, P., & Klopfenstein, T. (2022). Increased COVID-19 Severity among Pregnant Patients Infected with SARS-CoV-2 Delta Variant, France. *Emerg Infect Dis*, *28*(5), 1048-1050. https://doi.org/10.3201/eid2805.212080

Zhang, C., Ma, H. M., Dong, S. S., Zhang, N., He, P., Ge, M. K.,…Shen, S. M. (2022). Furin extracellularly cleaves secreted PTENα/β to generate C-terminal fragment with a tumor-suppressive role. *Cell Death Dis*, *13*(6), 532. https://doi.org/10.1038/s41419-022-04988-2

Zhang, J. J., Dong, X., Liu, G. H., & Gao, Y. D. (2023). Risk and Protective Factors for COVID-19 Morbidity, Severity, and Mortality. *Clin Rev Allergy Immunol*, *64*(1), 90-107. https://doi.org/10.1007/s12016-022-08921-5

Zhang, L., Jackson, C. B., Mou, H., Ojha, A., Peng, H., Quinlan, B. D.,…Choe, H. (2020). SARS-CoV-2 spike-protein D614G mutation increases virion spike density and infectivity. *Nat Commun*, *11*(1), 6013. https://doi.org/10.1038/s41467-020-19808-4

Zhang, Q., Chen, Z., Huang, C., Sun, J., Xue, M., Feng, T.,…Dai, J. (2021). Severe Acute Respiratory Syndrome Coronavirus 2 (SARS-CoV-2) Membrane (M) and Spike (S) Proteins Antagonize Host Type I Interferon Response. *Front Cell Infect Microbiol*, *11*, 766922. https://doi.org/10.3389/fcimb.2021.766922

Zhao, M.-M., Yang, W.-L., Yang, F.-Y., Zhang, L., Huang, W.-J., Hou, W.,…Yang, J.-K. (2021). Cathepsin L plays a key role in SARS-CoV-2 infection in humans and humanized mice and is a promising target for new drug development. *Signal Transduction and Targeted Therapy*, *6*(1), 134. https://doi.org/10.1038/s41392-021-00558-8

Zhao, Y., Wang, C. L., Gao, Z. Y., Qiao, H. X., Wang, W. J., Liu, X. Y., & Chuai, X. (2023). Ferrets: A powerful model of SARS-CoV-2. *Zool Res*, *44*(2), 323-330. https://doi.org/10.24272/j.issn.2095-8137.2022.351

Zhu, Q., Xu, Y., Wang, T., & Xie, F. (2022). Innate and adaptive immune response in SARS-CoV-2 infection-Current perspectives. *Front Immunol*, *13*, 1053437. https://doi.org/10.3389/fimmu.2022.1053437

Zmora, P., Hoffmann, M., Kollmus, H., Moldenhauer, A.-S., Danov, O., Braun, A.,…Pöhlmann, S. (2018). TMPRSS11A Activates the Influenza a Virus Hemagglutinin and the MERS Coronavirus Spike Protein and Is Insensitive Against Blockade by HAI-1. *Journal of Biological Chemistry*. https://doi.org/10.1074/jbc.ra118.001273

Štefek, M., Chalupská, D., Chalupský, K., Zgarbová, M., Dvořáková, A., Krafčíková, P.,…Nencka, R. (2023). Rational Design of Highly Potent SARS-CoV-2 nsp14 Methyltransferase Inhibitors. *ACS Omega*, *8*(30), 27410-27418. https://doi.org/10.1021/acsomega.3c02815

Vita

Stephanie Kehl received a BS in Biological Sciences and a BS in Chemistry from the University of Alabama in Huntsville (UAH) in May 2012. In August 2014, she received her MS in Biological Sciences from UAH. The title of her master's thesis was "Doc of Bacteriophage P1 is an enzyme that inhibits translation and phosphorylates a protein target". This work involved investigating the effects of the toxin-antitoxin system of bacteriophage P1 on *E. coli* and confirmed that the toxin inhibits translation by inducing phosphorylation of a host protein.

Stephanie has held various teaching and professional roles, including laboratory research assistant and graduate teaching assistant at the University of Alabama in Huntsville. After graduating with her master's degree, she joined the Tacoma Community College Biology teaching staff as an adjunct professor. Following this, she attended two years of graduate school at the University of New Mexico (UNM) in the Biomedical Sciences Graduate Program, where she studied autophagy processes and regulation. At UNM, her research focused on delineating the role of the selective autophagy receptor p62 as a signaling platform. It led to the discovery of a novel role for TAK1 (a kinase involved in inflammatory signaling) in regulating p62's autophagic function. This work resulted in a first-author publication in *EMBO Reports* titled "TAK1 converts Sequestosome 1/p62 from an autophagy receptor to a signaling platform".

In January 2020, she transferred to the Biosciences Graduate Program at the University of Texas at El Paso (UTEP). Her time at the UTEP has resulted in the publication of two papers titled "A novel eccentric therapeutic approach for individuals recovering from COVID-19" (published in *Cardiopulmonary Physical Therapy Journal)* and "An intranasal nanoparticle vaccine elicits protective immunity against Mycobacterium tuberculosis" (published in *Vaccine*). Her Ph.D. conferral date will be August 2024.